UILU-ENG-95-2004

CIVIL ENGINEERING STUDIES

STRUCTURAL RESEARCH SERIES NO. 601

ISSN: 0069-4274

Performance Evaluation of a Dual-Level Design Using 1994 Northridge Earthquake Records

By
KENNETH J. ELWOOD
and
Y. K. WEN

Technical Report of Research
Sponsored by the NATIONAL EARTHQUAKE HAZARDS REDUCTION PROGRAM
(FEMA, USGS, NSF, NIST)
(Under Grant NSF CMS 94-15726)

DEPARTMENT OF CIVIL ENGINEERING
UNIVERSITY OF ILLINOIS AT
URBANA-CHAMPAIGN
URBANA, ILLINOIS
MAY 1995

50272-101

REPORT DOCUMENTATION PAGE	1. REPORT NO. UILU-ENG-95-2004	2.	3. Recipient's Accession No.

4. Title and Subtitle
Performance Evaluation of a Dual-Level Design Using 1994 Northridge Earthquake Records

5. Report Date
May 1995

6.

7. Author(s)
K. J. Elwood and Y. K. Wen

8. Performing Organization Report No.
SRS 601

9. Performing Organization Name and Address
University of Illinois at Urbana-Champaign
Department of Civil Engineering
205 N. Mathews Avenue
Urbana, Illinois 61801

10. Project/Task/Work Unit No.

11. Contract(C) or Grant(G) No.
NSF CMS94-15726

12. Sponsoring Organization Name and Address
National Science Foundation
1800 "G" Street, NW
Washington, D.C. 20550

13. Type of Report & Period Covered

14.

15. Supplementary Notes

16. Abstract (Limit: 200 words)

A Dual-level seismic design procedure, in which a building structure is designed for both an ultimate and a serviceability level force, is proposed and used to design a seven story RC moment frame. The performance of the structure is monitored by a nonlinear pushover analysis and the design is adjusted accordingly. For comparison, a seven story RC moment frame is also designed according to the 1991 NEHRP provisions. The two designs are modeled using DRAIN-2DX and subjected to 84 strong ground motion records from the 1994 Northridge Earthquake. Response quantities for the two designs, such as damage indices and global and local drifts, are compared. Using this data, the reliabilities of the two designs at different response levels, given an event similar to the Northridge earthquake, are evaluated. It is concluded that the Dual-level design procedure results in better drift and damage control for severe ground motions that force the building into the inelastic range. Thus, excessive structural and non-structural damage may be avoided with little or no interruption to the building occupation after the earthquake.

17. Document Analysis a. Descriptors

Dual-level Design, Seismic Design, Nonlinear Dynamic Analysis, 1994 Northridge Earthquake, PRESSS Guidelines, Reliability, Reinforced Concrete Design, Damage Index, Global and Local Drifts, DRAIN-2DX

b. Identifiers/Open-Ended Terms

c. COSATI Field/Group

18. Availability Statement	19. Security Class (This Report)	21. No. of Pages
Release Unlimited	UNCLASSIFIED	117
	20. Security Class (This Page) UNCLASSIFIED	22. Price

(See ANSI-Z39.18)

OPTIONAL FORM 272 (4-77)
Department of Commerce

Acknowledgements

This report summarizes the research conducted as part of the National Earthquake Hazards Reduction Program (NEHRP) supplemental funding to study the causes and effects of the Northridge Earthquake of January 17, 1994. The strong ground motion records from the Northridge earthquake were processed and distributed by the California Strong Motion Instrumentation Program. The support of the National Science Foundation under grant CMS 94–15726 is gratefully acknowledged.

The authors would like to thank Prof. S. L. Wood, Dr. K. R. Collins, Dr. T. Saito, and Prof. A. Shibata for their advise and comments during the course of this study.

TABLE OF CONTENTS

LIST OF TABLES

TABLE

LIST OF FIGURES

FIGURE

CHAPTER 1

INTRODUCTION

Although the earthquake resistant design philosophy of most building codes states that buildings should resist small earthquakes with no damage, moderate earthquakes with limited non–structural damage, and large earthquakes without collapse, the codes only require buildings to be designed for one ultimate force level. Thus, in effect, the buildings are only designed for the third criteria of the design philosophy. The extensive damage caused by the 1994 Northridge earthquake, and the unprecedented economic losses, have caused designers and owners alike to consider how the above design philosophy can be more fully realized in order to protect economic investments.

This research proposes that a Dual–level design procedure may result in buildings that come closer to attaining the original design philosophy. Such a Dual–level design would require the building to remain elastic under a serviceability level force (corresponding to a design earthquake with a return period of, say, 10 years) and allow limited inelastic deformations under an ultimate level force (corresponding to the accepted 475 year return period). It has been shown (Goel and Chopra, 1994) that a serviceability limit state governs for long period structures (period > 0.3 seconds), while an ultimate limit state governs for short period structures (period < 0.2 seconds). Thus, simply designing for the higher force level, as the codes today require, may produce an unconservative design.

The first stage of this study involves the design of two seven–story reinforced concrete special moment resisting frames (SMRF) located in Los Angeles, California. One is designed according to the proposed Dual–level design procedure, while the other is designed by the 1991 National Earthquake Hazards Reduction Program Recommended Provisions for New Buildings (BSSC, 1991). The Dual–level design procedure requires that the building satisfy certain performance objectives for forces at both the serviceability and ultimate levels. For example, no flexural hinges should form under the serviceability level force, while the formation of flexural hinges should be limited to the beams and column bases to ensure a strong–column–weak–beam collapse mechanism under the ultimate level force. This design procedure generally follows the design philosophy in

the "Ultimate Strength Design Guidelines for Reinforced Concrete Buildings" (PRESSS Guidelines, 1992) (under review for adoption in Japan). Details of these guidelines and the two designs are presented in chapter 2.

Only the perimeter frames of the NEHRP design are used to resist the seismic loads. While many may argue with the effectiveness of perimeter frames for resisting seismic loads, this form of design remains common practice in California. The dual–level design, however, employs all frames to resist the seismic loading. The redundancy of the multiple frames should result in a more reliable structural system.

The nonlinear dynamic analysis program DRAIN–2DX (Prakash, Powell, and Campbell, 1993; Powell, 1993) is used to model the two designs. Chapter 3 describes the methods used to develop the moment–curvature and axial force–moment relationships needed for each member, and the assumptions and shortcomings of DRAIN–2DX models.

Response quantities from the two designs, such as, global roof drift, local interstory drift, plastic hinge locations, and damage indices, are compared for three acceleration time histories chosen to represent severe, moderate, and small ground motions. Damage indices are calculated according to a linear combination of damage due to excessive deformation and damage from repeated cyclic loading (Park, Ang and Wen, 1984). Details of the damage index calculations and the comparison of response quantities are presented in chapter 4.

Finally, the two designs are subjected to 84 strong ground motion records from the January 17, 1994 Northridge earthquake. The reliabilities, or probabilities of exceeding given thresholds for each response quantity, are evaluated for each frame. A method is developed to consider the distribution of epicentral distances in the reliability calculations. Important aspects of the Northridge records and conclusions from the reliability calculations are presented in chapter 5.

Although both methodologies are referred to as "Dual–level" designs, there are significant differences between the procedure recently proposed by Collins, Wen, and Foutch (1995) and the procedure proposed in this study. Collins et al's methodology quantifies the uncertainties at each

stage of the design processes in order to ensure that the structure meets specified probabilistic performance goals at both serviceability and ultimate limit states. Furthermore, the procedure proposed by Collins et al represents a significant departure from current design procedures by using an "equivalent" single–degree–of–freedom model and uniform hazard response spectra. In contrast, the procedure proposed herein simply requires the designer to check the design for two force levels and perform a nonlinear pushover analysis to confirm that the design meets specified performance objectives. This method does not make any attempt to account for the uncertainties in the design process or ensure a target reliability of the final design. The reliability of the design, given the occurrence of an earthquake event similar to the 1994 Northridge earthquake (i.e. $M \approx 6.7$ on a blind thrust fault), is evaluated. The probability of occurrence of $M \approx 6.7$ blind thrust events and the possibility of other magnitudes or source mechanisms, however, have not been considered.

CHAPTER 2

DESIGN OF NEHRP AND DUAL–LEVEL FRAMES

Two seven–story reinforced concrete moment–resisting frames were designed for this study. Each frame was presumed to belong to a building located in Los Angeles, with plan and elevation views as shown in figures 2.1 and 2.2. One frame was designed according to the 1991 National Earthquake Hazards Reduction Program (NEHRP) Recommended Provisions (BSSC, 1991), while the other was designed according to the proposed Dual–level design procedure. This procedure generally follows the design philosophy of the "Ultimate Strength Design Guidelines for Reinforced Concrete Buildings", prepared by the Japan PRESSS (PREcast Seismic Structural System) Guideline Drafting Working Group, hereafter referred to as the PRESSS guidelines (PRESSS Guidelines, 1992; Saito and Wen, 1994). Since both frames were hypothetically located in the United States, the ACI 318–89 Building Code (ACI, 1992) was used in both cases. The following sections will describe in detail the design procedures and the final design configurations for both the NEHRP and Dual–level frames.

2.1 Design of NEHRP Frame

As is common in U.S. design practice, only the perimeter frames (i.e. frames A, H, 1, and 4 in figure 2.1) were designed to resist lateral loads. The rest of the frames were designed to resist only gravity loads and the floor slab should distribute the seismic loads to the perimeter frames. While many may rightly argue with the validity of these assumptions, and the effectiveness of perimeter frames, this form of design remains common–place in California. Thus, in order to compare common U.S. design procedures with the proposed Dual–level procedure, it is necessary to design the NEHRP building considering only the perimeter frame. A transverse frame (i.e. frame A or H) will be considered in this study.

2.1.1 Loads

Dead and live loads were chosen to represent a common seven–story office building. The dead loads are listed in Table 2.1. The floor live load was presumed to be 50 psf, while the roof live load was taken as 20 psf.

The minimum level of analysis for seismic design recommended by the NEHRP provisions is determined by the structure's Seismic Performance Category, which is dependent upon the importance of the structure and the site's anticipated future seismicity. The future seismicity is represented by an effective peak velocity–related acceleration (A_v) for an earthquake with a 10% probability of exceedance in 50 years. For an office building in Los Angeles ($A_v = 0.4$) the associated Seismic Performance Category is D, thus only requiring an equivalent lateral force analysis for buildings under 240 feet.

As with most building codes worldwide, the equivalent lateral force procedure involves determining a base shear and then distributing the base shear over the building's height. In the NEHRP provisions the design base shear, V, is given by:

$$V = C_s W \tag{2.1a}$$

$$\text{where, } C_s = \frac{1.2\ A_v\ S}{R\ T^{2/3}} < \frac{2.5\ A_a}{R} \tag{2.1b}$$

The above coefficients are defined as follows:

C_s is the seismic design coefficient.

W is the seismic weight, including only the dead and partition loads.

A_v is the effective peak velocity–related acceleration.

A_a is the effective peak ground acceleration.

S is the soil profile coefficient.

R is the response modification factor.

T is the period of the building.

Complete definitions for these coefficients are given in the NEHRP provisions and commentary.

For the building under consideration the seismic weight was determined to be 15274 kips. The soil profile coefficient was taken as 1.0, representing shallow firm soils or rock. This coefficient was used to avoid the uncertainty associated with scaling the base shear to account for soft soil effects. The frames were designed as reinforced concrete special moment resisting frames (RC SMRF), which are given a response modification factor of 8 in the NEHRP provisions. The period

of the building is estimated by:

$$T \simeq T_a = C_T \, h_n^{3/4} \tag{2.2}$$

where C_T is 0.03 for RC moment frames that resist 100% of the lateral force, and h_n is the height of the building in feet (i.e. $h_n = 94$ ft.). This approximate equation and the coefficient C_T were determined based on the response of instrumented buildings during the 1971 San Fernando earthquake. Thus, T_a estimates the true period of the building, not just the period of the bare frame. For the building under consideration, the period was estimated as $T_a = 0.906$ seconds. The resulting design base shear is V = 978 kips.

The base shear was distributed over the height of the building according to the following formula:

$$F_x = \frac{w_x \, h_x^k}{\sum_{i=1}^{n} w_i \, h_i^k} V \tag{2.3}$$

where, w_x and w_i are the portion of W assigned to level x or i, h_x and h_i are the height in feet from the base to level x or i, and k is a coefficient related to the period of the structure to account for higher mode effects. Table 2.2 gives the vertical distribution of forces for the NEHRP frame. Note that the sum of the distributed forces is V/2 since two identical moment frames are used to resist the seismic forces.

The load combinations given in the NEHRP provisions were used to determine the factored loads due to earthquake loading. The load combinations are as follows:

$$1.3Q_D + 1.0Q_E + 1.0Q_L \tag{2.4a}$$
$$1.3Q_D - 1.0Q_E + 1.0Q_L \tag{2.4b}$$
$$0.7Q_D + 1.0Q_E \tag{2.4c}$$
$$0.7Q_D - 1.0Q_E \tag{2.4d}$$
$$1.4Q_D + 1.7Q_L \tag{2.4e}$$

The load factor of 1.0 for earthquake induced forces is used, since the loads determined by the NEHRP provisions are already at a design level (BSSC, 1991). The live load factor is reduced to

1.0 from 1.7 when combined with earthquake loading to account for the lower values of instantaneous live load versus maximum lifetime live load (BSSC, 1991).

2.1.2 Deflection Check

The members were sized to ensure the interstory drifts (i.e. the displacement of one level relative to the level below) remained below the required limit of $0.015h_{sx}$, where h_{sx} is the height of the story below level x. For the first story this meant a maximum drift of 2.88 inches, while the rest of the stories were limited to 2.34 inches. The NEHRP provisions provide a deflection amplification factor, C_d, to convert deflections obtained from a static elastic analysis under design load to approximate true deflections accounting for nonlinear behavior (for RC SMRF C_d=5.5). Thus:

$$\Delta = \Delta_e C_d \tag{2.5a}$$

$$\text{or } \Delta_e = \frac{\Delta}{C_d} \tag{2.5b}$$

where, Δ and Δ_e are the true interstory drift and elastic interstory drift respectively. Thus, interstory drifts from an elastic analysis must be limited to 0.524 inches for the first story and 0.425 inches for all other stories. Note that the NEHRP Provisions allow higher fundamental periods calculated by an eigenvalue solution (or other such accepted techniques) to be used in the calculation of the base shear for the purpose of determining interstory drifts. Since a calculated fundamental period will only account for the bare frame, the period will be longer than the approximate period discussed above. Thus, the base shear used in the deflection calculations is less than that used for the strength design. The calculated period for the structure in question was determined using IGRESS–2 (1989) to be 1.75 seconds. This results in a base shear of 630.5 kips, approximately 1/3 less than the base shear required for the strength design.

The deflection check was performed on a standard elastic plane frame analysis program. Due to the inherent nonlinearity of reinforced concrete, it is very difficult to determine accurate beam and column stiffnesses to be used in an elastic analysis. However, it is the relative stiffnesses of beams and columns that is most important to determine accurate deflections and member forces (Pillai and Kirk, 1988). The ACI Building Code Commentary (318R–89) recommends that the member stiffnesses be estimated as one half of the full gross EI for the beams and the gross EI for

the columns. This will account for the greater concentration of cracking expected in the beams compared to the columns. Thirty inches of the 5 inch thick slab was also included in the calculation of the moment of inertia for the beams as required by ACI 318–89. The beam and column dimensions shown in figure 2.3 ensured the frame met the drift requirements.

2.1.3 Steps for Flexural Design of Members in NEHRP Frame

Once the section dimensions were chosen to comply with the deflection requirements, a plane frame analysis program was used to compute the member forces. Given the design forces for the beams, FORTRAN programs were developed to determine the required steel areas and moment capacities according to ACI 318–89 and basic reinforced concrete design principles (see Appendix B). The effect of the slab was included in the calculation of the flexural capacity since a stronger beam will require stronger columns in order to satisfy the strong–column–weak–beam (SCWB) requirement (discussed below). For special moment resisting frames in seismic regions the longitudinal reinforcement should be continuous through the joints. Therefore, the required reinforcement for the interior joints was chosen based on the maximum of the positive and the maximum of the negative moments for the two beams framing into the joint.

The columns were designed for the maximum of the forces from the elastic analysis or the moments from the SCWB requirement of ACI 318–89. This requirement states that,

$$\sum M_c = 6/5 \sum M_g \tag{2.6}$$

where M_c and M_g are the design moments of the columns and girders respectively. Such a restriction is intended to avoid a soft story collapse, and allow for more energy dissipation by providing more plastic hinges prior to the formation of a collapse mechanism (see figure 2.4). In general, the SCWB requirement governed the design of the columns. The design software STAAD–III (1993) was used to choose the required reinforcing steel for the columns.

For the bottom corner columns, the load cases given by equations 2.4c and 2.4d resulted in tensile axial loads. This was the governing load case since the column needed to carry a high moment

in addition to the tensile axial load. However, STAAD–III (1993) ignored any load case where the columns were in tension. This difficulty was overcome by the method described in Appendix A.

The columns were designed with reinforcement on all four sides since the required reinforcement ratio was not found to drop significantly when the requirement was considered on only two sides. Furthermore, providing reinforcement on all four sides will increase the confinement and provide better support in the case of bi–axial bending.

Finally, after all the members had been designed, the number of bars and bar sizes were adapted to improve the constructability of the overall design. For example, the number of different bar sized was reduced to avoid confusion on the job site. The reinforcement required for the final design of the NEHRP frame is shown in figure 2.5. Note that reinforcement in the columns changes at the floor levels. This was done to simplify the model discussed in section 3 (i.e. each column element has the same properties top and bottom). In reality, the reinforcement splices would occur at the column mid–height to avoid the region of highest moment.

2.2 Overview of the PRESSS Guidelines

Before the Dual–level design procedure is discussed, it is necessary to discuss some details of the PRESSS guidelines. Two limit states are considered in these guidelines: severability and ultimate. For each limit state an equivalent lateral force is applied and certain performance objectives are satisfied. Regardless of the limit state, the design i^{th} **story shear**, Q_i, is given by:

$$Q_i = C_i W_i \tag{2.7a}$$

$$\text{where,} \quad C_i = Z R_t A_i C_B \tag{2.7b}$$

The above coefficients are defined as follows:

C_i is the story shear coefficient

W_i is the "seismic weight" at and above the i^{th} story

Z is the seismic zone coefficient

R_t is the vibrational characteristic coefficient

A_i is the coefficient for story shear distribution

C_B is the standard base shear coefficient

Alternatively, equation 2.7 may be expressed in terms of the design **base** shear

$$V = C\ W \tag{2.8a}$$
$$C = Z\ R_t\ C_B \tag{2.8b}$$

The coefficient A_i is used to determine the specific story shears (note: these are shears, not forces as in the NEHRP provisions). Only the standard base shear coefficient, C_B, changes depending on the limit state under consideration. Each term will be discussed in more detail below.

Unlike U.S. guidelines, the seismic weight, W, includes both dead load and live load. However, since the design earthquake is a rare event, only a fraction of the live load used in gravity load design is included in the seismic weight (e.g. 16 psf for office buildings) (ATC , 1986). Strictly speaking, the fraction of the live load included in the seismic weight should be lower for the ultimate limit state since this event has a lower probability of occurrence than the serviceability limit state. However, the PRESSS guidelines do not consider this and use the same value of live load regardless of the limit state. Since the majority of "continuous" live load, such as office equipment, will add to the inertia weight of the building, the inclusion of the live load in the seismic weight seems reasonable, and therefore, was used in this study.

The seismic zone coefficient, Z, indicates the relative seismicity of the chosen site. Z varies from 1.0 to 0.7 as indicated in figure 2.6. Since the design procedure used in the study is currently site specific (see discussion of C_B), there is no need to scale the force for different zones, and thus, $Z = 1.0$ was used.

The vibration characteristic coefficient, R_t, approximately accounts for the soil–structure interaction, and the variation of the base shear with period (i.e. the shape of the design response spectrum). R_t is given by:

$$R_t = 1.0 \qquad \text{for } T < T_c$$
$$R_t = 1.0 - 0.2\ (T/T_c - 1.0)^2 \qquad \text{for } T_c < T < 2T_c \tag{2.9}$$

$$R_t = 1.6\ (T_c/T) \qquad \text{for } 2T_c < T$$

where T_c is the critical period of the subsoil and T is the fundamental period of the building. T_c is defined as:

T_c = 0.4 seconds for Type 1 (i.e. rock, stiff sand, or gravel)

T_c = 0.6 seconds for Type 2 (i.e. anything other than Type 1 or 3)

T_c = 0.8 seconds for Type 3 (i.e. alluvium consisting of soft soils)

In order to account for the effects of non–structural components, T is often approximated as:

$$T = 0.02h \tag{2.10}$$

where h is the building height in meters. This approximation results in a slightly smaller fundamental period than the estimated period using equation 2.2. For example, for the building considered in this study, equation 2.2 estimated the period as 0.906 seconds, while equation 2.10 estimated the period as 0.573 seconds. This difference results in a higher base shear when equation 2.10 is used. The proposed Dual–level design procedure used equation 2.10 and T_c = 0.4 seconds for stiff soil sites.

The coefficient for story shear distribution, A_i, is given by:

$$A_i = 1.0 + (\frac{1}{\sqrt{\alpha_i}} - \alpha_i)\frac{2\ T}{1 + 3\ T} \tag{2.11}$$

$$\text{where, } \alpha_i = W_i\ /\ W_1$$

The effects of higher modes are approximately accounted for by making A_i period dependent. This distribution was also adopted for the current study.

The standard base shear coefficient, C_B, is dependent on the limit state considered. For serviceability, C_B = 0.2 regardless of the structural type. For the ultimate limit state, C_B is a function of the percentage of base overturning moment resisted by structural walls (see table 2.3). Since the building considered in this study consists of only moment frames, C_B was taken as 0.3.

The physical meaning of C_B, for both limit states, is unclear. Although it is not explicitly stated in the PRESSS guidelines, the serviceability level (i.e. C_B = 0.2) seems to represent the elastic short period ($T \simeq 0.3$ seconds) base shear coefficient (i.e. V/W) (Shibata – personal correspondence,

1994). In other words, the serviceability design earthquake should result in an elastic base shear of $0.2W$ for buildings with a fundamental period of approximately 0.3 seconds. It is important to remember that this is an elastic force, and therefore, no reduction is included to account for inelastic behavior.

For the ultimate limit state nonlinear inelastic behavior is allowed, and thus, the design base shear should include some reduction from the elastic base shear value. Unlike U.S. codes, however, this reduction is only implicitly included in the base shear coefficient, C_B. In previous Japanese codes, C_B for the ultimate limit state was taken as 1.0 (Bertero, Anderson, Krawinkler and Miranda, 1991). A factor of 0.3 was then applied to account for nonlinear inelastic behavior (this factor may be compared to $1/R$ from the NEHRP provisions). For the PRESSS guidelines considered in this study, it appears that these coefficients have been combined to arrive at $C_B = 0.3$ for the ultimate limit state. In other words, the ultimate design earthquake should result in an elastic base shear of $1.0W$ for a building with a fundamental period of approximately 0.3 seconds. However, the ultimate design base shear is reduced to $0.3W$ to account for expected nonlinear inelastic behavior. Figure 2.7 shows a comparison of the serviceability and ultimate design spectra with the design spectra from the NEHRP provisions.

The question remains: What are the return periods associated with the serviceability and ultimate design earthquakes discussed above? According to the PRESSS guidelines, the serviceability limit state shall be satisfied for "small to medium intensity earthquake motions", and the ultimate limit state shall be satisfied for "intense earthquake motions" (PRESSS Guidelines, 1992). Japanese codes do not attach a return period to the standard base shear coefficients. Thus, the implicit return periods can only be estimated by considering the seismicity of Japan. It has been estimated by some Japanese researchers that the return period of the serviceability earthquake is approximately 100 years, while the return period for the ultimate earthquake is approximately 400 years (Saito – personal correspondence, 1994). Other U.S. researchers have used a serviceability return period of 10 years and an ultimate return period of 450 years, when applying a dual–level type design (Bertero and Bertero, 1992). There is no consensus on what return periods the different limit states represent.

Thus, the return periods of the limit states considered in this study were determined by experience and a trial and error procedure discussed in section 2.3.

Besides designing the members for the force levels described above, the PRESSS guidelines require that different performance criteria be satisfied for each limit state. The performance is determined by a static nonlinear pushover analysis, including both geometric (P–Δ effects) and material nonlinearities. Although the nonlinear analysis is only strictly required for buildings over 31 meters in height, it will be employed in this study to investigate the effect of including a more realistic and complex analysis in the design process.

Under the design equivalent lateral force corresponding to the serviceability limit state, the following criteria shall be satisfied:

1) No flexural hinging shall occur in the structural members.

2) The interstory drift of the i^{th} story shall not exceed 1/200 h_i, where h_i is the height of the i^{th} story.

The first criteria ensures that the building remains elastic at the serviceability limit state, and validates the use of an elastic base shear (i.e. no reduction factor).

The performance criteria for the ultimate limit state requires that at an interstory drift of 1/100 h_i, the story shear at any story must be greater than 0.9 times the ultimate design story shear. Furthermore, at an interstory drift of 1/50 h_i, the story shear at any story must be greater than the ultimate design story shear. In other words, as the equivalent lateral force is increased monotonically, the interstory drifts are monitored until one reachers the first limit of 1/100 h_i. At this limit, the story shears achieved in the structure from the pushover analysis (i.e. the actual resistances) must exceed 0.9 times the ultimate design story shears (i.e. the resistance goal). Similarly, as the maximum interstory drift reaches 1/50 h_i during the pushover analysis, the story shears achieved in the structure (i.e. the actual resistances) must exceed the ultimate design story shears (i.e. the resistance goal). Furthermore, the SCWB design is confirmed by checking that all the yielding during the pushover analysis occurred in the beams and column bases. These performance checks avoid the

use of general deflection amplification factors (C_d) as in the NEHRP provisions, and thus, allows the designer to satisfy the performance criteria by providing specialized detailing. However, the lack of precision in modelling nonlinear behavior must always be considered when interpreting the results of a pushover analysis.

2.3 Design of Dual–Level Frame

In contrast to the NEHRP design, each frame within the building was designed to resist the seismic forces. This was done for two reasons: (1) due to the larger design base shear, a perimeter frame system would require abnormally large sections; (2) the redundancy of multiple frames should result in a more reliable structural system (Wang – research in progress, 1995). The frame designed for this study was a typical interior frame (i.e. frames B through G of figure 2.1). The dead loads are listed in table 2.4. Although reduced live loads were included in the "seismic weight" (see section 2.2), the same live loads used in the NEHRP design were used in any live load analysis of the the Dual–level design.

The Dual–level design procedure proposed in this study generally follows the PRESSS guidelines. The following sections will discuss the primary changes to the PRESSS guidelines and the resulting final design.

2.3.1 Serviceability and Ultimate Force Levels

The proposed Dual–level design procedure uses the same formulation for the design story shear discussed in the previous section (equation 2.7). However, for the ultimate limit state, the standard base shear coefficient from the PRESSS guidelines shall be discussed as the product of an elastic base shear coefficient, $(C_e)_{ult}$, and a base shear reduction factor, K, to explicitly account for the nonlinear response of the structure. Thus,

$$(C_B)_{ult} = K\ (C_e)_{ult} \tag{2.12}$$

Referring to equation 2.8, the **ultimate** design base shear may be expressed as:

$$V_{ult} = C_{ult}\ W \tag{2.13a}$$

$$C_{ult} = Z\ R_t\ K\ (C_e)_{ult} \tag{2.13b}$$

Equation 2.12, with $K = 1$, may be considered for the serviceability limit state since the structure must remain elastic. Thus,

$$(C_B)_{serv} = 1 * (C_e)_{serv} \tag{2.14}$$

Similarly, the **serviceability** design base shear may be expressed as:

$$V_{serv} = C_{serv}\, W \tag{2.15a}$$

$$C_{serv} = Z\, R_t\, (C_e)_{serv} \tag{2.15b}$$

Tables 2.5 and 2.6 summarize the coefficients and loads used for the design of the seven story office building in Los Angeles (see figures 2.1 and 2.2). All of the coefficients, except the standard base shear coefficients and the base shear reduction factor, were calculated according to the PRESSS guidelines (see section 2.2).

The elastic base shear coefficients, $(C_e)_{ult}$ and $(C_e)_{serv}$, were chosen such that the design spectra from equations 2.13b and 2.15b approximated the uniform hazard elastic response spectra developed for Los Angeles, California, at the desired return periods for the ultimate and serviceability design earthquakes. (The uniform hazard response spectra were developed by K. R. Collins, and are discussed in Collins and Wen, 1995). The best approximations were achieved by setting $(C_e)_{serv}$ and $(C_e)_{ult}$ equal to the base shear coefficient (V/W) of the uniform hazard elastic response spectra at T = 0.3 seconds (see figures 2.8 and 2.9). It should be noted that since the uniform hazard elastic response spectra were developed for approximately stiff soil sites in Los Angeles, the corresponding design spectra (equations 2.13b and 2.15b) are also site specific to both stiff soil conditions and the seismic hazard associated with Los Angeles.

Since the PRESSS guidelines gave no indication regarding the desired return periods for the serviceability and ultimate design earthquakes, the choice of the return periods, and thus $(C_e)_{serv}$ and $(C_e)_{ult}$, was done using a trial and error process. To remain consistent with the ultimate design level in U.S. codes, a return period of 475 years (or 10% probability of exceedance in 50 years) was chosen for the ultimate design earthquake. Using the uniform hazard response spectra developed by Collins, a 475 year return period corresponded to a short period elastic base shear coefficient, $(C_e)_{ult}$,

of 0.92 (see figure 2.9). This result seems reasonable since the PRESSS guidelines implicitly used a short period elastic base shear coefficient of 1.0 for the highest seismic zones of Japan (see section 2.2). The reduction to 0.92 for Los Angeles seems appropriate, since the seismic risk in Los Angeles is generally not as high as in the highest seismic regions of Japan, such as Tokyo (Wen, 1995). The choice of the base shear reduction factor, K, shall be discussed later in this section.

The choice of the serviceability return period was not as simple. Three possibilities were considered: 50, 15, and 10 years. The 50 year return period was ruled out immediately, since to remain elastic at such a high force level, would require abnormally large member cross sections. The frame was initially designed for a 15 year return period (i.e. $(C_e)_{serv} = 0.19$, see figure 2.8) and then adjusted slightly to meet the serviceability and ultimate performance criteria discussed in section 2.2 ($K = 0.3$ was used for this preliminary performance check). The final design was modelled analytically and subjected to the Sylmar record from the 1994 Northridge earthquake. The results indicated that the Dual–level design experienced only 1/3 of the maximum interstory drift experienced by the NEHRP design, and negligible permanent displacement. This response was deemed over–conservative for a ground motion considered to be nearly representative of the ultimate design earthquake (see section 4). Thus, the frame was redesigned for the 10 year return period response spectrum (i.e. $(C_e)_{serv} = 0.1$, see figure 2.8).

As discussed above, the serviceability base shear coefficient, $(C_B)_{serv}$, was reduced from 0.2 in the PRESSS guidelines to 0.1 for the current study. Thus, the ultimate standard base shear coefficient, $(C_B)_{ult}$, should also be reduced from 0.3 used in the PRESSS guidelines. Since the elastic base shear coefficient, $(C_e)_{ult}$, has been chosen as 0.92 to comply with a 475 year return period design earthquake, a base shear reduction factor, K, less than 0.3 must be used to reduce $(C_B)_{ult}$ (see equation 2.12). K was chosen as 0.15 for this study, however, much more research is needed to determine appropriate values of K.

The ultimate and serviceability design base shears for a typical interior frame were finally calculated as 307 kips and 223 kips, respectively.

2.3.2 Flexural Design of Members in Dual–Level Frame

Since the Dual–level design was assumed to be located in Los Angeles, the member design must satisfy the ACI 318–89 Building Code. The procedure followed for the flexural design is discussed in section 2.1.3. The serviceability force level was used for the initial flexural design. Due to overstrength, this design was also sufficient to pass the ultimate limit state performance criteria (see section 2.3.3). The reinforcement and member dimensions for the final design are given in figures 2.10 and 2.11.

2.3.3 Performance Criteria

After the initial elastic design for the serviceability force level was completed (see section 2.3.2), the frame was modelled on DRAIN–2DX (see section 3) and a nonlinear pushover analysis was conducted. The resulting base shear–interstory drift curve for the first story is shown in figure 2.12 (the first story exhibited the highest interstory drifts). Figure 2.12 shows that the design complied with the serviceability limit state performance criteria (i.e. remaining elastic at the serviceability design base shear (223 kips) and limiting the maximum interstory drift to less than 0.5% at the same base shear).

The ultimate limit state performance criteria specified in the PRESSS guidelines, was changed for the proposed Dual–level design procedure. Figure 2.12 demonstrates that, for the assumed model, a nearly elastic–plastic pushover curve will result. Thus, there is no reason to include two force levels at which to check the performance of the structure. For example, if the structure achieved the ultimate design base shear at a maximum interstory drift of 2%, then it would automatically achieve 90% of the ultimate design base shear at a maximum interstory drift of 1%. Therefore, only the first performance criteria specified in the PRESSS guidelines was used for this analysis (i.e. at a maximum interstory drift of 2%, the mobilized base shear must be greater than or equal to the ultimate design base shear). Figure 2.12 demonstrates that the final design of the Dual–level frame complies with the above performance criteria. Furthermore, the pushover analysis also demonstrated that the required SCWB collapse mechanism was achieved.

Roof	Width (in)	Depth (in)	Length (in)	Density (pcf)	Number	Weight (kips)
Slab	1080	5.0	1680	150	1	787.5
Ext. Column	30	30	78	150	20	121.9
Int. Column	20	20	78	150	12	32.6
Beams EW	20	30	1680	150	4	350.7
Beams NS	20	30	1080	150	8	450.9
Ext. Wall	1.2	78	5520	150	1	44.9
					Subtotal =	**1788.5**

3rd – 7th Floors	Width (in)	Depth (in)	Length (in)	Density (pcf)	Number	Weight (kips)
Slab	1080	5.0	1680	150	1	787.5
Ext. Column	30	30	156	150	20	243.8
Int. Column	20	20	156	150	12	65.2
Beams EW	20	30	1680	150	4	350.7
Beams NS	20	30	1080	150	8	450.9
Ext. Wall	1.2	156	5520	150	1	89.8
Partitions	1080	1.6	1680	150	1	252.0
					Subtotal =	**2239.9**

2nd Floor	Width (in)	Depth (in)	Length (in)	Density (pcf)	Number	Weight (kips)
Slab	1080	5.0	1680	150	1	787.5
Ext. Column	30	30	174	150	20	271.9
Int. Column	20	20	174	150	12	72.7
Beams EW	20	30	1680	150	4	350.7
Beams NS	20	30	1080	150	8	450.9
Ext. Wall	1.2	174	5520	150	1	100.2
Partitions	1080	1.6	1680	150	1	252.0
					Subtotal =	**2285.9**

Total Dead Load = 1788.5 + 5 x 2239.9 + 2285.9 = ***15273.9 kips***

Table 2.1: Dead Loads for NEHRP Design

Floor Level	w_x (kips)	h_x (ft)	k (for T=0.9)	F_x (kips)	$F_x/2$ (kips)
roof	1788.5	94	1.2	217.9	108.9
7	2239.9	81	1.2	228.2	114.1
6	2239.9	68	1.2	185.0	92.5
5	2239.9	55	1.2	143.4	71.7
4	2239.9	42	1.2	103.8	51.9
3	2239.9	29	1.2	66.5	33.3
2	2285.9	16	1.2	33.3	16.6

Table 2.2: Vertical Distribution of Earthquake Loads for NEHRP Frame

% of base overturning moment resisted by structural walls	C_B (ultimate limit state)
0.0 – 0.3	0.30
0.3 – 0.7	0.35
0.7 – 1.0	0.40

Table 2.3: Standard Base Shear Coefficient for Ultimate Limit State
(PRESSS Guidelines, 1992)

Roof	Width (in)	Depth (in)	Length (in)	Density (pcf)	Number	Weight (kips)
Slab	1080	5.0	1680	150	1	787.5
Ext. Column	28	28	78	150	20	106.2
Int. Column	28	28	78	150	12	63.7
Beams EW	20	29	1680	150	4	338.3
Beams NS	20	29	1080	150	8	435.0
Ext. Wall	1.2	78	5520	150	1	44.9
					Subtotal =	**1775.6**

3rd – 7th Floors	Width (in)	Depth (in)	Length (in)	Density (pcf)	Number	Weight (kips)
Slab	1080	5.0	1680	150	1	787.5
Ext. Column	28	28	156	150	20	212.3
Int. Column	28	28	156	150	12	127.4
Beams EW	20	29	1680	150	4	338.3
Beams NS	20	29	1080	150	8	435.0
Ext. Wall	1.2	156	5520	150	1	89.8
Partitions	1080	1.6	1680	150	1	252.0
					Subtotal =	**2242.3**

2nd Floor	Width (in)	Depth (in)	Length (in)	Density (pcf)	Number	Weight (kips)
Slab	1080	5.0	1680	150	1	787.5
Ext. Column	28	28	174	150	20	236.8
Int. Column	28	28	174	150	12	142.1
Beams EW	20	29	1680	150	4	338.3
Beams NS	20	29	1080	150	8	435.0
Ext. Wall	1.2	174	5520	150	1	100.2
Partitions	1080	1.6	1680	150	1	252.0
					Subtotal =	**2291.9**

Total Dead Load = 1775.6 + 5 x 2242.3 + 2291.9 = ***15279.0 kips***

Table 2.4: Dead Loads for Dual–Level Design

Dual–Level Design Coefficients	
Z	1.0
T	0.573 seconds
R_t	0.96
$(C_e)_{serv}$	0.1
$(C_e)_{ult}$	0.92
K	0.15

Table 2.5: Summary of Design Coefficients used for Dual–Level Design

Floor Level	W_i[1] (kips)	A_i	$(Q_i)_{serv}$[2] (kips)	$(Q_i)_{ult}$[2] (kips)	$(F_x)_{serv}/7$[3] (kips)	$(F_x)_{ult}/7$[3] (kips)
roof	1813.0	2.21	385.4	531.9	55.1	76.0
7	4210.4	1.72	694.6	958.6	44.2	61.0
6	6607.8	1.49	944.7	1303.7	35.7	49.3
5	9005.2	1.33	1151.8	1589.5	29.6	40.8
4	11402.6	1.21	1321.4	1823.5	24.2	33.4
3	13800.0	1.10	1456.1	2009.4	19.3	26.6
2	16241.6	1.0	1559.2	2151.7	14.7	20.3

[1] Includes portion of live load (16 psf for each floor and 6.4 psf for the roof)
[2] Story shears
[3] Forces applied to each story for one typical interior frame

Table 2.6: Vertical Distribution of Earthquake Loads for Dual–Level Frame

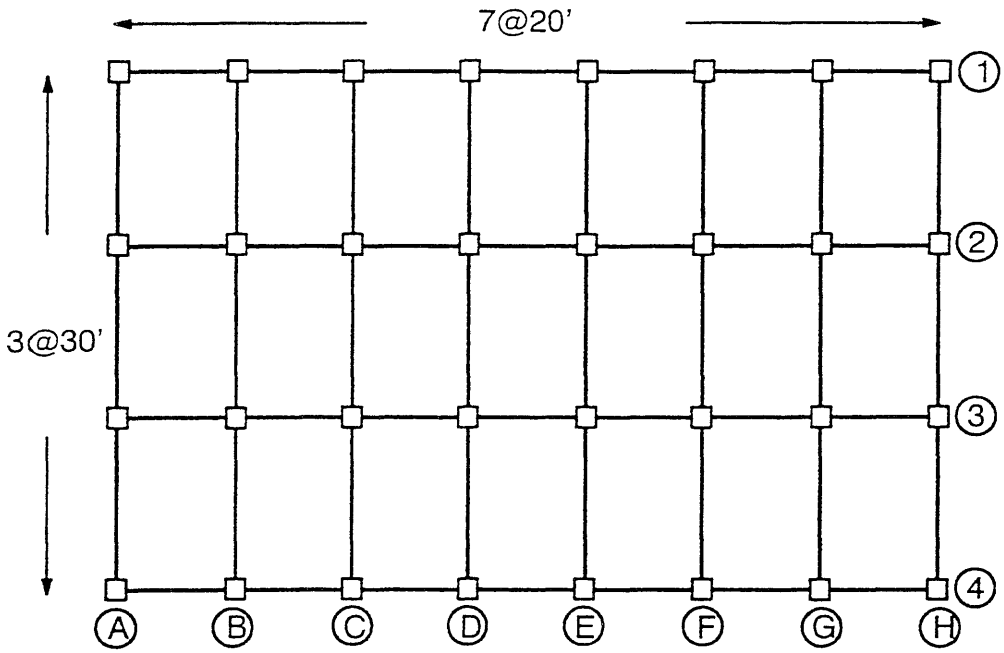

Figure 2.1: Plan view of 7–story building

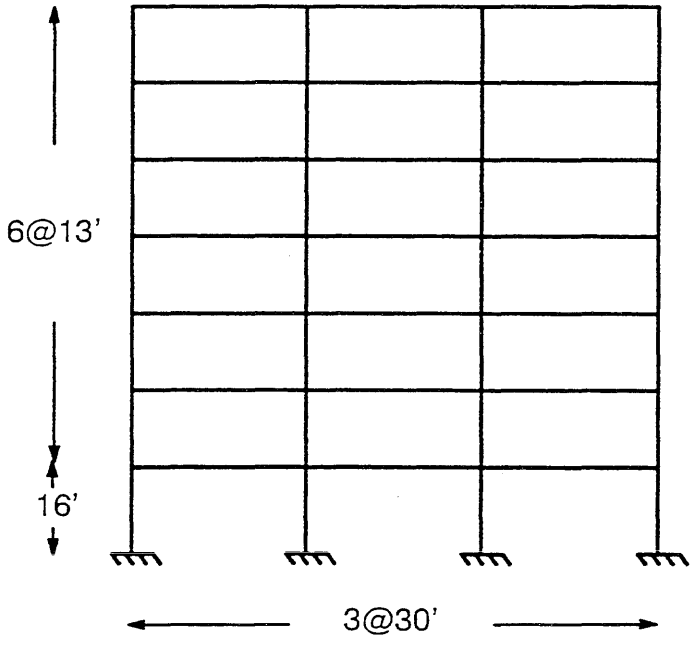

Figure 2.2: Elevation view of transverse frame

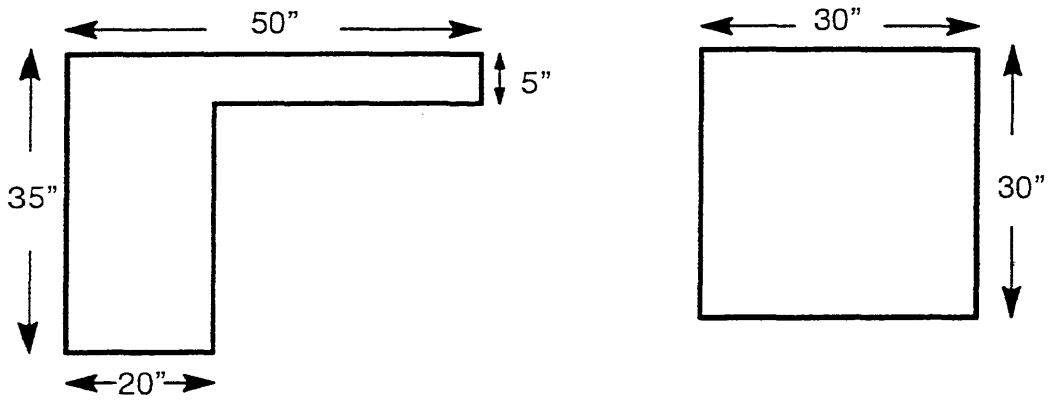

Figure 2.3: Member Sections for NEHRP Frame

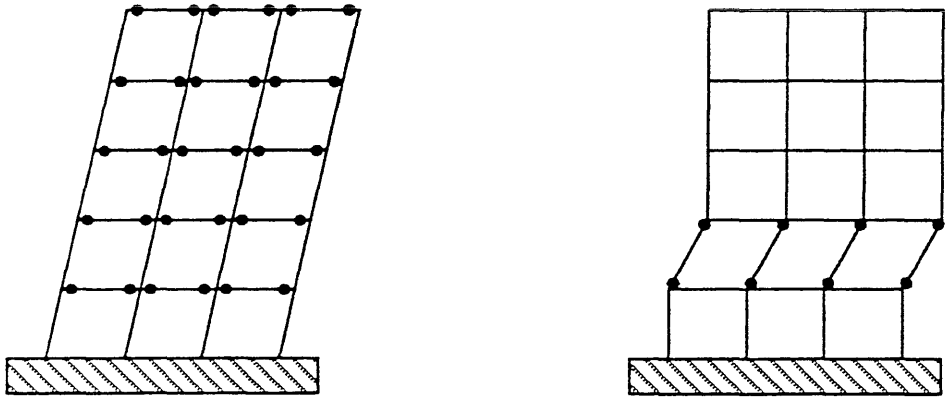

Figure 2.4: Collapse Mechanisms

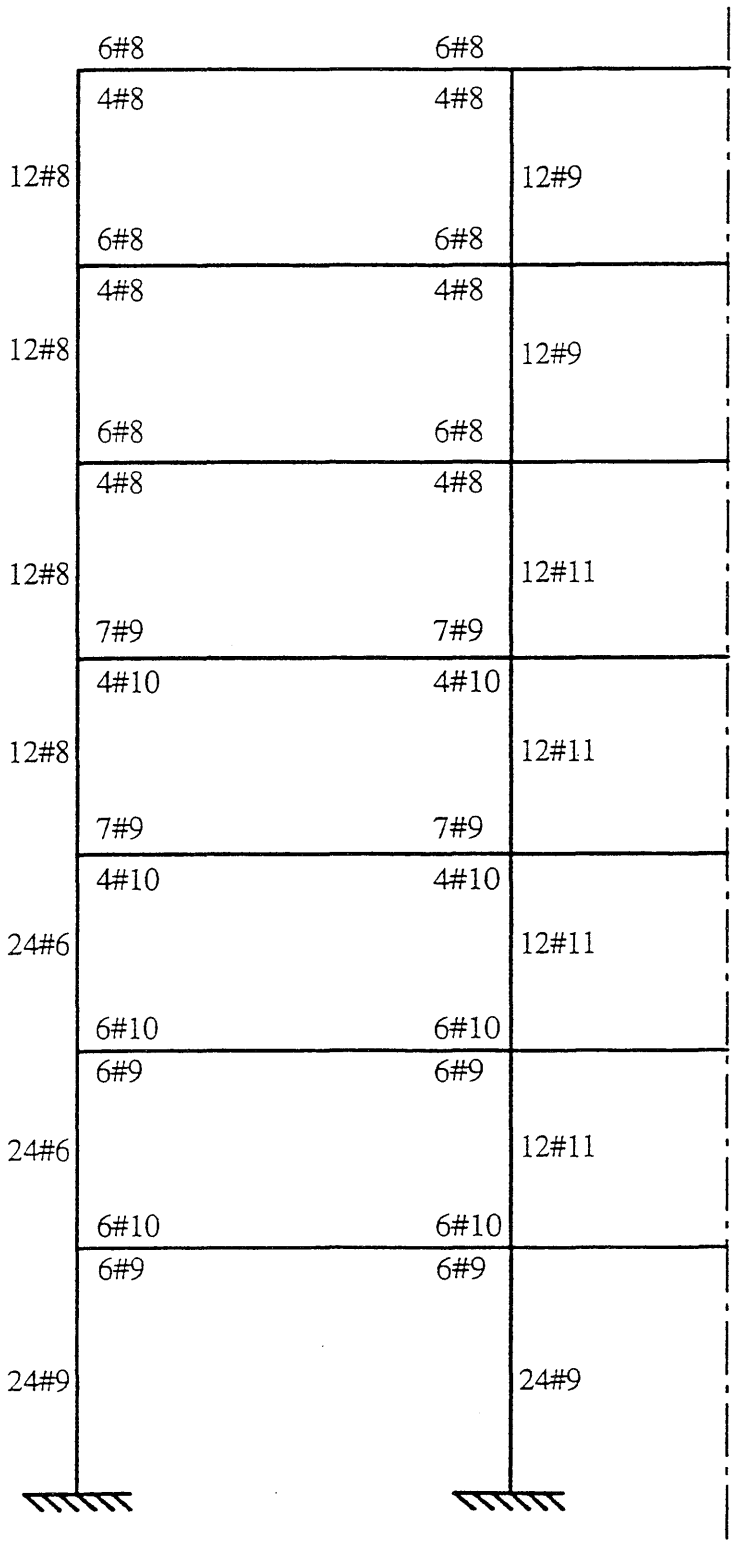

Figure 2.5: Flexural Reinforcement for NEHRP Design

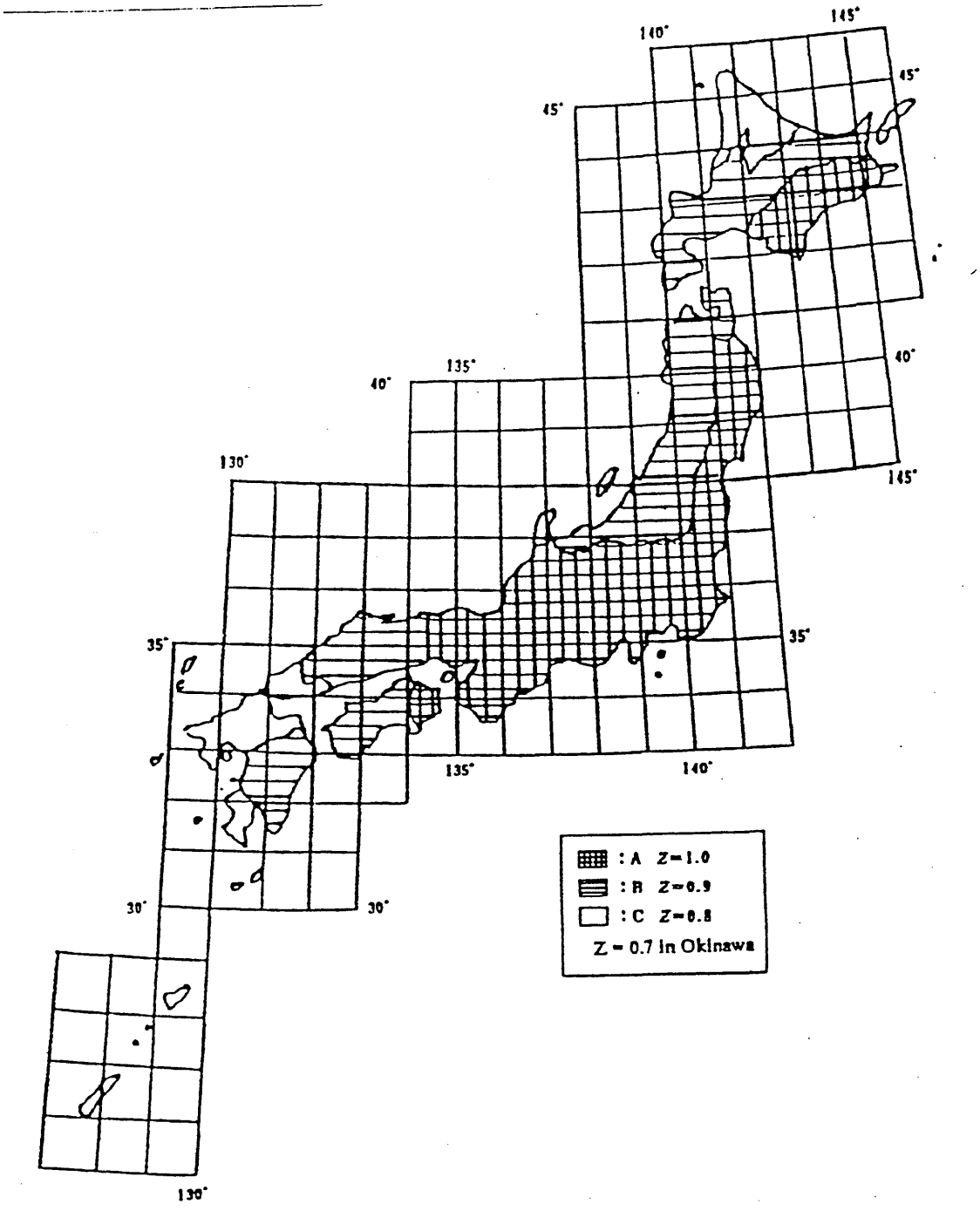

Figure 2.6: Seismic Zones of Japan (Otani, 1992)

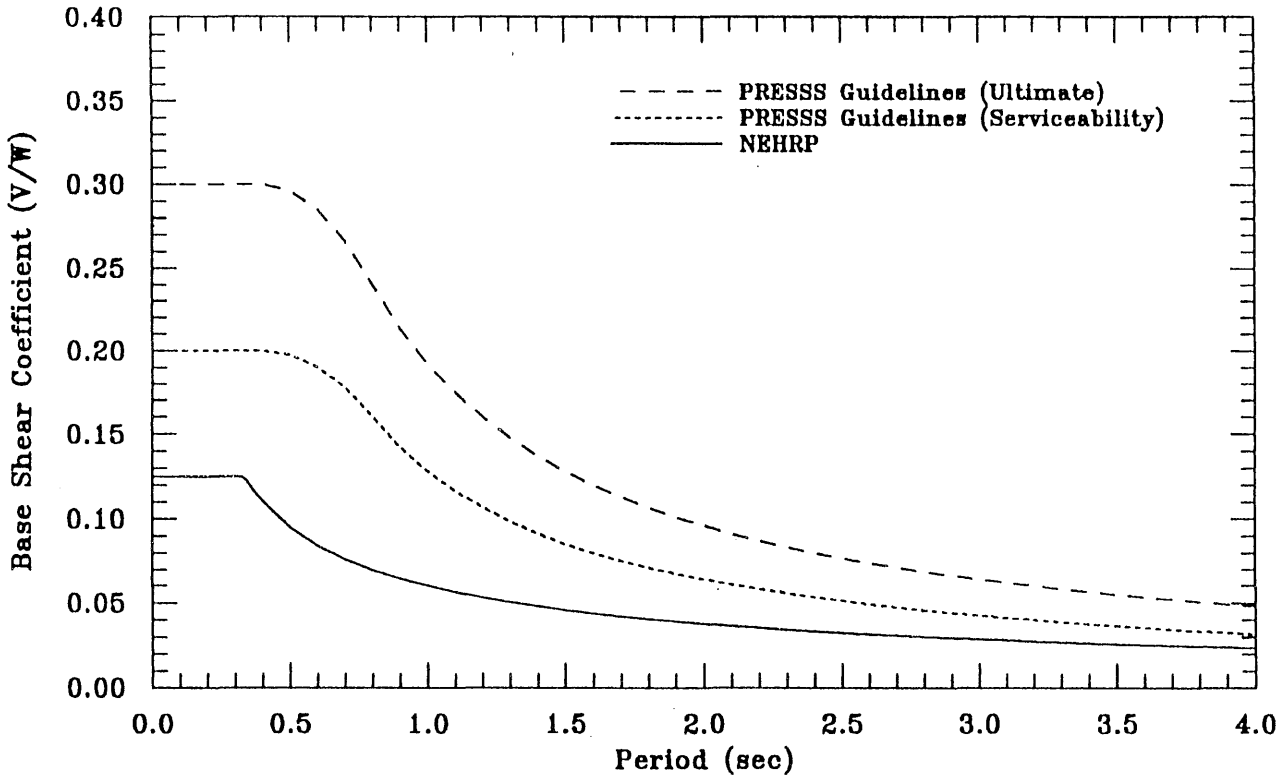

Figure 2.7: Design Responce Spectra for NEHRP Provisions and PRESSS Guidelines
(Shallow stiff soil and highest seismic zone)

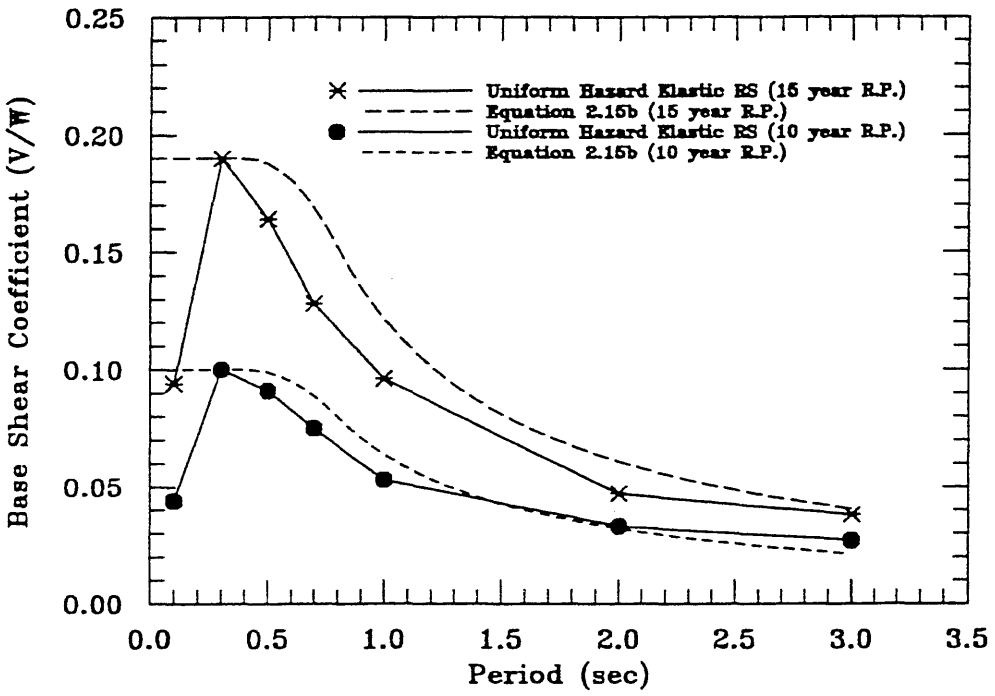

Figure 2.8: Serviceability Limit State Design Spectra for Dual–Level Design

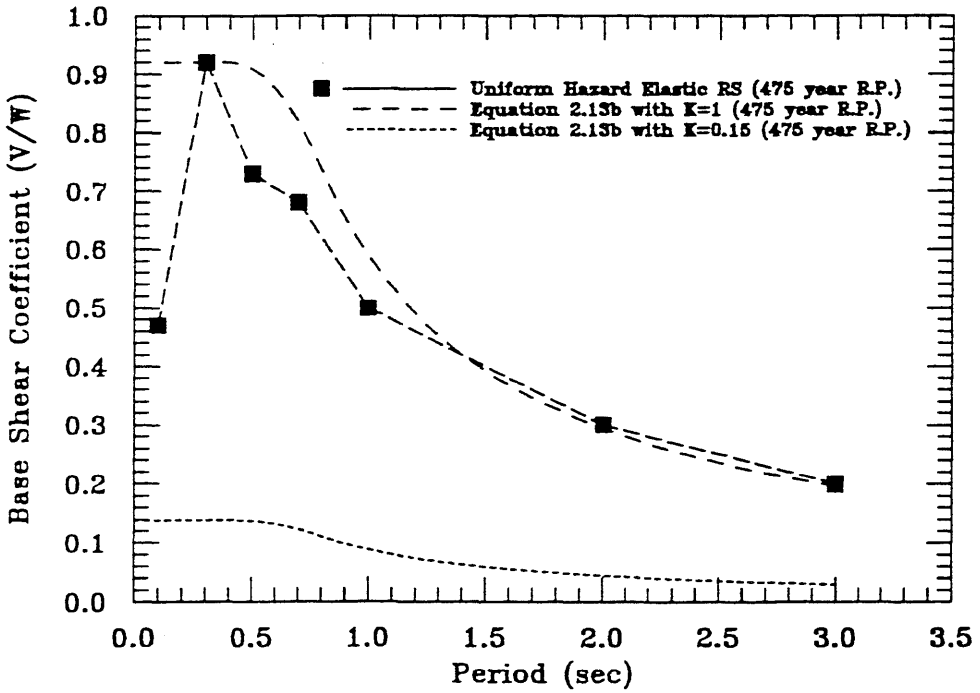

Figure 2.9: Ultimate Limit State Design Spectra for Dual–Level Design

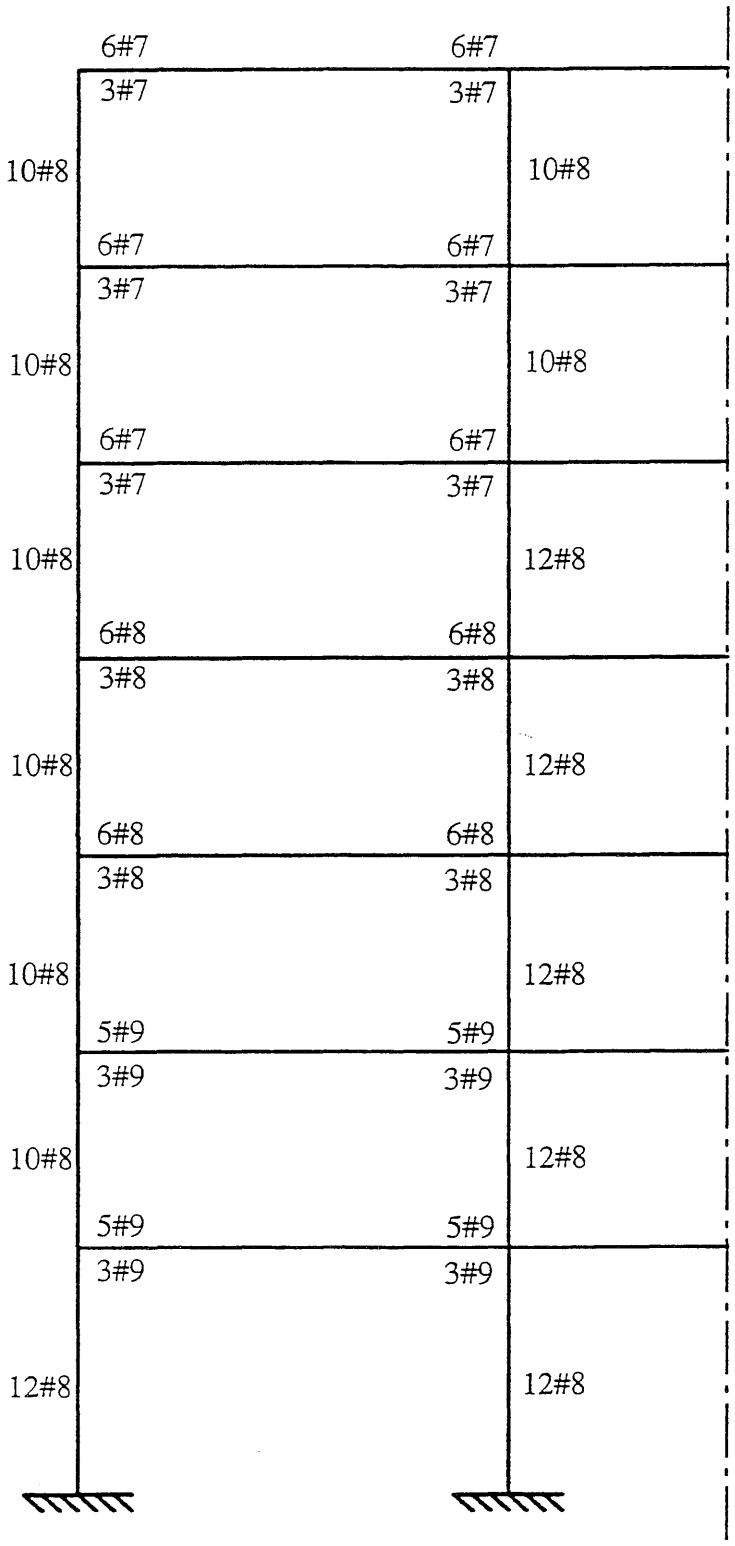

Figure 2.10: Flexural Reinforcement for Dual–Level Design

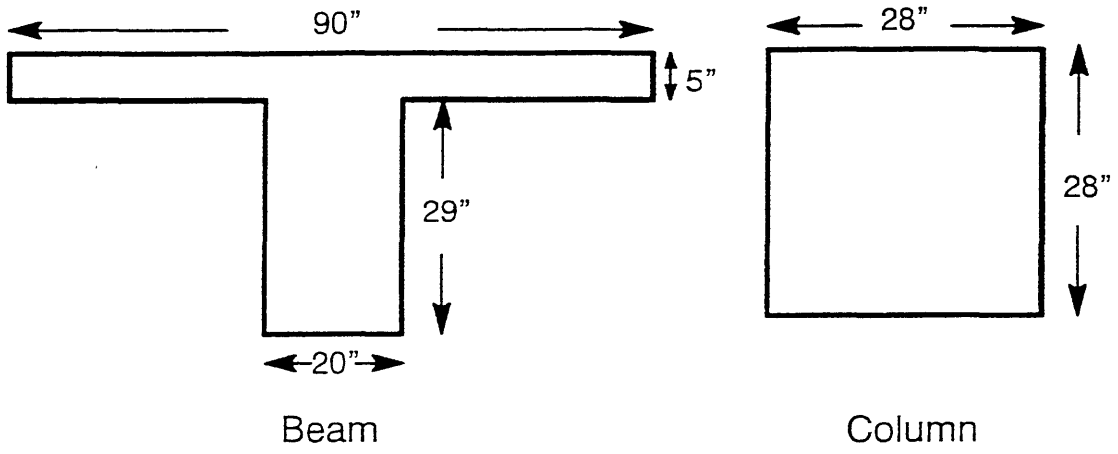

Figure 2.11: Member Sections for Dual–Level Frame

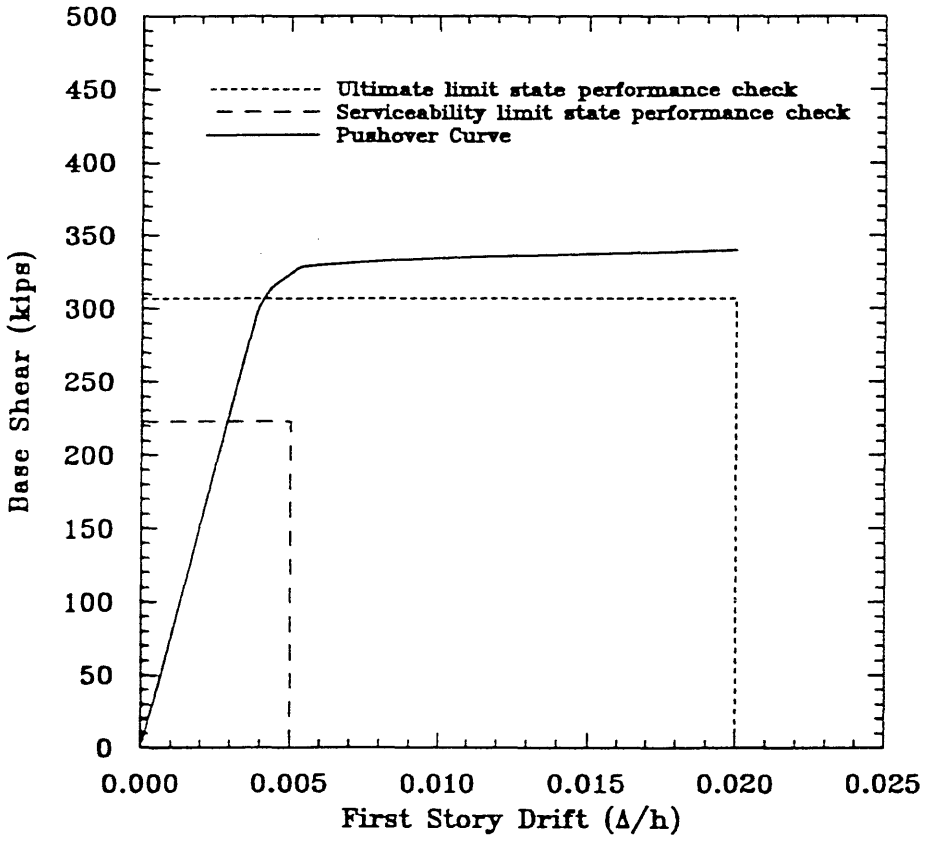

Figure 2.12: Load–Deflection Relationship for Dual–Level Frame and Performance Check for Ultimate and Serviceability Limit States

CHAPTER 3

MODELLING FOR NONLINEAR STATIC AND DYNAMIC ANALYSES

The nonlinear dynamic analysis program DRAIN–2DX (Prakash, Powell, and Campbell, 1993; Powell, 1993) was used to model the two frames discussed in the previous section. Using the beam–column elements, nonlinear behavior is assumed to occur only through flexural yielding at the member ends. Thus, moment–curvature (M–ϕ) relationships and axial force–moment (P–M) interaction diagrams are required to construct the DRAIN–2DX models. The following sections will discuss: (1) the methods used to develop the M–ϕ and P–M relationships, (2) particular details of the DRAIN–2DX models, and (3) the assumptions and shortcomings of DRAIN–2DX models.

3.1 M–ϕ Relationships

The FORTRAN program developed to calculate the M–ϕ relationship for any cross–section employs a standard method discussed in most reinforced concrete behavior textbooks MacGregor (1992) (the program is included in Appendix B). The method may be described by the following steps (refer to figure 3.1 for an explanation of the variables).

1. Divide the cross–section into layers (figure 3.1).
2. Arbitrarily choose the maximum compressive strain in the concrete, ε_c'.
3. Assume a neutral axis depth, c.
4. Calculate the strain at mid–depth of every layer of concrete and steel using similar triangles.

$$\text{i.e.} \quad \frac{\varepsilon'_c}{c} = \frac{\varepsilon_i}{c - d_i} \tag{3.1}$$

5. Calculate the stress in each layer of concrete (f_{c_i}) and steel (f_{s_i}) using the adopted stress–strain relationships (for this study the relationships are shown in figures 3.4a and 3.4b).
6. Calculate the force in each layer:

$$F_{c_i} = f_{c_i} * A_{c_i} \quad , \quad F_{s_i} = f_{s_i} * A_{s_i} \tag{3.2}$$

7. Sum the forces in every concrete and steel layer, ΣF.

- If ΣF = the axial force, P, then continue to step 8
- If $\Sigma F > P$, choose a smaller c and return to step 3
- If $\Sigma F < P$, choose a larger c and return to step 3

8. Calculate the moment and curvature for the chosen ε_c' as follows:

$$M = \sum_{\text{concrete layers}} d_{c_i} F_{c_i} + \sum_{\text{steel layers}} d_{s_i} F_{s_i} + P\frac{h}{2} \qquad (3.3)$$

$$\phi = \frac{\varepsilon_c'}{c}$$

This will give one point on the M–ϕ relationship. Return to step 2 and choose a new ε_c' to get the next point.

Several important comments should be made about the above procedure. First, convergence is most easily attained by initially assuming a very small neutral axis depth, c, (i.e. one half of the layer depth, Δh) and then increasing c until the residual force is approximately equal to the axial force. Secondly, for cross–sections under high axial loads, the smallest ε_c' must be sufficient to at least obtain the axial load in pure compression. Thirdly, accuracy and computation time increase with decreasing Δh. Choosing Δh such that there are approximately 20 layers above the neutral axis at capacity should provide sufficient accuracy. Typical M–ϕ relationships for a beam and column, developed using the above procedure, are shown in figure 3.2.

3.2 P–M Interaction Diagrams

The procedure used to develop the P–M interaction diagrams was very similar to the procedure described above for the M–ϕ relationships. However, in the case of the P–M relationship each point represents the ultimate capacity of the section. Thus, one value of the maximum concrete compressive strain, ε_c', is used for the entire curve, while the axial force, P, is varied from zero (i.e. pure bending) to P_{max} (i.e. pure compression). The interaction diagrams used for this study were developed using $\varepsilon_c' = 0.004$. A typical P–M interaction diagram is shown in figure 3.3. Below the balance point the tension steel yields before the strain in the concrete reaches ε_c' resulting in a ductile failure mode. Above the balance point the strain in the concrete reaches ε_c' before the tension steel yields, resulting in a brittle failure mode. It should be noted that the P–M interaction diagrams would not change significantly if yielding of the tension steel was used as the capacity criterion rather than the concrete compressive strain exceeding ε_c' (Park and Paulay, 1975). A program developed to calculate the P–M interaction diagrams is included in Appendix B.,

3.3 Material Models

The results from the above procedures agree very well with experimental test results if the exact stress–strain relationships for the steel and concrete are used. However, these relationships are not exactly known when modelling a structure prior to construction, and thus, realistic estimates must be used. Only the simplest of relationships has been used in the programs developed for this study.

Figure 3.4a shows the idealized stress–strain relationship used for the steel. A mean yield stress of 71 ksi was used to determine the M–ϕ and P–M relationships (Mirza and MacGregor, 1979). Note that the nominal yield stress of 60 ksi was used in the design procedure, thus introducing significant overstrength.

As shown in figure 3.4a, the steel stress–strain relationship used in this study did not include any strain hardening effects. The accuracy of the M–ϕ and P–M relationships could be improved by including modest strain hardening beyond a strain of 0.03. The effects of strain hardening were approximately accounted for by using a second slope of 0.02 *EI* in the DRAIN–2DX bilinear moment–rotation relationship for the beams (see section 3.4.1).

Hognestad's parabola was used to model the concrete stress–strain relationship (see figure 3.4b). No effects of confined concrete were included in this model, since the increase in the maximum compressive stress, f'_c, was approximated at less than 10% of f'_c using the modified Kent and Park model (Park, Priestley, and Gill, 1982). The accuracy of the M–ϕ and P–M relationships may be improved by including the effects of confined concrete. In particular, two models may be used: one for the unconfined concrete in the cover, and one for the confined concrete in the core. Although less accuracy is attained by ignoring the effect of the confined concrete, the purpose of this study is the comparison of two designs, and thus, as long as the models of the two designs are consistent and **reasonably** accurate, the increased complexity is not necessary to improve the accuracy of the analytical results.

3.4 DRAIN–2DX Model

DRAIN–2DX is a complex nonlinear dynamic analysis program commonly used by researchers to investigate the nonlinear response of structures to earthquake ground motions. As with any such program, DRAIN–2DX requires a thorough understanding of the fundamental theory and the implicit assumptions of nonlinear dynamic analysis. A review of the theory and assumptions is beyond the scope of this report, however, details are presented elsewhere (Prakash et al., 1993; Powell, 1993; Allahabodi and Powell, 1988; Clough and Penzien, 1993).

The DRAIN–2DX analysis was done in three stages: (1) the structure geometry, mass, and member properties were defined; (2) the unfactored gravity loads were applied; and (3) the nonlinear dynamic analysis was performed using a horizontal ground acceleration time history record. The beam–column elements (TYPE02) included in DRAIN–2DX were used to model the beams and columns of both frames. The following sections shall discuss the approximations and assumptions required for both beams and columns, and other details of the dynamic model necessary to properly interpret the results presented in sections 4 and 5.

3.4.1 Beams

The flexural stiffnesses of the beams were determined using the M–ϕ relationships discussed previously. The effective width of the slab (according to ACI 318–89) and the slab reinforcement within the effective width were included in the calculation of the beam flexural stiffness and capacity. Due to the use of a perimeter frame for the NEHRP design, the slab extended only to one side of the beam (see figure 2.3). Although this unsymetric shape would produce torsional forces in the beam, this cannot be considered in the two dimensional DRAIN–2DX model.

The use of the effective width of the slab and slab reinforcement (recommended by French and Moehle, 1991) is only an approximation since as beams go further into the inelastic range more slab reinforcement begins to contribute (Miranda and Bertero, 1989). At the modelling stage, however, the amount of inelastic action is unknown, and thus, the amount of contributing slab reinforcement must be estimated.

The model of the beams is further approximated since DRAIN–2DX only allows one stiffness for each beam. Since in most beams the positive and negative steel areas are not equal, the positive and negative stiffnesses are also unequal. Furthermore, in positive bending the beams act as T–beams, while in negative bending they act as rectangular sections. For this study an average of the positive and negative stiffnesses was used for the DRAIN–2DX model.

The beam–column element in DRAIN–2DX only allows the use of a bilinear non–degrading hysteretic model. Although a stiffness–degrading model (such as the Tekeda model) more accurately represents the true behavior of RC members, the bilinear model usually produces the same maximum response (Teran–Gilmore and Bertero, 1993). It also may be argued that given our lack of understanding of the true behavior of RC members, the bilinear model may serve as a good simple approximation. The bilinear model also allows for easy calculation of the total hysteretic energy (see section 4.1). Once again, it should be remembered that the purpose of this study is the comparison of responses, and therefore, the inaccuracy of the absolute response of one frame due to the use of the bilinear model is not important as long as the relative response of the two frames is accurately determined by using consistent hysteretic models in the two frames.

The yield moment, M_y, was determined by detecting during the construction of the M–ϕ curve the point at which the tension steel first yields. The effect of axial load on the moment capacity was ignored by using the yield surface shown in figure 3.5. The axial load was also ignored in the construction of the M–ϕ relationship. A strain hardening ratio of 0.02 was used for the beams to approximately account for the strain hardening of the steel.

Rigid joint lengths of one half of the column width were used to account for the increase in stiffness in the joint region. The joints were assumed to be properly designed such that the plastic hinges are forced into the beams, avoiding severe shear distortions of the joint regions.

During seismic loading, the maximum moments generally occur at the beam ends. Therefore, the lumped plasticity model at the element ends used by the DRAIN–2DX beam column elements seems reasonable. There are, however, two shortcomings of this model. Firstly, under severe

seismic loading the nonlinear behavior will spread from the beam ends toward the center of the beam (Kunnath, Reinhorn, and Park, 1990). This phenomena cannot be modeled by the lumped plasticity at the element ends. Secondly, if the gravity loads are high relative to the lateral loads (e.g. in roof beams), then the highest moment may occur away from the beam ends. In this case, the DRAIN–2DX model would not form a plastic hinge at the proper location (Teran–Gilmore and Bertero, 1993).

3.4.2 Columns

As discussed in the previous section, DRAIN–2DX allows only one stiffness to be used for the beam–column elements. Although the columns are symmetric in cross–section, and thus have the same positive and negative bending stiffnesses, the column bending stiffness can change significantly depending on the axial load. During seismic loading the axial load in the columns will vary about the axial load due to the gravity loads alone. To ensure a ductile failure mode, the columns are designed such that the axial load due to gravity loads, P_{grav}, is well below P_{bal} on the P–M interaction diagram (see figure 3.2). Since this portion of the interaction diagram is nearly linear, the effects of varying compression about P_{grav} during seismic loading will effectively cancel out. Thus, the stiffness of the columns is determined using the axial load due to the unfactored gravity loads alone. This approximation is no longer accurate if the maximum compressive axial load during the seismic loading exceeds P_{bal}. To avoid such extreme axial force during seismic loading, several bays within one frame and the widest possible frame should be used.

The column yield surface is approximated by the simplified P–M interaction diagram shown in figure 3.6. Each point on the curve was determined using the P–M interaction diagrams developed using the method discussed in section 3.2. As mentioned previously, the interaction diagrams were developed using $\varepsilon_c' = 0.004$ as the ultimate criteria rather than the first yield of the reinforcement. This method approximates the true column yield surface.

Since the axial loads in the columns tend to result in an ultimate moment that is lower than the maximum moment attained (see figure 3.2), a strain hardening ratio of zero was deemed appropriate for the columns.

Since columns have multiple layers of reinforcement, and each layer yields at a different applied moment and curvature, the stiffness and yield moment for a bilinear model are not easily defined. Paulay and Priestley (1992) recommend a method illustrated in figure 3.7. The yield moment, M_y, is assumed (in this study the moment at $\varepsilon_c' = 0.006$ was used as a yield moment since a strain hardening ratio of zero was assumed). Then the curvature at $0.75M_y$, ϕ_y', is determined using the M–ϕ relationship (see figure 3.7). The stiffness is determined by connecting this point to the origin. Therefore,

$$EI = \frac{0.75M_y}{\phi_y'} = \frac{M_y}{\phi_y} \tag{3.4}$$

As with the beams, rigid ends with lengths equal to one half of the beam height were used to model the increase in stiffness at the column ends. The bilinear non–degrading hysteretic model was also used for the columns. The discussion in the previous section for beams also applies for the columns.

3.4.3 Dynamic Model

Since the NEHRP design only uses a perimeter frame the resist the lateral forces (see section 2.1), one half of the total mass of each floor level must be assigned to NEHRP frame model. On the other hand, the Dual–level design uses all of the transverse frames to resist the lateral load, and therefore, only 1/7 of the total mass at each floor level must be assigned to Dual–level frame model.

The masses were lumped at the nodes to create a diagonal mass matrix. However, the axial deformations of the floors were ignored, and therefore, all of the nodes on a single floor were "slaved" together. Prakash et al. (1993) warns that if slaving the nodes results in a non–diagonal mass matrix, then DRAIN–2DX will **ignore** the off–diagonal terms.

The models used in this study only considered the translational degrees of freedom at each floor level. This is a reasonable assumption since the rotational and vertical displacements during seismic shaking should be negligible when compared to the horizontal displacements.

DRAIN–2DX assumes the damping to be proportional to a combination of the mass and stiffness matrices (i.e. Rayleigh damping). Such a method allows the damping to be exactly specified for two modes, but only approximated for any other modes (Clough and Penzien, 1993). For both frames, damping of 5% was specified for the first two modes, since higher modes do not significantly influence the response of building structures. It should be noted that the stiffness matrix used by DRAIN–2DX to determine the damping matrix remains constant throughout the analysis. Therefore, the decrease in stiffness as the frame yields is not considered when calculating the the damping matrix (Prakash et al., 1993)

The fundamental periods of the DRAIN–2DX models of the NEHRP and Dual–level designs are 2.12 seconds and 1.47 seconds, respectively. These are much larger than the periods estimated by equations 2.2 and 2.10 since only the bare frames are included in the models.

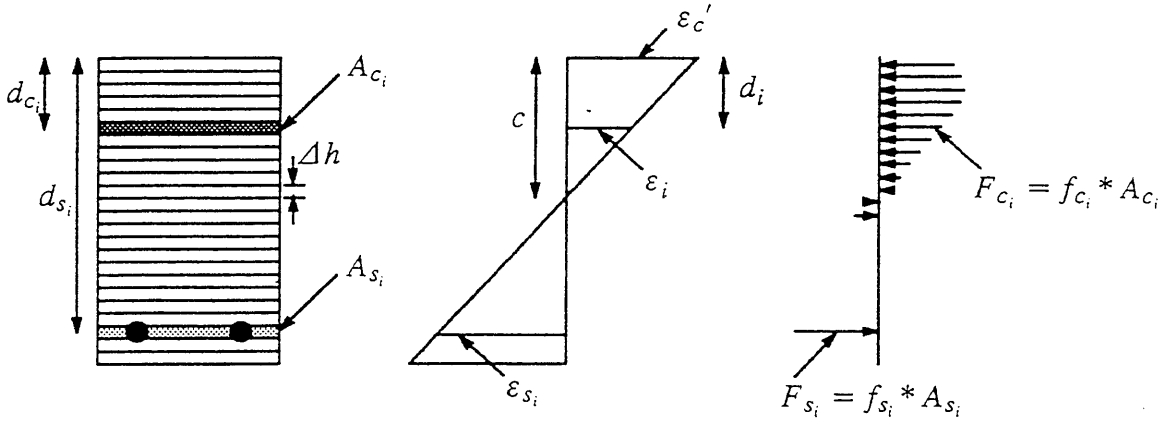

Figure 3.1: Section Details for Development of M–ϕ Relationships

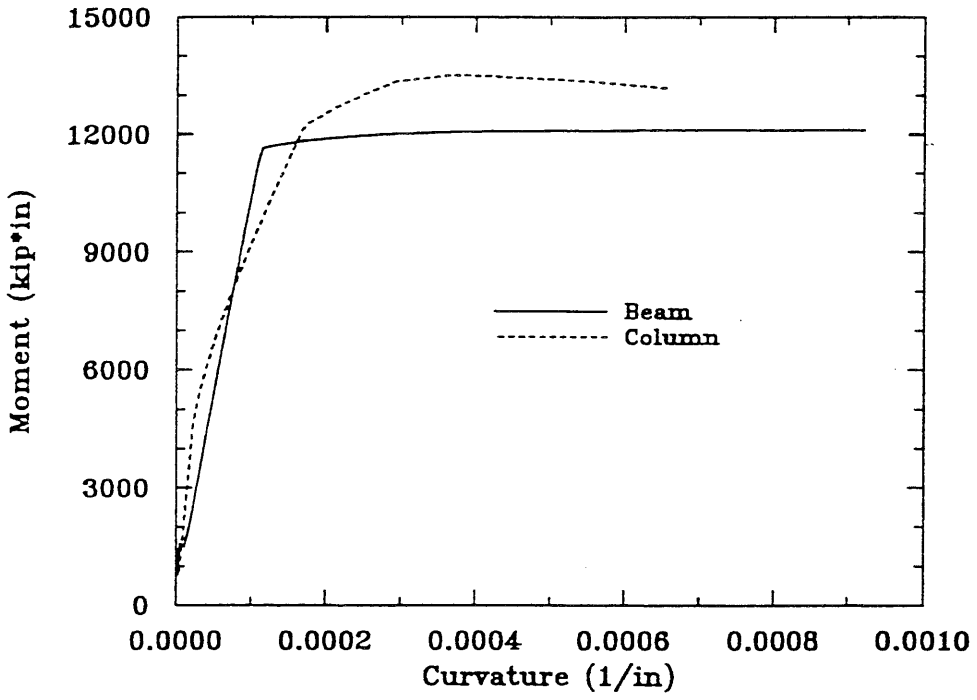

Figure 3.2: Typical Moment–Curvature Relationships

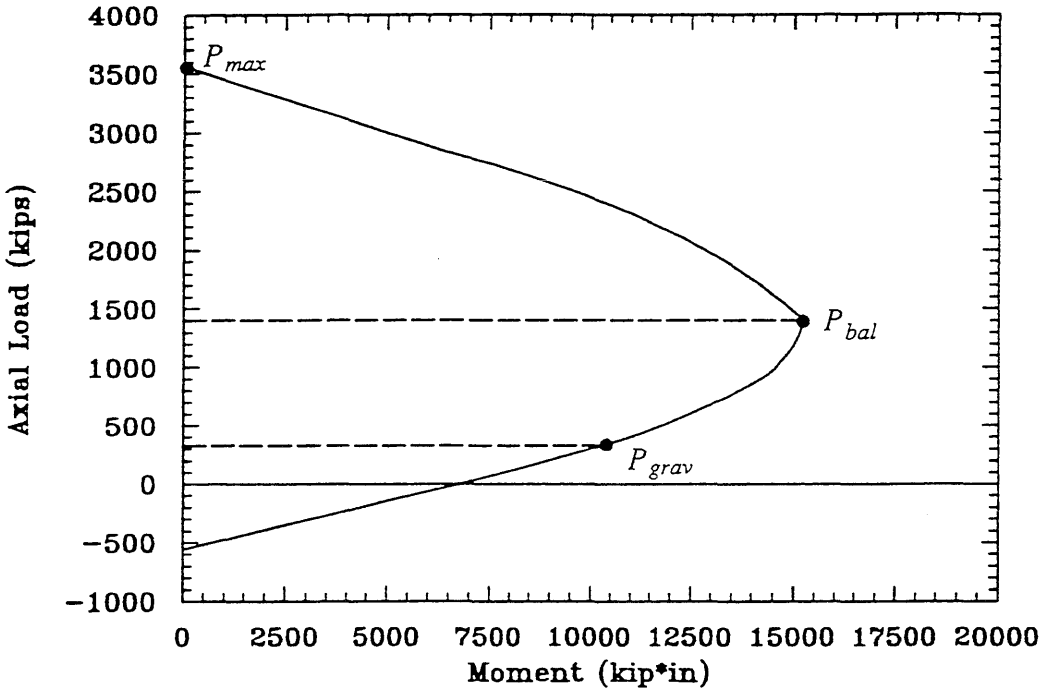

Figure 3.3: Typical Axial Load–Moment Interaction Diagram

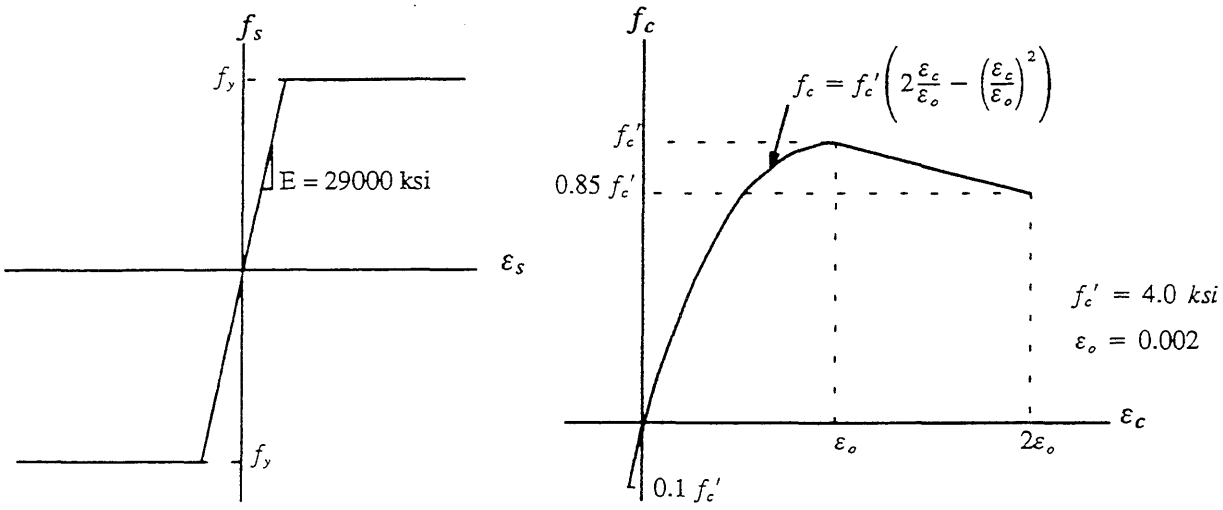

(a) Steel (b) Concrete

Figure 3.4: Material Models

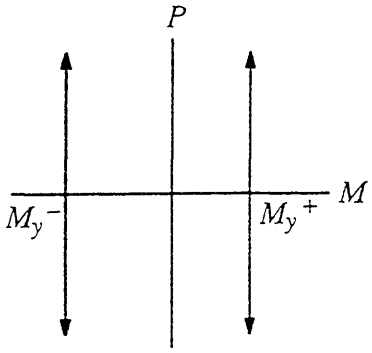

Figure 3.5: Beam Yield Surface

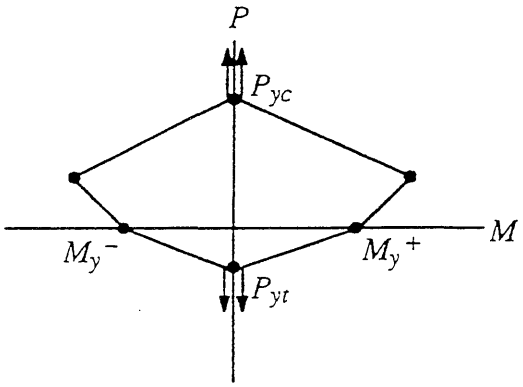

Figure 3.6: Column Yield Surface

(Adapted from Powell, 1993)

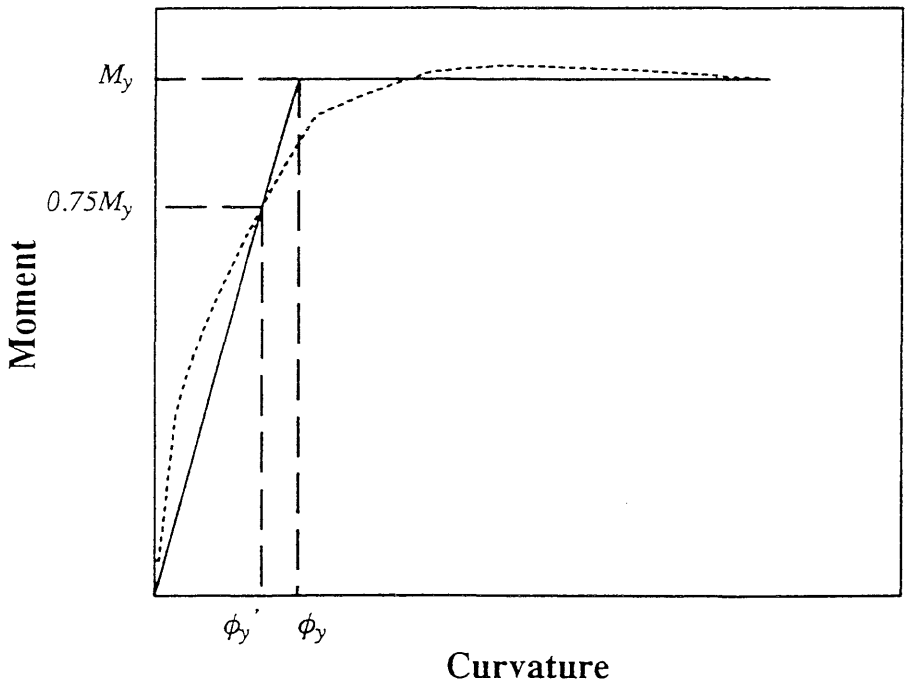

Figure 3.7: Approximate Moment–Curvature Diagram for Columns
(Adapted from Paulay and Priestley, 1992)

CHAPTER 4

COMPARISON OF RESPONSES OF DUAL–LEVEL AND NEHRP DESIGNS

This section will discuss and compare the responses of two frames modeled on DRAIN–2DX and subjected to three strong ground motion records. As discussed in section 2, one frame is designed according to the 1991 NEHRP provisions, while the other is designed according to the proposed Dual–level procedure. Three ground motion records (Sylmar from the 1994 Northridge earthquake, El Centro from the 1940 Imperial Valley earthquake, and Castaic from the 1971 San Fernando earthquake) were chosen to approximately represent strong, moderate, and small ground motions respectively. Three response quantities are compared: global roof displacement, interstory drift, and damage indices. Some details of the concept and calculation of damaged indices are presented in the following.

4.1 Damage Index

A variation of the damage index (*DI*) developed by Park, Ang, and Wen (1984) is used in this study to approximately define the state of damage in the frames due to each ground motion excitation. Structural damage is expressed as a linear combination of damage due to excessive deformation and damage from repeated cyclic loading (Park, Ang, and Wen, 1984). Since in the DRAIN–2DX model plastic rotations (i.e. deformations) only occur at the element ends (see section 3.4), the damage indices are defined for each member end as follows:

$$DI = \frac{\theta_p}{\theta_u} + \beta \frac{E_H}{E_{H_{mon}}} \tag{4.1}$$

This definition of *DI* is also used by Bertero and Bertero (1992) and Teran–Gilmore and Bertero (1993). Each of the variables in equation 4.1 will be discussed in detail below.

Since damage at a local level does not provide useful information for the direct comparison of the overall damage experienced by two different frames, the local damage indices are weighted over the entire frame to get a frame damage index, DI_{frame}.

$$DI_{frame} = \sum_{member\ ends} \lambda_i\, DI_i$$

$$\text{where,} \quad \lambda_i = \frac{E_{H_i}}{\sum_{member\ ends} E_{H_i}} \tag{4.2}$$

The original Park, Ang, and Wen model used the total absorbed energy (i.e. including the elastic strain energy) to define the weighting function, λ_i. For the current study, only the hysteretic energy was used for the following reasons: (1) the elastic strain energy stored in a structure is generally negligible after a long ground motion record that allows the structure to essentially return to rest, (2) given the output available from DRAIN–2DX, the hysteretic energy is much simpler to compute (discussed in detail below). Note that IDARC, a nonlinear dynamic analysis program that employs the Park, Ang, and Wen damage index, currently uses the hysteretic energy to define the weighting function, λ_i (Kunnath, Reinhorn, and Lobo, 1992).

4.1.1 Definition of θ_p

θ_p is the largest plastic rotation (either positive or negative) experienced by the hinge during the ground motion record (see figure 4.1). Note that θ_p would be zero if the "hinge" remained elastic. This value is attained directly from the output of DRAIN–2DX.

4.1.2 Definition of θ_u

θ_u is the ultimate plastic rotation capacity of the member. Either the positive or negative value is used, depending on the direction of θ_p (i.e. if $\theta_p{}^+ > \theta_p{}^-$, then $\theta_u{}^+$ should be used and visa versa). However, the ultimate capacity of any member is not easily defined. For this study θ_u is estimated by:

$$\theta_u = l_p\ (\phi_u - \phi_y) \tag{4.3}$$

where l_p is the plastic hinge length and ϕ_u and ϕ_y are the ultimate and yield curvatures respectively. The question still remains: How shall l_p and ϕ_u be defined? A conservative and common estimate of l_p is $h/2$, where h is the total depth of the member (Teran–Gilmore and Bertero, 1993). Although

more sophisticated models have been developed (Corely, 1966; Paulay and Priestley, 1992), $h/2$ was deemed adequate for use in an already approximate damage index calculation.

The ultimate curvature, ϕ_u, was initially determined using the procedure discussed in section 3.1 with $\varepsilon_c' = 0.004$. This resulted in very small ultimate plastic rotations for the columns with high axial load. Thus, other definitions of ϕ_u were explored. Park and Sampson (1972) recommended a curvature ductility of at least 15 for good seismic design.

$$\text{i.e.} \quad \frac{\phi_u}{\phi_y} \geq 15 \tag{4.4}$$

A curvature ductility of 15 should, in turn, result in a displacement ductility, μ, of approximately four (Park and Sampson, 1972). Since both frames are designed according to the current ACI building code, which emphasizes ductile construction, a curvature ductility of 15 was chosen as a conservative estimate of the member ductilities. Thus, the ultimate curvature was determined as:

$$\phi_u \geq 15\ \phi_y \tag{4.5}$$

To avoid overconservatism, ϕ_u was taken as the larger of 15 ϕ_y or the value determined using the procedure discussed in section 3.1 with $\varepsilon_c' = 0.004$.

4.1.3 Definition of β

β is a model parameter that reflects the effect of cyclic loading on structural damage. Since the strength capacity of a reinforced concrete beam will deteriorate through cyclic loading, β may be considered a correlation between strength degradation and damage (Kunnath et al., 1992). In the original study by Park, Ang, and Wen, data from 261 cyclic tests on reinforced concrete elements were analyzed and regression curves were obtained to express β in terms of the shear span ration, the axial force, and the amount of longitudinal and transverse steel. However, the large data scatter resulted in a coefficient of variation of 60%. β values ranging from –0.3 to 1.2, with a median of approximately 0.15, are reported in the literature (Cosenza, Manfredi and Ramasco, 1993). β equal to 0.15 shall be used in this study. This value of β has also been used by Teran–Gilmore and Bertero (1993), and Bertero and Bertero (1992).

4.1.4 Definition of E_H

The dissipated irrecoverable hysteretic energy, E_H, is defined as the total area enclosed by the hysteretic loops. Thus, E_H includes the effects of duration and low–cycle fatigue, and provides a good measure of the damage potential of earthquake ground motions (Naeim and Anderson, 1993). For an elastic–plastic system, the hysteretic energy due to positive and negative rotations ($E_H{}^+$ and $E_H{}^-$ respectively) are given by:

$$\begin{aligned} E_H^+ &= M_y^+ \sum \Delta\theta_p^+ = M_y^+ \theta_{acc}^+ \\ E_H^- &= M_y^- \sum \Delta\theta_p^- = M_y^- \theta_{acc}^- \end{aligned} \tag{4.6}$$

where M_y is the yield moment, $\Delta\theta_p$ is the change in plastic rotation, and θ_{acc} is the accumulated plastic rotations (figure 4.1 illustrates the relationship between θ_{acc} and $\Delta\theta_p$). The total hysteric energy is, therefore, given by (Teran–Gilmore and Bertero, 1993):

$$E_H = E_H^+ + E_H^- = M_y^+ \theta_{acc}^+ + M_y^+ \theta_{acc}^+ \tag{4.7}$$

If the positive and negative yield moments are equal (i.e. for columns) then equation 4.7 reduces to:

$$E_H = M_y \, (\theta_{acc}^+ + \theta_{acc}^-) \tag{4.8}$$

$\theta_{acc}{}^+$ and $\theta_{acc}{}^-$ are attained directly from the output of DRAIN–2DX. $M_y{}^+$ and $M_y{}^-$ are calculated according to the procedures outlined in section 3 and are used in the DRAIN–2DX input files.

The elastic–plastic formulation of E_H holds for the columns of both frames, since no strain–hardening was assumed. For the beams, a bilinear hysteresis with a strain hardening of 2% was assumed, and thus, equation 4.7 is not strictly correct. However, Nassar and Krawinkler (1991) state that "the error [in E_H] for strain hardening of 10% is typically less than 1%". Therefore, equation 4.7 has been adopted to estimate the hysteretic energy dissipated by plastic hinges in both beams and columns.

4.1.5 Definition of $E_{H_{mon}}$

$E_{H_{mon}}$ is the irrecoverable hysteretic energy from a monotonic push–over analysis. For an elastic–plastic system with equal positive and negative yield moments (i.e. the columns in the current study), $E_{H_{mon}}$ is given by:

$$E_{H_{mon}} = M_y \, \theta_u \tag{4.9}$$

For the beams, on the other hand, strain hardening exists and the positive and negative yield moments and ultimate rotations are not equal. As with E_H, the effect of strain hardening is neglected. In order to account for both positive and negative bending, the average of $E^{+}_{H_{mon}}$ and $E^{-}_{H_{mon}}$ is used. That is, $E_{H_{mon}}$ for the beams is given by:

$$E_{H_{mon}} = \frac{1}{2}(E^{+}_{H_{mon}} + E^{-}_{H_{mon}}) = \frac{1}{2}(M_y^{+}\theta_u^{+} + M_y^{-}\theta_u^{-}) \tag{4.10}$$

Some may argue that since E_H includes all of both $E_H{}^{+}$ and $E_H{}^{-}$, $E_{H_{mon}}$ should also include all of both $E^{+}_{H_{mon}}$ and $E^{-}_{H_{mon}}$. However, the model parameter β has been determined using equation 4.9 as the definition of $E_{H_{mon}}$. Since $\beta = 0.15$ has been chosen based on previous studies, for consistency $E_{H_{mon}}$ must be determined by equation 4.9 or 4.10.

4.1.6 Physical Significance of Damage Indices

It should be noted that equation 4.1 will result in a damage index of zero for any member that remains elastic. This differs from the original Park, Ang and Wen formulation where θ_p included the elastic rotations, and thus, resulted in a non–zero damage index for even the smallest ground motion records. For the original formulation, Park, Ang, and Wen (1984) determined that $DI_{frame} \leq 0.4$ indicated repairable damage, $DI_{frame} > 0.4$ indicated unrepairable damage, and $DI_{frame} > 1.0$ indicated total collapse. To satisfy the current code requirements of life safety, the overall damage index for the frame must be less than 1.0. These conclusions may be used as a rough guideline when evaluating the damage indices resulting from equations 4.1 and 4.2. The FORTRAN program developed to determine the damage indices based on the DRAIN–2DX output is given in Appendix B.

4.2 Comparison of Responses to the 1994 Northridge Earthquake (Sylmar Record)

The January 17, 1994 Northridge earthquake (M_w = 6.7) resulted in several near–field records, including one at the Sylmar County Hospital 16 km from the epicenter. This record is characterized by two very large acceleration pulses (PGA = 0.91g). The significant strong ground motion lasts for only approximately 6 seconds, however, the blast of the initial shock is enough to cause significant damage. The Sylmar response spectrum and acceleration time history are shown in figures 4.2 and 4.3a.

The global drifts (i.e. the roof displacement as a fraction of the total height of the building) for both the NEHRP and Dual–level designs subjected to the Sylmar record are shown in figure 4.3b. The maximum global drift of the NEHRP design is 1.4 times that of the Dual–level design, and both occur within the first displacement excursion, indicating the importance of the blast of the initial acceleration pulse. The lower stiffness of the NEHRP design (T_{fund} = 2.12 seconds versus T_{fund} = 1.47 seconds for the Dual–level design) is evident in the longer period of vibration. The longer period of vibration may also be partially explained by the larger amount of inelastic deformation experienced by the NEHRP design (see discussion of flexural hinges below). It is interesting to note that the final permanent global drift is essentially the same for both designs, and remains very small considering the large maximum displacement.

The local interstory drifts for the first and second stories of the two designs are shown in figures 4.3c and 4.3d. The maximum interstory drifts for the NEHRP design exceed that of the Dual–level design for both stories. It is interesting to note that while the global drifts of both designs remained below 2% (recommended by Sozen (1981) as a maximum limit for drift), the interstory drifts for the second story exceeded 3% and 2% for the NEHRP and Dual–level designs, respectively. This would appear to indicate a concentration of drifts in the lower stories. The interstory drifts for the second stories of both designs are generally larger than those for the first story, indicating the possibility of a soft story collapse.

Further understanding of the seismic performance may be gained by observing the distribution of flexural hinges throughout the two designs (see figure 4.4). Flexural hinges are formed when

the moment at the end of a member exceeds the specified yield moment, and thus, hinges are still able to resist a moment of M_y (or higher if the strain hardening is included). It should be noted that no distinction has been made in figure 4.4 between hinges that have just barely yielded (i.e. small plastic hinge rotations) and hinges that have undergone extensive plastic high rotations.

For several stories (2, 3, 4, and 6) the NEHRP frame hinges have formed across all four columns, indicating the formation of a strong–beam–weak–column collapse mechanism (see figure 2.4). Collapse is not necessarily guaranteed in an earthquake since, upon formation of the column hinges, the inertial forces may be reversed by a reversal of the shaking motion. Nevertheless, the formation of a possible collapse mechanism threatens life safety, and thus, threatens the primary goal of the NEHRP provisions – to protect life safety during severe earthquake ground motion.

Although hinges have formed in many of the center columns of the Dual–level frame (see figure 4.4), no single story has hinges across all four columns (except at the base). Thus, a soft story collapse is not imminent. Formation of the hinges in the beams, prior to the columns, allows for increased hysteretic energy dissipation and evenly distributes the interstory drifts over the height of the frame. The improved performance of the columns in the Dual–level design may again be attributed to the performance check on the SCWB design (see section 2.3).

Although not within the original scope of this study, one point should be noted about the SCWB requirement of ACI 318–89. Clause 21.4.2.2 requires that at any joint the sum of the design moments in the columns must be equal to or greater than the sum of the design moments in the beams times 1.2. That is,

$$\sum M_c \geq \frac{6}{5} \sum M_b \tag{4.11}$$

Since the **design** moments are used for the beams, a strength reduction factor, ϕ, less than 1.0 and the nominal steel yield stress are used in the calculation of M_b. However, in a capacity type design, such as clause 21.4.2.2, a $\phi = 1.0$ and a **mean** steel yield stress should be used to calculate the **true capacity** of the beams. The design moments of the columns may still employ a $\phi < 1.0$ and

the nominal yield stress to give a conservative estimate of the capacity of the columns. This form of capacity design has been incorporated in the Canadian Concrete Code (CSA, 1984).

The overall frame damage index for the NEHRP design is 0.98. This would suggest that the frame has experienced very nearly total collapse, thus not satisfying the life safety requirement of the NEHRP provisions. It should be noted that the DRAIN–2DX model assumes unlimited ductility in each member, and thus, is not able to detect member failure due to exceedance of the ultimate rotation capacity. The damage index attempts to detect this form of failure, and then determines the effect in the entire frame by weighting the individual member damage indices by the dissipated hysteretic energy. This explains why the time history of the global drift (figure 4.3b) does not suggest the collapse of the frame (i.e. no large permanent displacements), while the overall frame damage index suggests that collapse is imminent.

The overall frame damage index for the Dual–level design is 0.78. According to the original Park, And, and Wen model, this would suggest that the frame has suffered significant structural damage and will be torn down, but has not collapsed, and thus, has not threatened life safety. Since the Sylmar record was chosen to represent severe earthquake ground motions, the above performance may be considered acceptable. It should be noted that the individual damage indices for the hinges at the base of the columns are greater than 1.0. These large values may be partially explained by the fact that an interior frame was used to represent the Dual–level design, and thus, carries higher gravity loads than the exterior frame used to represent the NEHRP design. The higher gravity loads result in reduced ductility capacity, and in turn, higher damage indices.

It should be noted that structures designed according to current standards performed quite well in the Northridge earthquake. This observation conflicts with the conclusion above that a building designed according to the NEHRP provisions would have suffered nearly total collapse. This conflict has also been noted by Naeim (1995). Such discrepancy between observed damage and expected damage from analysis must be addressed before an adequate performance–based design philosophy can be developed (Naeim, 1995).

The damage indices are best used for a comparison of the seismic performance of the NEHRP and Dual–level designs. In this light, the Dual–level design performed much better than the NEHRP design for the Sylmar record.

4.3 Comparison of Responses to the 1940 Imperial Valley Earthquake (El Centro Record)

The 1940 Imperial Valley earthquake (M = 7.0) resulted in the world's first significant strong ground motion record from a station in El Centro, California. Since then this record has been used extensively by engineers to define design ground motions (consequently, the 1940 earthquake is often referred to as the El Centro earthquake). Since the El Centro record has formed the basis for many aspects of current design codes, it should be interesting to note the performance of the NEHRP and Dual–level designs when subjected to the El Centro record. This record has been chosen to represent moderate earthquake ground shaking. The acceleration time history and response spectra are shown in figures 4.2 and 4.5a.

The global drifts for the NEHRP and Dual–level designs are shown in figure 4.5b. The maximum global drift for the NEHRP design is 2.0 times that of the Dual–level design. The most obvious difference in the performance of the two designs is the permanent drift of approximately 0.4% that remains in the NEHRP design (note that although the record is longer than the 30 seconds shown in figure 4.5, no significant changes in the behavior occur after 30 seconds). It should be noted that the global drifts of both designs remain below 1%, and thus, should experience little or no structural damage.

The local interstory drifts for the first and second stories of the two designs are shown in figures 4.5c and 4.5d. The maximum interstory drifts for the NEHRP design exceed those of the Dual–level design for both stories. As in the global drifts, the NEHRP design experiences a permanent drift while the Dual–level design remains plumb. Unlike the Sylmar record, the interstory drifts for the NEHRP design are nearly equal to the global drifts, suggesting that the drifts are well distributed over the height of the frame. Note that the maximum interstory drift exceeds 0.5% for both designs,

thus indicating that non–structural damage may result from this ground motion. However, non–structural damage is generally acceptable for a moderate earthquake.

The distribution of flexural hinges for both designs is shown in figure 4.6. For the NEHRP design, nearly all the beams have formed flexural hinges, resulting in a very good SCWB design. However, it is disconcerting to note the extensive yielding that has occurred for only a moderate ground motion. The Dual–level design, on the other hand, remained nearly elastic. It is interesting to note that if the El Centro record is taken as a model for the deterministic "design" earthquake, as many have done in the past, the NEHRP frame would be considered very well designed. However, the performance under the Sylmar record clearly demonstrates the NEHRP frame is not adequate and the El Centro record can no longer be considered a model for the deterministic "design" earthquake.

Since the Dual–level design remained nearly elastic, the overall damage index is only 0.02. Thus, no structural repairs should be needed for the Dual–level design. The overall damage index for the NEHRP design is 0.26. This indicates that some moderate structural damage may need to be repaired after ground motions similar to the El Centro record. This is currently adequate performance for moderate ground motions, however, the incidental cost associated with repairing structural damage (e.g. profits lost from business closure, relocation of personal, etc.) have recently forced many engineers to consider stricter performance goals for moderate ground motions.

4.4 Comparison of Responses to the 1971 San Fernando Earthquake (Castaic Record)

The 1971 San Fernando earthquake resulted in one of the first extensive set of strong ground motion records from a single earthquake. One of these records was the Castaic – Old Ridge Route record. The acceleration time history and response spectra are shown in figures 4.2 and 4.7a.

Both the NEHRP and Dual–level designs remained elastic when subjected to the Castaic record. Thus, the global drifts for both designs (see figure 4.7b) were relatively small (i.e. less than 0.25%). The interstory drifts for the first and second stories (see figures 4.7c and 4.7d) were generally larger than the global drifts, indicating a concentration of displacement in the lower stories. How-

ever, the interstory drifts remained well below 0.5% (a threshold used by Foutch, Yu, and Wen (1992) as the interstory drift needed for non–structural damage).

The Dual–level design exhibits larger maximum global and interstory drifts than the NEHRP design, and a significantly different time–displacement response. The Dual–level design appears to react in the first mode, while the NEHRP design reacts in the higher modes. This may be explained by the lower column to beam strength ratio in the NEHRP design allows higher modes to participate; while in the assured SCWB design of the Dual–level design may force the frame to remain in the first mode. The elastic response spectra peaks at a low period (i.e. approximately 0.4 seconds), and thus, the stiffer Dual–level design should be expected to respond more severely than the softer NEHRP design.

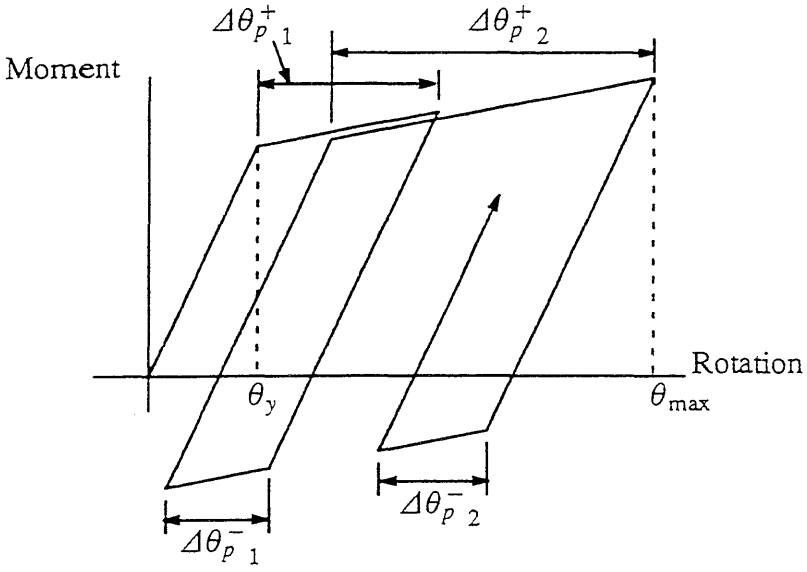

$$\theta_{acc}^{+} = \Delta\theta_p^+{}_1 + \Delta\theta_p^+{}_2$$

$$\theta_{acc}^{-} = \Delta\theta_p^-{}_1 + \Delta\theta_p^-{}_2$$

$$\theta_p = \theta_{max} - \theta_y$$

Figure 4.1: Illustration of θ_p, $\Delta\theta_p$, and θ_{acc}
(Adapted from Powell, 1993)

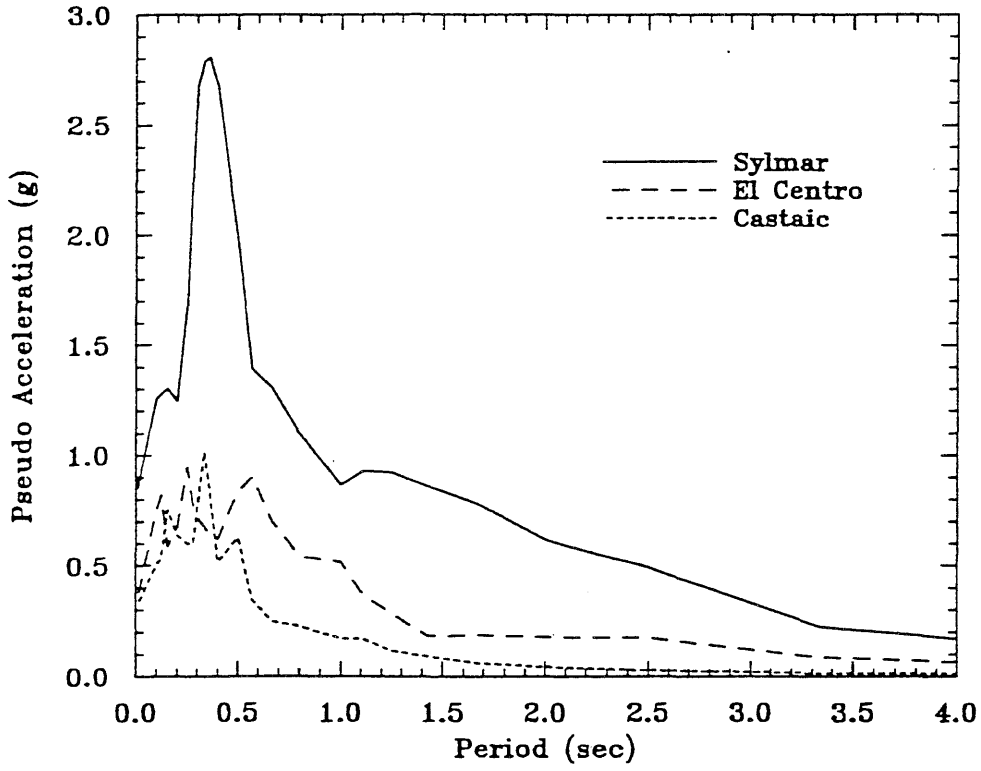

Figure 4.2: Elastic Pseudo Acceleration Response Spectra

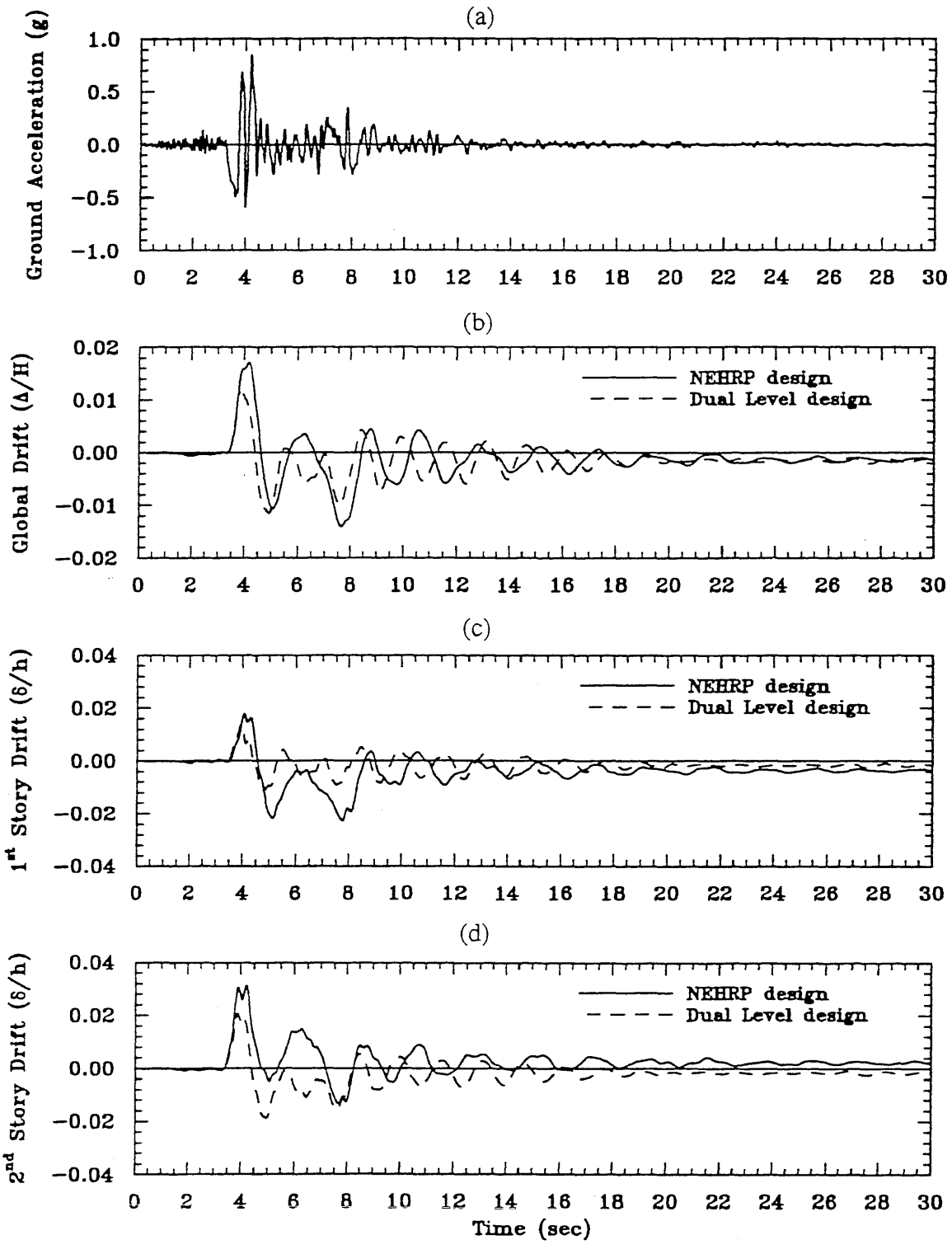

Figure 4.3: Ground Motion and Structural Responses for Sylmar Record
(a) ground acceleration, (b) global drift, (c) first story drift, (d) second story drift

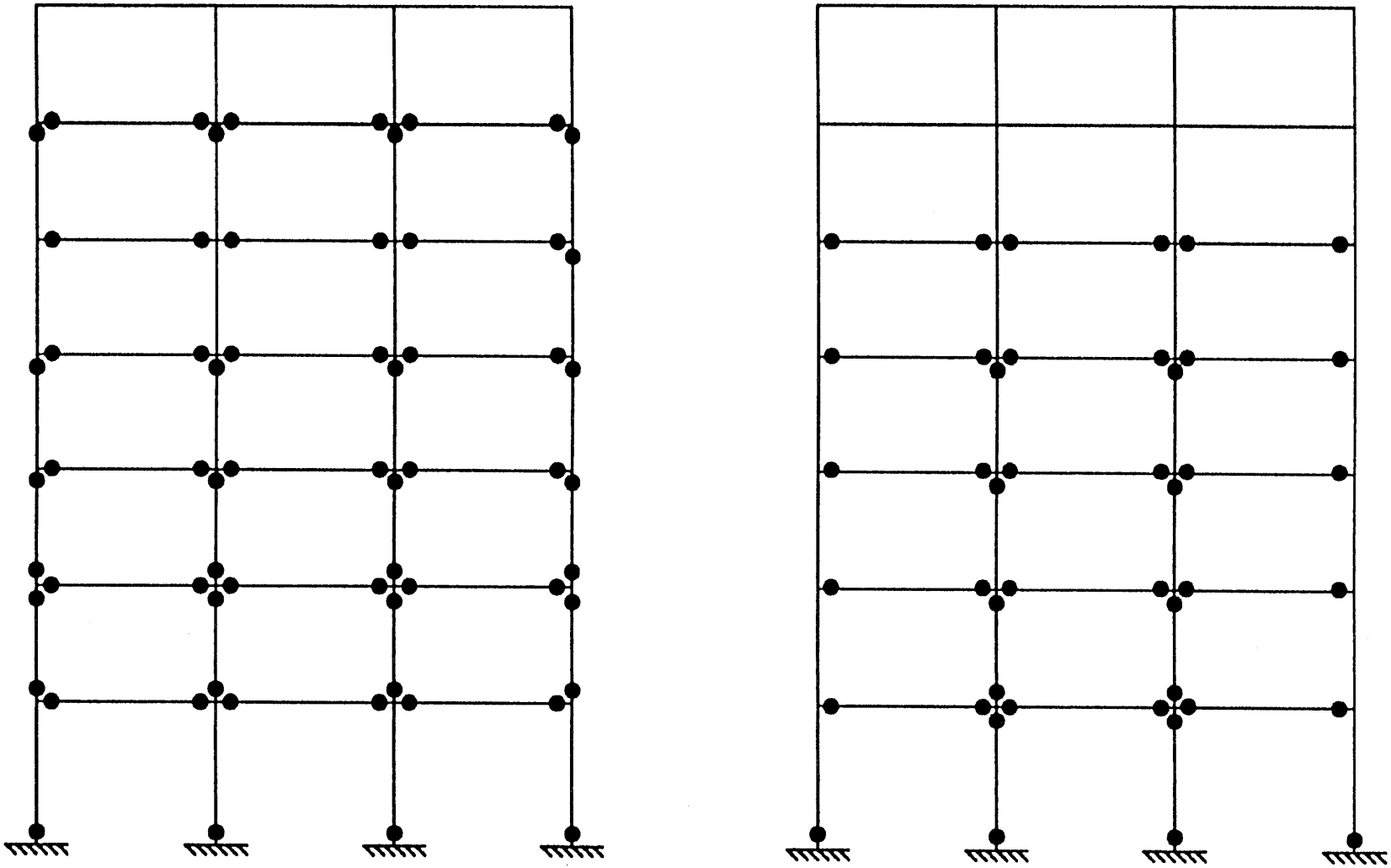

Figure 4.4: Flexural Hinges Resulting from Sylmar Record

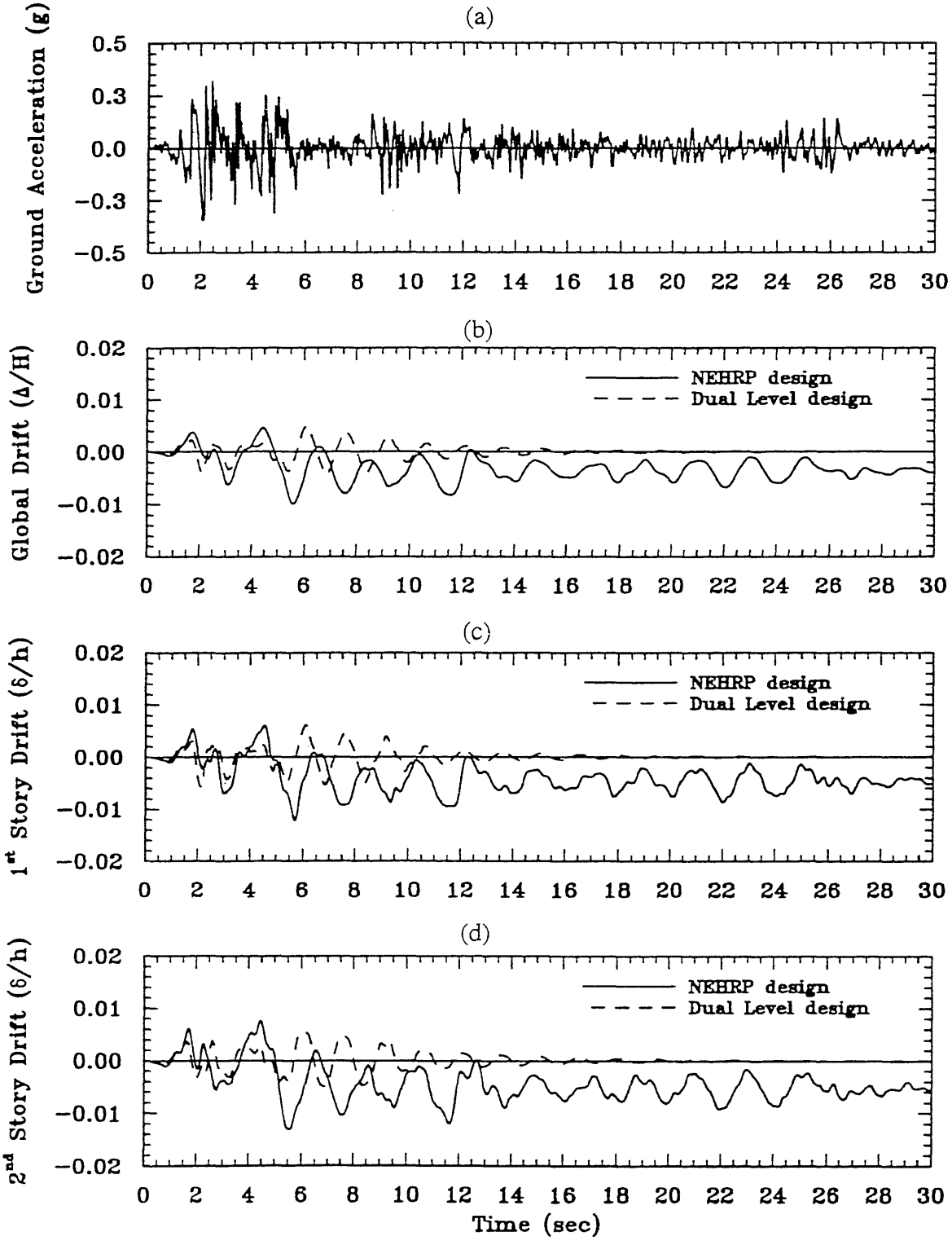

Figure 4.5: Ground Motion and Structural Responses for El Centro Record
(a) ground acceleration, (b) global drift, (c) first story drift, (d) second story drift

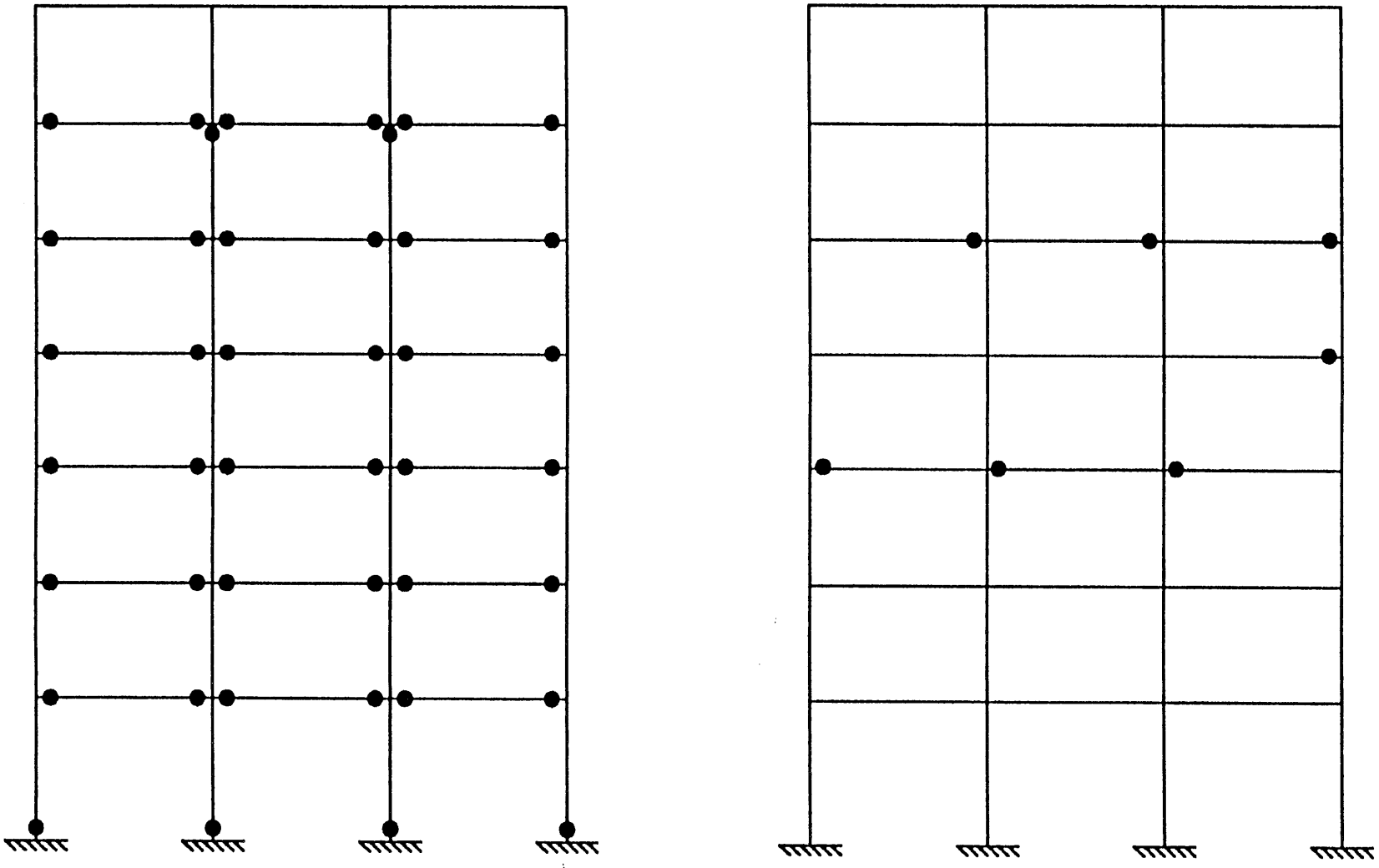

Figure 4.6: Flexural Hinges Resulting from El Centro Record

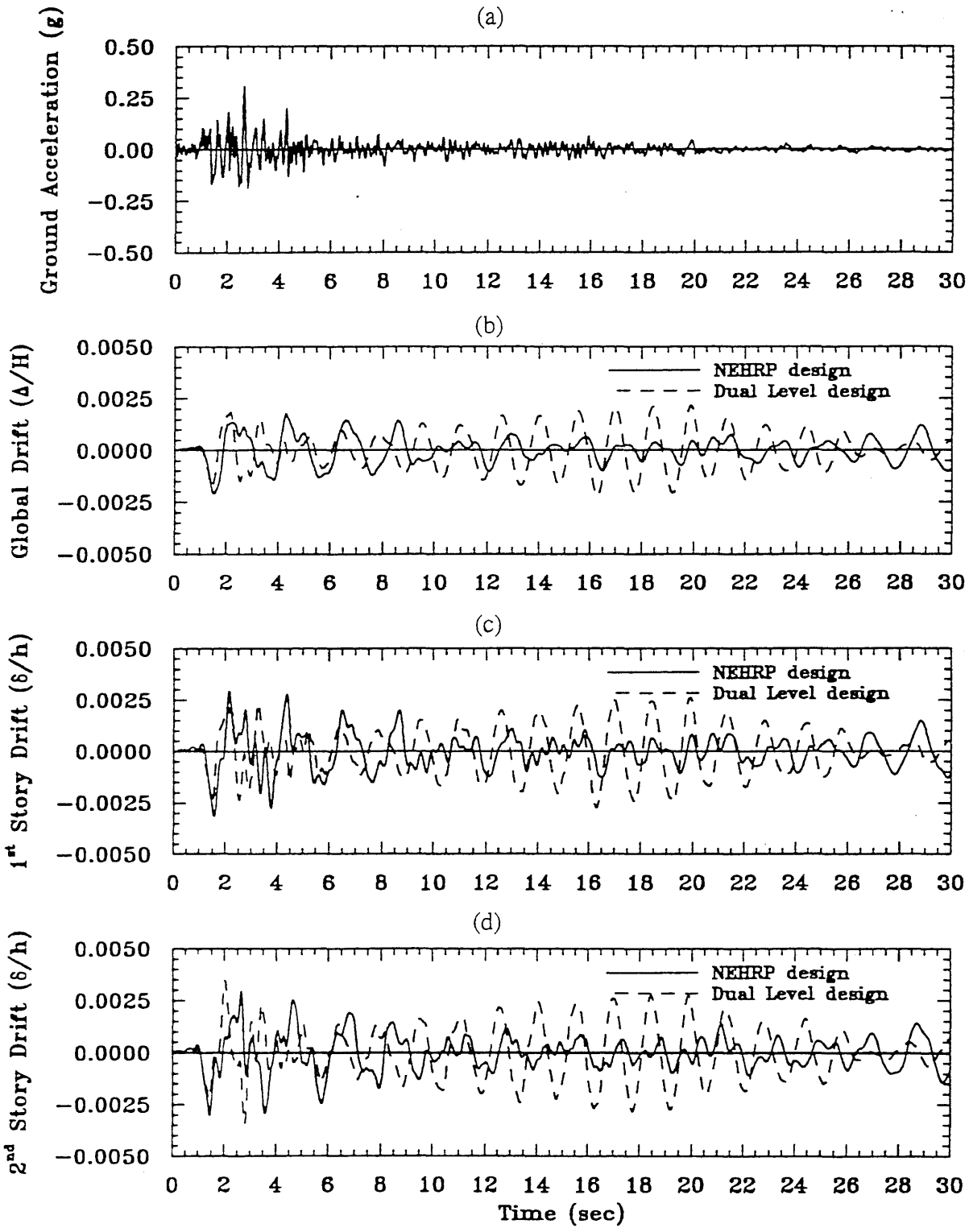

Figure 4.7: Ground Motion and Structural Responses for Castaic Record
(a) ground acceleration, (b) global drift, (c) first story drift, (d) second story drift

CHAPTER 5

IMPLICATIONS OF THE 1994 NORTHRIDGE EARTHQUAKE TO DUAL–LEVEL DESIGN

Given the extensive number of strong ground motion records recorded during the 1994 Northridge earthquake, it is possible to evaluate the reliability of the NEHRP and Dual–level designs given an earthquake event similar to the 1994 Northridge earthquake. The effect of epicentral distance is considered when evaluating the reliability. Before the method used to determine the reliability is discussed, certain aspects of the Northridge earthquake deserve special attention.

5.1 The 1994 Northridge Earthquake

The 1994 Northridge earthquake occurred on a blind thrust fault dipping southward under the Santa Susana Mountains and the San Fernando Valley, including the city of Northridge, California. Although the earthquake resulted in a moment magnitude of only $M_w = 6.7$, its close proximity to the highly populated Los Angeles basin and relatively shallow hypocenter (approximately 12 miles) resulted in extensive damage to buildings, parking structures, bridges, and lifelines. More details of the seismological aspects of the Northridge earthquake are presented elsewhere (EERI, 1994; Trifunac, Todorovska, and Ivanovic, 1994; EQE, 1994).

Fortunately, this region had been extensively instrumented after the 1971 San Fernando earthquake, and thus, many strong ground motion records are available to researchers to evaluate the implications of the Northridge earthquake. 84 corrected horizontal strong ground motion records from 42 stations have been used in this study to evaluate the reliability of the NEHRP and Dual–level designs. (These records are available to the public on the Internet (ftp at ftp.netcom.com, directory pub/cs/csmip_eq_data/northridge) courtesy of the California Strong Motion Instrumentation Program. Further details of the records are available in Shakal et al., 1994.) Table 5.1 gives the station name, component, peak ground acceleration (PGA), and epicentral distance for each strong ground motion record. Figure 5.1 shows the spatial distribution of the stations over the Los Angeles basin area. The site soil conditions for each station could be approximated as stiff soil or

rock, thus remaining consistent with the choice of soil factors for the design of the two frames (see section 2).

Naeim (1995) has discussed many interesting aspects of the Northridge strong ground motion records; several points deserve attention here. Naeim (1995) comments that there is a lack of correlation between epicentral distance and ground motion characteristics (such as PGA, response and energy spectral values, etc.) in the north–west San Fernando valley. This may be explained by the fact that these stations (such as Newhall) are located close to or on top of the fault rupture zone, and thus, the epicentral distance does not necessarily represent the closest distance to the point of largest energy release (Naeim, 1995). Therefore, the reliability evaluation to be described in section 5.2.2 should be repeated using the closest distance to the fault rupture zone (or another descriptor of earthquake distance), instead of epicentral distance, when this information is available from seismologists.

To appreciate the significance of the Northridge records, Naeim (1995) compared the ground motion characteristics with those from North and Central American earthquakes from 1933 to 1993. Although not all the records considered in this study were included in Naeim's investigation, Naeim (1995) found that several Northridge records exhibited PGAs within the top 10 PGAs recorded since 1933 (i.e. PGA > 0.8g). The Northridge records also exhibited very high peak ground velocities (PGV), a better representation of the damage potential for the mid–period range. In fact, the Sylmar record produced the highest PGV of any earthquake considered. On the other hand, the peak ground displacements (PGD) from the Northridge records were all relatively small, indicating that the Northridge earthquake did not seriously affect long period structures. Figure 4.2 demonstrates that the response spectrum from the Sylmar record (360 degrees) is significantly higher than response spectra previously considered in earthquake resistant design, particularly in the short period range. This is also true with other Northridge records, such as Santa Monica and Newhall.

Naeim (1995) also found that some of the Northridge records exhibited the highest input energies of any California earthquake for natural periods less than 2.5 seconds (i.e. low or medium–rise

building structures). It is also interesting to note that for several records the input energies rise to nearly their maximum values within a very short period of time (i.e. approximately 1.5 seconds). Due to the short time span for the input energy increase the structure does not have time to respond through cyclic vibration, and therefore, the damping dissipation is not very efficient (Naeim, 1995). Thus, very little input energy is dissipated through damping, resulting in a large percentage of the input energy being dissipated through hysteretic energy. Since hysteretic energy is achieved through plastic deformations, the amount of input energy dissipated through hysteretic energy is directly related to the amount of damage in the structure.

Probably the most important aspect for many of the Northridge records is the presence of a substantial acceleration pulse, particularly evident in the near–field records (such as Sylmar – see figure 4.3). The effect of this impulse type loading on the NEHRP and Dual–level designs is discussed in detail in section 4.2.

5.2 Distributions of Response Quantities

Three response quantities are used in this study to evaluate the performance of the NEHRP and Dual–level frames when subjected to the Northridge earthquake records; i.e. overall frame damage index, global drift, and local drift. The overall frame damage index is defined and discussed in detail in section 4.1. The global drift is given by:

$$GD = \frac{Maximum\ roof\ displacement\ relative\ to\ the\ base}{Height\ of\ frame} \times 100 \qquad (5.1)$$

The local drift is the maximum interstory drift experienced by any story over the whole frame. That is:

$$LD = \frac{Maximum\ displacement\ of\ a\ story\ relative\ to\ the\ story\ below}{Height\ between\ the\ stories} \times 100 \qquad (5.2)$$

The response quantities for each frame when subjected to the 84 Northridge records are given in table 5.1.

The results presented in table 5.1 seem reasonable since records from stations closer to the epicenter generally produced higher responses than those at a greater distance. Note that the re-

sponse quantities are very small at epicentral distances greater than 80 kilometers. It is interesting to note that records with a very high PGA (i.e. Tarzana and Pacoima Dam) do not result in a damage index as high as those determined using the Sylmar or Newhall records. This agrees with the generally accepted belief that PGA is not a very good measure of the damage potential of earthquake ground motions.

5.2.1 Distributions of Response Quantities NOT Considering Spatial Distribution of Records

The histograms and probabilities of exceedance for the overall frame damage indices are shown in figures 5.2 and 5.3, respectively. It should be noted that for the formulation of the damage index presented in section 4.1, the overall frame damage index will be zero if the frame remains elastic. Thus, the probability of exceedance is not equal to 1.0 at DI = 0 as shown in figure 5.3. None of the Northridge records resulted in a damage index large enough to exceed a threshold of DI = 0.8 for the Dual–level frame and DI = 1.0 for the NEHRP frame. Therefore, the probabilities of exceedance at or above these threshold values are not accurately know and are not included in figure 5.3. The histogram in figure 5.2 indicates that both frames remain elastic for 70% of the records. On the other hand, the damage index for the Dual–level frame exceeds 0.4 (the level set by Park, Ang, and Wen (1984) for irreparable damage – see section 4.1.6) for approximately 5% of the records, compared to approximately 11% of the records for the NEHRP frame. Since the probability of exceedance for the Dual–level frame remains consistently below the probability of exceedance for the NEHRP frame (except at low damage levels), the Dual–level frame may be considered less likely to be seriously damaged than the NEHRP frame.

The histograms and probabilities of exceedance for the global drifts are shown in figures 5.4 and 5.5, respectively. Figure 5.4 shows that the distribution of global drifts for the Dual–level frame is more skewed to the left (i.e. low global drifts) than the distribution of global drifts for the NEHRP frame. Once again, the probability of exceedance for the Dual–level frame is consistently below the probability of exceedance for the NEHRP frame, indicating that the Dual–level frame is a better design if the engineer wishes to limit the global drift of the structure.

The histograms and probabilities of exceedance for the local drifts are shown in figures 5.6 and 5.7, respectively. As with the global drifts, the distribution of local drifts for the Dual–level frame is more skewed to the left (i.e. low local drifts) than the distribution of local drifts for the NEHRP frame. Similarly, the probability of exceedance for the Dual–level frame is consistently below the probability of exceedance for the NEHRP frame, indicating the Dual–level frame is a better design if the engineer wishes to limit the local drifts of the structure. For both frames, the local drifts are larger than the global drifts, suggesting that drifts are concentrated in only a few stories.

It may be concluded from figures 5.2 – 5.7 and the above discussion that, without considering the spatial distribution of the records and given an earthquake event similar to the Northridge earthquake (i.e. $M \approx 6.7$ on a blind thrust fault), the Dual–level frame has a higher reliability than the NEHRP frame. In other words, for the same probability level, the response or damage index of the Dual–level frame is much smaller than that of the NEHRP frame.

5.2.2 Distributions of Response Quantities Considering Spatial Distribution of Records

In the previous section, the distributions of response quantities were determined by simply counting the number of records that resulted in a response less than a given threshold value. This method, however, does not account for the fact that stations are more likely to be located at a larger epicentral distance than at a smaller epicentral distance.

The response statistics can be used to estimate the probability of attaining a drift or damage index threshold due to future earthquakes with similar magnitude and intensity of the 1994 Northridge earthquake. Since the location of future blind thrust fault events cannot be predicted, one can assume a reference area with a spatially uniform distribution of the epicenters. Or conversely, for a given event, the coordinates of the site can be assumed to be random and uniformly distributed within a circle reference area shown in figure 5.8. If x_1 and x_2 are the coordinates of a station and are uniformly distributed within a circle of radius R_{max}, then a station is more likely to be located in region A than in region B, even though $r_1 = r_3 - r_2$. Therefore, a more accurate representation

of the distributions of response quantities should be obtained by considering the distribution of epicentral distances within the sample area, a circle of radius R_{max}.

Based on the total probability theorem (Ang and Tang, 1975) and given the occurrence of the earthquake and a site within the reference area, the probability that a response X will exceed a given threshold x_o is given by:

$$P(X > x_o) = \int_0^{R_{max}} P(X > x_o \mid R = r)\, f_R(r)\, dr \tag{5.3}$$

where $f_R(r)$ is the probability density function of the epicentral distance. This conditional probability can be regarded as a measure of the performance of a building during future events similar to the Northridge earthquake, taking into consideration the random spatial distribution of the epicenter. If the coordinates x_1 and x_2 are uniformly distributed within a circle of radius R_{max}, then $f_R(r)$ may be derived as follows:

$$\begin{aligned} f_R(r) &= \frac{d}{dr} F_R(r) \\ &= \frac{d}{dr} \frac{\pi r^2}{\pi R_{max}^2} \\ &= \frac{2r}{R_{max}^2} \end{aligned} \tag{5.4}$$

The integral of equation 5.3 is evaluated numerically as follows:

$$P(X > x_o) = \sum_{i=1}^{84} P(X > x_o \mid R = r_{sta_i})\, A_i$$

i.e. $$P(X > x_o) = \sum_{i=1}^{84} \frac{\#\ of\ times\ X > x_o\ at\ a\ distance\ r_{sta_i}}{\#\ of\ records\ at\ a\ distance\ r_{sta_i}} \frac{2r_i}{R_{max}^2} \Delta r_i \tag{5.5}$$

where all the variables are defined in figure 5.9. Since the furthest station, Phelan, has an epicentral distance of 98 km, R_{max} = 100 km was used to find the distributions presented later in this section. The implications of this assumption shall be investigated in section 5.2.3. The FORTRAN program developed to calculate the probabilities of exceedance using equation 5.5 is included in Appendix B.

Several approximations have been made in equation 5.5. The probability of exceedance, $P(X > x_o \mid R = r_{sta_i})$, must be evaluated at the epicentral distance of the station for the i^{th} record, r_{sta_i}. However, the incremental area under the probability density function, A_i, is evaluated at the average epicentral distance within the width of the incremental area, r_i (see figure 5.9). This approximation was necessary to correctly integrate the area under the probability density function. Furthermore, the above formulation does not consider the effect of the direction of the path from the Northridge epicenter to the station, θ. This may be an important consideration since stations along the path of the fault rupture should produce severe records due to directivity effects. As shown in figure 5.1, however, there are very few stations to the south–west and north–west due to the ocean and mountains, respectively. Thus, the uniform distribution of the samples is only approximately correct.

Figure 5.10 shows the histograms of damage indices derived using equation 5.5. Comparing figures 5.2 and 5.10 it is evident that the probability that either frame will remain elastic (i.e. DI = 0) increases when the distribution of epicentral distance is considered. Furthermore, the distribution of the damage index for the Dual–level frame appears more skewed to the left than the distribution of the damage index for the NEHRP frame when the effect of epicentral distance is considered. This implies that, by considering the distribution of the epicentral distance, the calculated reliability of the Dual–level frame increases more than the reliability of the NEHRP frame.

The probabilities of exceedance for the overall frame damage indices are shown in figure 5.11. The points designated by squares and triangles were calculated using equation 5.5 (i.e. using the data shown in the histograms of figure 5.10). The fitted lines shown in figure 5.11 were calculated using a tail biased generalized extreme value distribution developed by Maes and Breitung (1993). Since in structural reliability one is usually interested in the extreme values of random variables, extreme value distributions are often used to model the observed data. However, the appropriate distribution must be chosen from three popular extreme value distributions; Gumbel (type I), Fréchet (type II), or Weibull (type III) (Ang and Tang, 1984). The generalized extreme value distribution developed by Maes and Breitung (1993), given below, avoids the need to choose a distribution.

$$F(x \mid \alpha,\beta,\gamma) = \exp\left\{-\left[1 - \frac{\gamma(x-\alpha)}{\beta}\right]^{1/\gamma}\right\} \tag{5.6}$$

The three parameters, α, β, and γ, are chosen such that the best fit of equation 5.6 to the observed data is obtained in the tail region of the distribution. Thus, the following sum of squared error (*SSE*) should be minimized.

$$SSE(\alpha,\beta,\gamma) = \sum_{i \in T}\left[\frac{\frac{1}{1-F(x_i \mid \alpha,\beta,\gamma)} - \frac{1}{1-p_i}}{\frac{1}{1-F(x_i \mid \alpha,\beta,\gamma)}}\right]^2 \tag{5.7}$$

where p_i is the probability of not exceeding the threshold value calculated using the observed data, and T is the tail region of the distribution. The type of extreme value distribution is determined by the choice of γ: for $\gamma = 0$, equation 5.6 reduces to a type I distribution; for $\gamma < 0$, equation 5.6 reduces to a type II distribution; and for $\gamma > 0$, equation 5.6 reduces to a type III distribution. The values of α, β, and γ that minimized equation 5.7 for each response quantity and each frame are given in table 5.2. More details of the generalized extreme value distribution are given in Maes and Breitung (1993).

Although the points shown in figure 5.11 calculated using equation 5.5 for the Dual–level frame (i.e. the squares) remain almost entirely below the points for the NEHRP frame (i.e. the triangles), the fitted extreme value distributions indicate that the Dual–level frame exhibits a lower probability of exceedance than the NEHRP frame only for $0.15 < DI < 0.75$. However, since the generalized extreme value distribution discussed above is fitted to the tail region, these distributions should not be used to imply the reliability of the frames for small damage indices. Furthermore, none of the Northridge records result in a damage index large enough to exceed a threshold of DI = 0.8 for the Dual–level frame and DI = 1.0 for the NEHRP frame. Therefore, no data for damage indices above these threshold values were included in the fitting of the extreme value distributions, and thus, the fitted distributions should be used with caution when evaluating the reliability of the Dual–level and NEHRP frames above DI = 0.8 and DI =1.0, respectively.

The histograms and probabilities of exceedance, considering the effect of epicentral distance, for the global drifts are shown in figures 5.12 and 5.13, respectively. Figure 5.13 has been provided on a log scale to avoid the congestion of points with very low probabilities of exceedance. The same trends can be observed that were noted for figures 5.4 and 5.5 (i.e. (1) the histogram of global drifts for the Dual–level frame is more skewed to the left (i.e. low global drifts) than the histogram of global drifts for the NEHRP frame; and (2) the probability of exceedance for the Dual–level frame is consistently below the probability of exceedance for the NEHRP frame, indicating that the Dual–level frame is a better design if the engineer wishes to limit the global drift of the structure). Once again, the extreme value distributions should not be used to imply the reliability of the frames at very low global drift levels.

It should be noted that the difference in the probabilities of exceedance for the two frames at high global drift levels (i.e. GD > 1.0%) decreases significantly when the effect of epicentral distance is considered (i.e. the difference in the probabilities of exceedance calculated without considering the epicentral distances is approximately 6 times the difference in the probabilities of exceedance when the epicentral distances are considered). This effect of considering the epicentral distances in equation 5.5 may be explained by observing the distribution of the epicentral distances for each station versus the assumed uniform distribution discussed previously, as shown in figure 5.14. The highest response quantities, and thus, the greatest difference between the two designs, will result from the stations closest to the epicenter. However, these stations are over–represented in the sample from the Northridge earthquake, and therefore, the probabilities of exceedance calculated without considering the epicentral distances (figure 5.5) will over–estimate the difference between the two designs at high response levels. By including the uniform distribution of epicentral distances in equation 5.5, the over–representation of the near field stations is compensated for. The resulting probabilities of exceedance for the two design are closer together at high response levels (see figure 5.13) since the most severe records (i.e. the closest stations) are given less weight in the calculation of the probabilities of exceedance (see equation 5.5).

The histograms and probabilities of exceedance, considering the effect of epicentral distance, for the local drifts are shown in figures 5.15 and 5.16, respectively. Once again, figure 5.16 has been provided on a log scale to avoid the congestion of points with very low probabilities of exceedance. As with the global drifts, the probability of exceedance for the Dual–level frame is consistently above the probability of exceedance for the NEHRP frame, indicating the Dual–level frame is a better design if the engineer wishes to limit the local drift of the structure. However, the difference in the left–skewness of the local drift histograms is not as obvious as for the global drifts. The probability of exceedance at low drift levels (i.e. $0.25\% < LD < 1.0\%$) appears to decrease considerably when the effect of the epicentral distance is considered. Similar to the global drifts, the difference in the probabilities of exceedance for the two frames decreases at high local drift levels (i.e. $LD > 2.0\%$) when the effects of epicentral distance are considered (i.e. the difference in the probabilities of exceedance calculated without considering the epicentral distances is approximately 5 times the difference in the probabilities of exceedance when the epicentral distances are considered). As discussed above for the global drifts, this effect of considering the epicentral distances in equation 5.5 may be explained by observing the distribution of the epicentral distances for each station versus the assumed uniform distribution, as shown in figure 5.14.

Figures 5.10–5.16 and the above discussion suggest that when the epicentral distance is considered, the probabilities of exceedance for both frames are lower than when the distribution of the epicentral distances is ignored. Although the Dual–level frame still has a lower probability of exceedance than the NEHRP frame when the epicentral distance is considered, the difference between the probabilities for the two frames decreases particularly at high response quantities. It must be remembered that the calculated reliabilities assume the occurrence of a Northridge type earthquake (i.e. $M \approx 6.7$ on a blind thrust fault).

5.2.3 Effect of the Choice of R_{max}

To determine if the choice of $R_{max} = 100$ km provides a large enough sample area to accurately estimate the probabilities of exceedance, $R_{max} = 50$ km shall be used and the resulting probabilities compared to those obtained when $R_{max} = 100$ km is used. The ratios of the probabilities of excee-

dance calculated using R_{max} = 50 km and R_{max} = 100 km are shown in figure 5.17. For DI > 0.2, GD > 0.8%, and LD > 1.0%, the ratio is exactly 4.0. This illustrates that R_{max} = 100 km is large enough to provide a good estimate of the probabilities of exceedance, since if R_{max} is decreased to 50 km (i.e. the sample area is decreased by 4), then the probabilities of exceedance should increase by 4. Similarly, if the probability of occurrence of a Northridge type earthquake (i.e. M≈6.7 on a blind thrust fault) was found assuming a uniform spatial distribution of such earthquakes within the sample area, then the probability of occurrence should be approximately 4 times greater for R_{max} = 100 km than for R_{max} = 50 km. Therefore, the factors of 4 will cancel out when the final probabilities of exceedance, considering the probability of earthquake occurrence, are computed.

As shown in figures 5.17(b) and 5.17(c), at low drifts the ratio of probabilities of exceedance for R_{max} = 50 km and R_{max} = 100 km are less than 4.0. This discrepancy deserves some attention here. For very small drifts, the probabilities of exceedance are nearly the same for both R_{max} = 50 km and R_{max} = 100 km since the drift resulting from a large earthquake will always exceed some small finite value. Therefore, the ratio is close to unity. As the drift considered is increased, the probability of exceedance within R_{max} = 50 km will increase faster than that for R_{max} = 100 km, and therefore, the ratio will increase steadily until 4.0 is reached. If R_{max} is increased to 200 km and compared to 100 km then the slope of the initial portion in figures 5.17(b) and 5.17(c) will be steeper since 200 km will be good enough for still smaller global and local drifts. Note that the Dual–level frame curves in figures 5.17(b) and 5.17(c) are steeper since the finite drift that will be exceeded at both 100 km and 50 km is less than the finite drift exceeded by the NEHRP frame.

Table 5.1: Ground Motion Records and Response Quantities

#	Station Name	Comp.	PGA (g)	Epicnt. Dist. (km)	NEHRP Frame			Dual–Level Frame		
					DI[1]	GD[2]	LD[3]	DI[1]	GD[2]	LD[3]
37	Tarzana Cedar Hill Nursery	090	1.82	5	0.62	1.31	2.68	0.51	1.31	1.96
		360	1.06	5	0.69	1.46	2.56	0.76	1.18	2.44
3	Arleta Nordhoff Ave. Fire Sta.	090	0.35	10	0.2	0.71	1.12	0.15	0.67	0.88
		360	0.29	10	0.1	0.71	0.89	0.02	0.52	0.63
36	Sylmar County Hosp. Park. Lot	090	0.61	16	0.65	1.12	2.03	0.49	1.51	2.05
		360	0.91	16	0.98	1.71	3.11	0.78	1.23	2.18
18	Los Angeles UCLA Grounds	090	0.32	18	0	0.30	0.50	0	0.36	0.51
		360	0.66	18	0.3	0.85	1.35	0.2	0.51	0.83
28	Pacoima Kagel Canyon	090	0.3	18	0.27	0.69	1.29	0.09	0.64	0.91
		360	0.44	18	0.25	0.82	1.13	0.14	0.60	0.85
42	Pacoima Dam Downstream	175	0.42	19	0.08	0.29	0.85	0.14	0.34	0.73
		265	0.44	19	0.04	0.38	0.62	0.05	0.50	0.67
41	Pacoima Dam Upper Left Abutment	104	1.22	19	0.26	0.50	1.27	0.16	0.64	1.01
		194	1.53	19	0.49	1.11	2.32	0.3	1.06	1.62
6	Century City LACC North	090	0.27	20	0.08	0.61	0.84	0.12	0.52	0.70
		360	0.24	20	0.06	0.56	0.75	0.1	0.55	0.68
26	Newhall LA County Fire Sta.	090	0.63	20	0.42	1.04	1.81	0.39	0.78	1.46
		360	0.61	20	0.89	1.79	2.65	0.65	1.15	1.99
34	Santa Monica City Hall Grounds	090	0.93	23	0.42	1.06	1.86	0.25	0.67	1.02
		360	0.42	23	0.2	0.73	1.07	0.15	0.58	0.76
13	Los Angeles Baldwin Hills	090	0.24	28	0.09	0.62	0.84	0	0.36	0.47
		360	0.27	28	0	0.44	0.55	0.04	0.49	0.60
16	Los Angeles Pico & Sentous	090	0.1	31	0	0.38	0.48	0	0.23	0.31
		180	0.19	31	0	0.21	0.36	0	0.22	0.30
17	Los Angeles Temple & Hope	090	0.13	32	0	0.34	0.51	0	0.33	0.44
		180	0.19	32	0	0.22	0.48	0	0.35	0.46
21	Malibu Point Dume	090	0.13	32	0	0.30	0.39	0	0.18	0.25
		360	0.1	32	0	0.39	0.52	0	0.19	0.25
22	Moorpark	090	0.3	33	0.06	0.43	0.68	0	0.40	0.54
		180	0.19	33	0.03	0.47	0.71	0	0.39	0.50
19	Los Angeles Univ. Hosp. Grounds	005	0.49	36	0	0.13	0.50	0.03	0.28	0.58
		095	0.22	36	0	0.14	0.26	0	0.18	0.28

#	Station Name	Comp.	PGA (g)	Epicnt. Dist. (km)	NEHRP Frame			Dual–Level Frame		
					DI[1]	GD[2]	LD[3]	DI[1]	GD[2]	LD[3]
40	Vasquez Rocks Park	090	0.15	37	0	0.24	0.36	0	0.18	0.28
		360	0.16	37	0	0.34	0.49	0	0.26	0.45
14	Los Angeles City Terrace	090	0.26	38	0	0.20	0.33	0	0.26	0.34
		180	0.32	38	0	0.22	0.35	0	0.32	0.46
1	Alhambra Fremont School	090	0.12	39	0	0.18	0.27	0	0.26	0.34
		360	0.09	39	0	0.17	0.21	0	0.11	0.15
15	Los Angeles Obregon Park	090	0.36	39	0	0.24	0.40	0	0.24	0.36
		360	0.42	39	0	0.22	0.55	0.01	0.34	0.58
9	Lake Hughes 12A	090	0.18	40	0	0.20	0.25	0	0.09	0.14
		180	0.26	40	0	0.19	0.22	0	0.11	0.16
20	Los Angeles 116th St. School	090	0.2	41	0	0.33	0.47	0	0.21	0.30
		360	0.15	41	0	0.24	0.31	0	0.13	0.21
5	Castaic Old Ridge Route	090	0.59	41	0.36	1.05	1.76	0.25	0.82	1.07
		360	0.54	41	0.5	1.11	1.78	0.32	0.93	1.59
8	Lake Hughes #9	090	0.24	44	0	0.13	0.18	0	0.08	0.13
		360	0.17	44	0	0.12	0.19	0	0.09	0.16
24	Mt. Wilson Caltech Seismic Sta.	090	0.14	45	0	0.07	0.11	0	0.07	0.09
		360	0.23	45	0	0.07	0.11	0	0.09	0.15
4	Camarillo	180	0.12	50	0	0.41	0.52	0	0.39	0.50
		270	0.11	50	0	0.36	0.44	0.11	0.52	0.66
32	Rolling Hills Estates Rancho Vista School	090	0.12	50	0	0.09	0.16	0	0.11	0.21
		360	0.11	50	0	0.08	0.15	0	0.09	0.11
2	Anaverde Valley City Ranch	090	0.04	52	0	0.16	0.21	0	0.08	0.12
		180	0.06	52	0	0.19	0.28	0	0.09	0.14
7	Elizabeth Lake	090	0.16	52	0	0.13	0.24	0	0.12	0.16
		180	0.11	52	0	0.20	0.36	0	0.16	0.22
30	Point Mugu Naval Air Station	090	0.17	54	0	0.44	0.56	0	0.26	0.33
		360	0.19	54	0	0.23	0.46	0	0.20	0.27
12	Long Beach City Hall Grounds	090	0.06	58	0	0.22	0.30	0	0.14	0.18
		360	0.06	58	0	0.12	0.17	0	0.10	0.13
11	Littlerock Brainard Canyon	090	0.07	60	0	0.08	0.17	0	0.07	0.12
		180	0.06	60	0	0.15	0.20	0	0.07	0.09

#	Station Name	Comp.	PGA (g)	Epicnt. Dist. (km)	NEHRP Frame			Dual–Level Frame		
					DI[1]	GD[2]	LD[3]	DI[1]	GD[2]	LD[3]
33	Sandberg Bald Mountain	090	0.09	62	0	0.23	0.39	0	0.16	0.22
		180	0.1	62	0	0.15	0.23	0	0.10	0.17
10	Lancaster Fox Airfield Grounds	090	0.07	66	0	0.19	0.25	0	0.17	0.22
		360	0.09	66	0	0.27	0.34	0	0.20	0.26
35	Seal Beach Office Bld. Parking Lot	000	0.09	66	0	0.16	0.21	0	0.10	0.13
		090	0.06	66	0	0.19	0.23	0	0.14	0.17
38	Ventura Harbor & California	090	0.06	70	0	0.30	0.37	0	0.37	0.50
		360	0.07	70	0	0.41	0.51	0	0.30	0.40
25	Neenach Sacatara Creek	090	0.06	71	0	0.36	0.44	0	0.17	0.27
		180	0.07	71	0.08	0.62	0.78	0	0.26	0.36
23	Mt. Baldy Elementary School	090	0.08	81	0	0.04	0.10	0	0.04	0.08
		180	0.07	81	0	0.03	0.09	0	0.04	0.08
39	Wrightwood Swarthwood Valley	090	0.05	83	0	0.06	0.12	0	0.05	0.09
		180	0.06	83	0	0.05	0.09	0	0.03	0.06
27	Newport Beach Newport & Coast Hwy.	090	0.11	86	0	0.18	0.26	0	0.11	0.14
		180	0.08	86	0	0.17	0.22	0	0.10	0.13
31	Rancho Cucamonga Deer Canyon	090	0.07	89	0	0.08	0.12	0	0.06	0.07
		180	0.05	89	0	0.05	0.11	0	0.07	0.10
29	Phelan Wilson Ranch Road	090	0.05	98	0	0.18	0.23	0	0.06	0.09
		180	0.06	98	0	0.13	0.17	0	0.08	0.11

[1]DI = Overall Frame Damage Index (where 0 indicates elastic response – see section 4.1)

[2]GD = Global Drift (roof displacement / building height x 100)

[3]LD = Maximum Local Drift (maximum interstory displacement / story height x 100)

Table 5.2: Parameters Chosen for Tail Biased Generalized Extreme Value Distributions

Parameters	Damage Index		Global Drift		Local Drift	
	NEHRP frame	Dual–level frame	NEHRP frame	Dual–level frame	NEHRP frame	Dual–level frame
α	–1.028	–0.055	0.084	–0.012	0.035	0.129
β	0.481	0.023	0.163	0.140	0.256	0.132
γ	0.108	–0.671	–0.237	–0.262	–0.289	–0.350

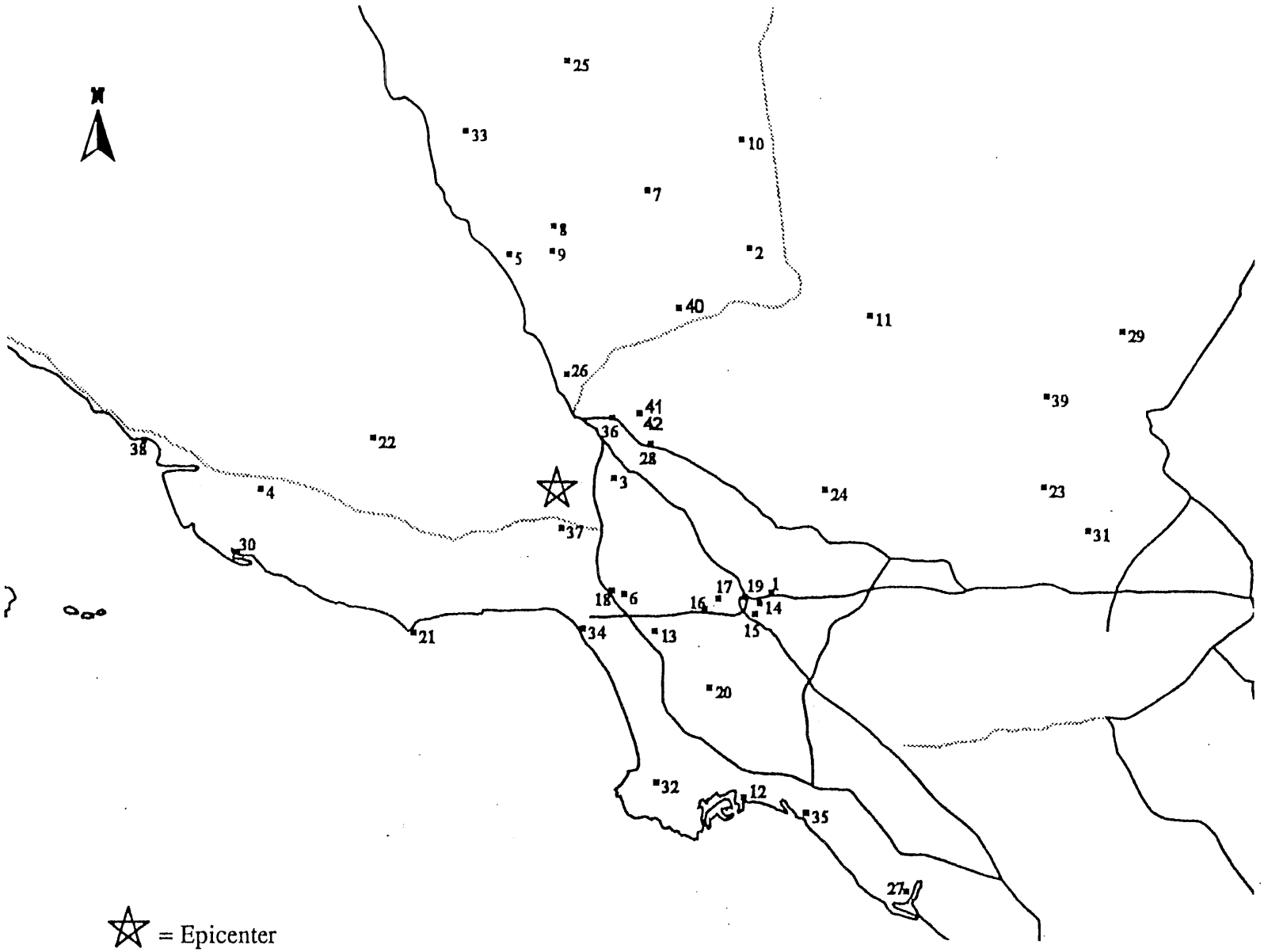

Figure 5.1: Distribution of Strong Ground Motion Stations from 1994 Northridge Earthquake

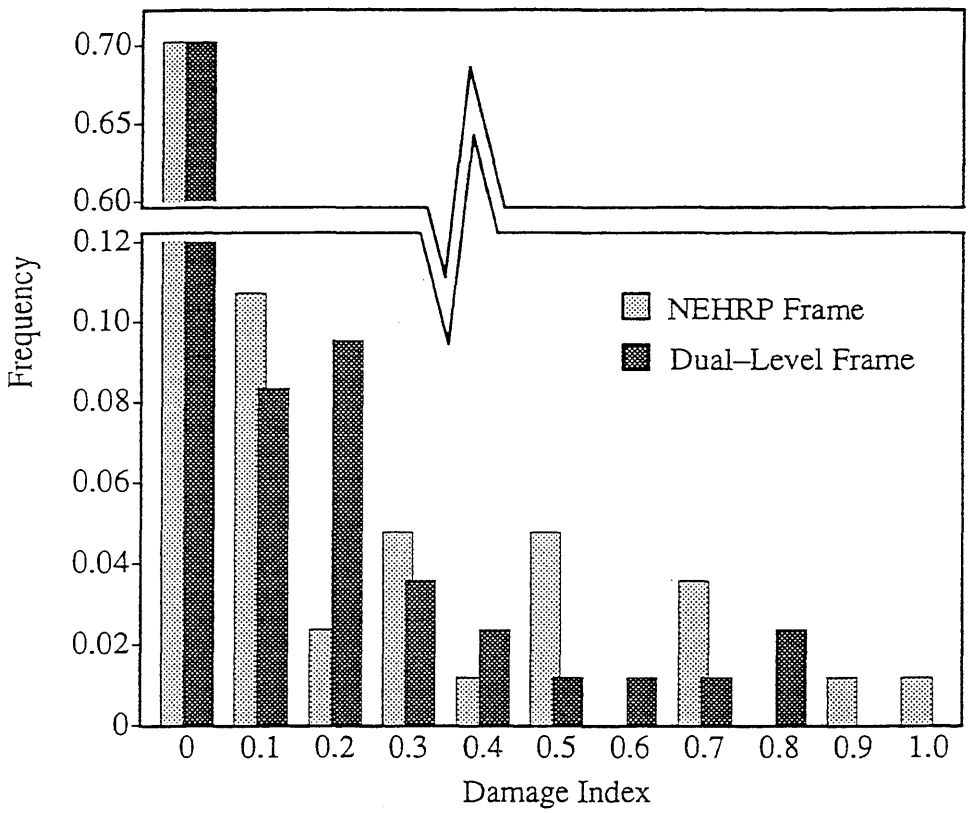

Figure 5.2: Histogram of Damage Indices

(note: DI = 0 indicates elastic response)

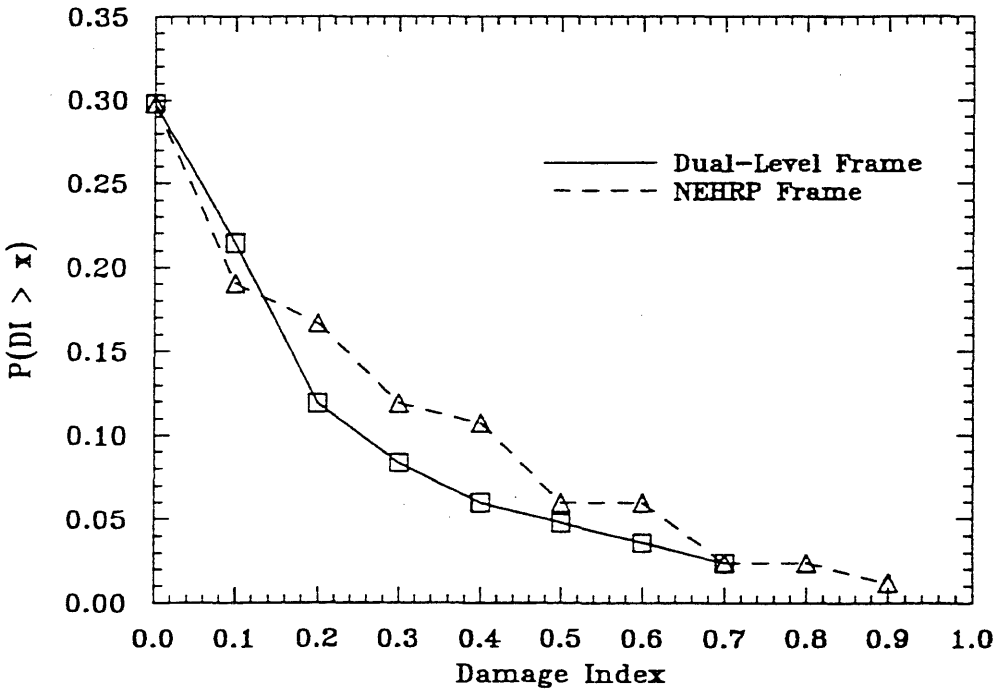

Figure 5.3: Probability of Exceedance for Damage Indices

(note: DI = 0 indicates elastic response)

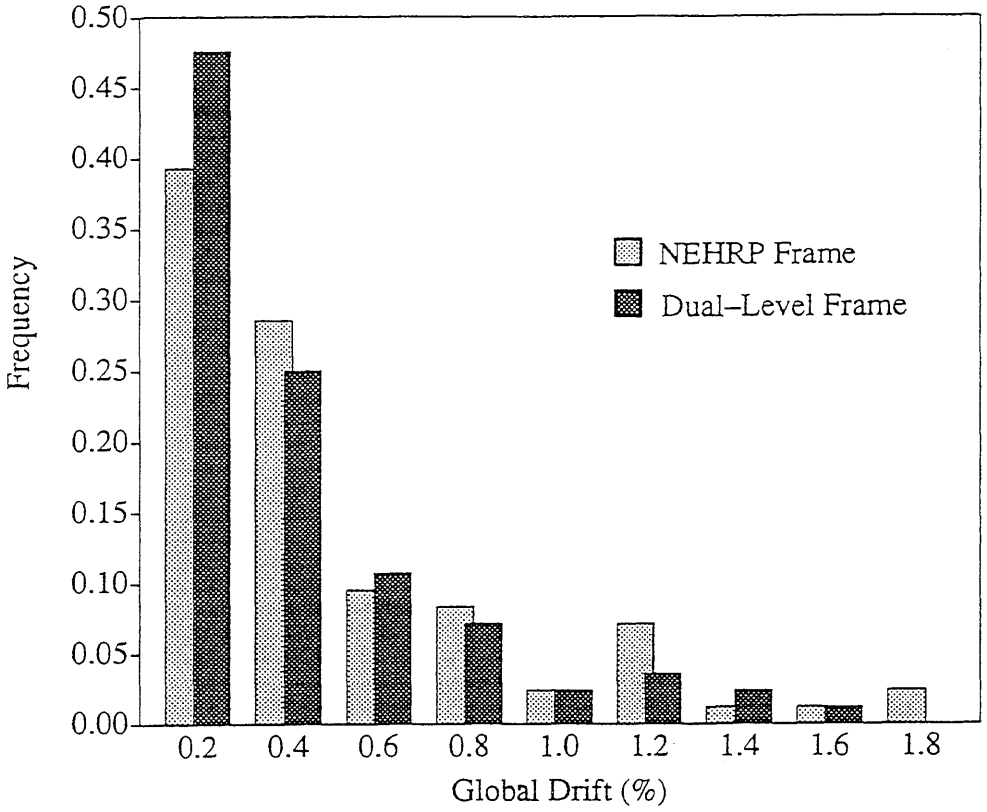

Figure 5.4: Histogram of Global Drifts

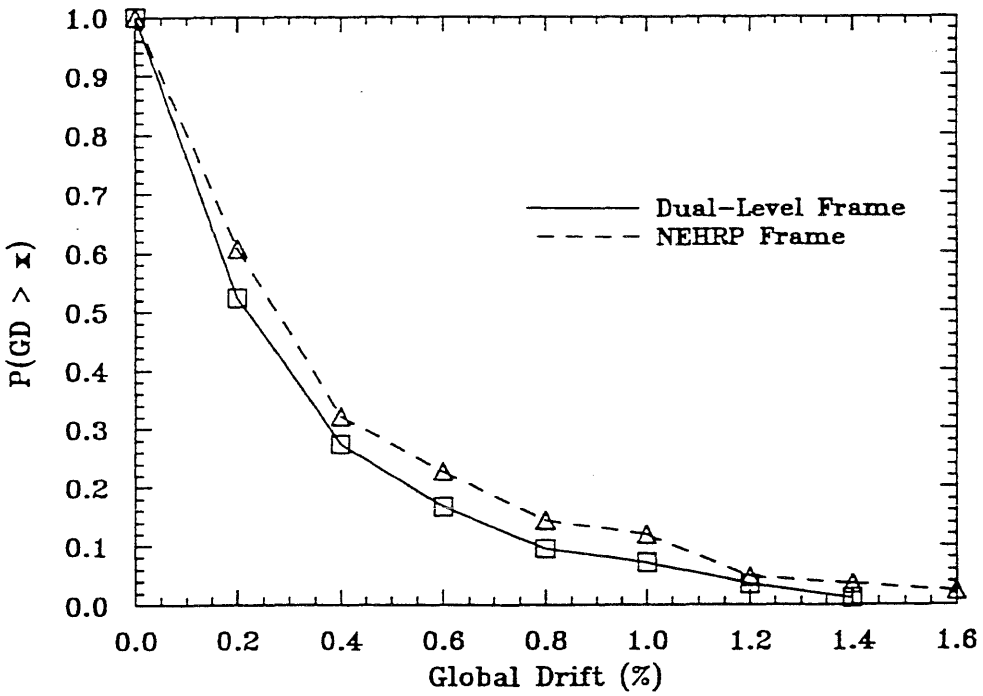

Figure 5.5: Probability of Exceedance for Global Drifts

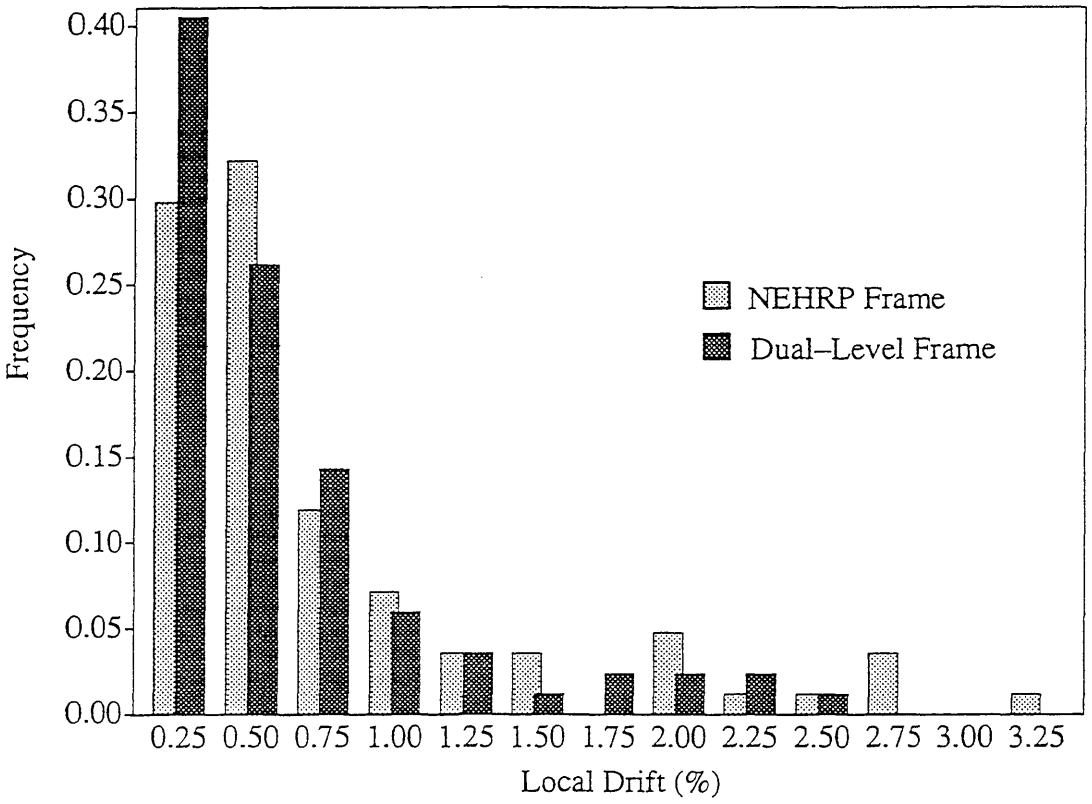

Figure 5.6: Histogram of Local Drifts

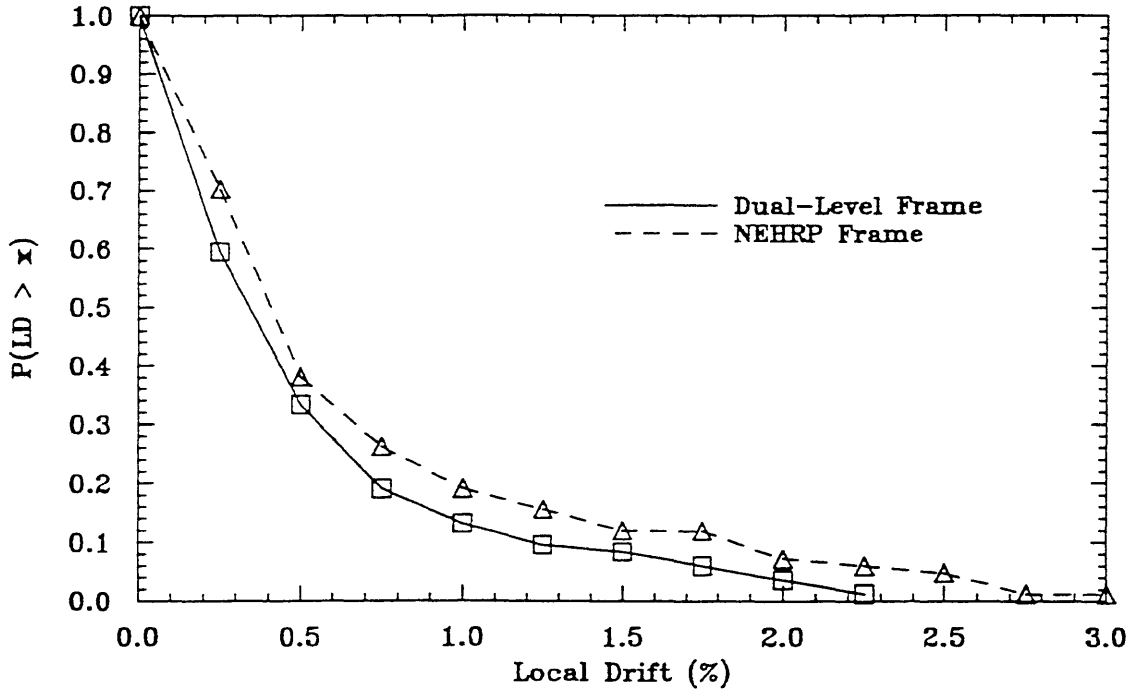

Figure 5.7: Probability of Exceedance for Local Drifts

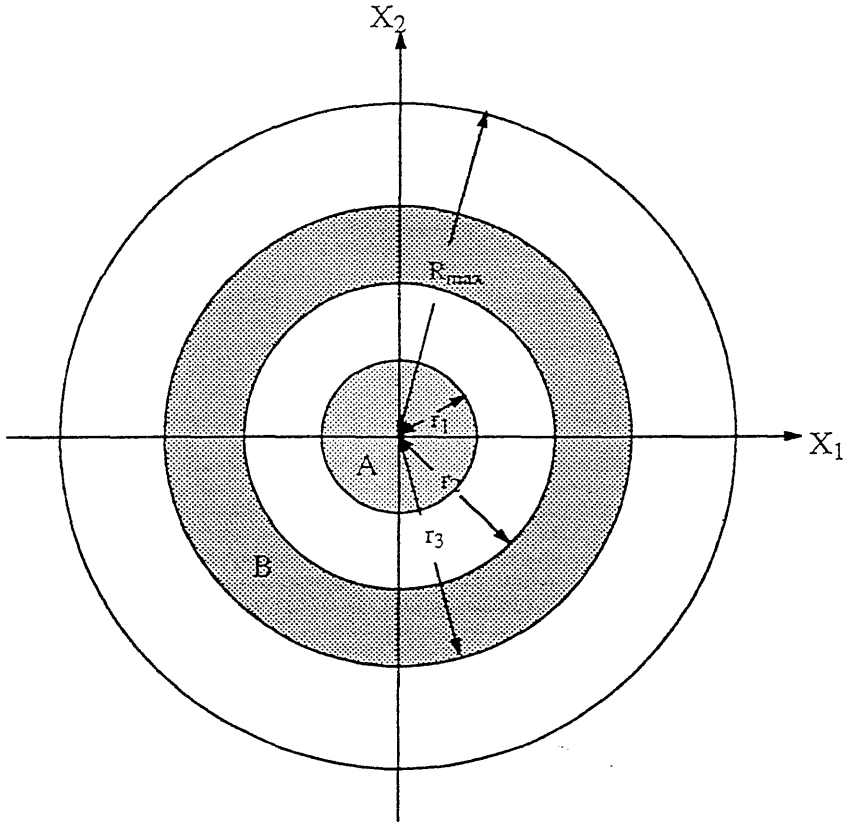

Figure 5.8: Reference Area of Radius R_{max}

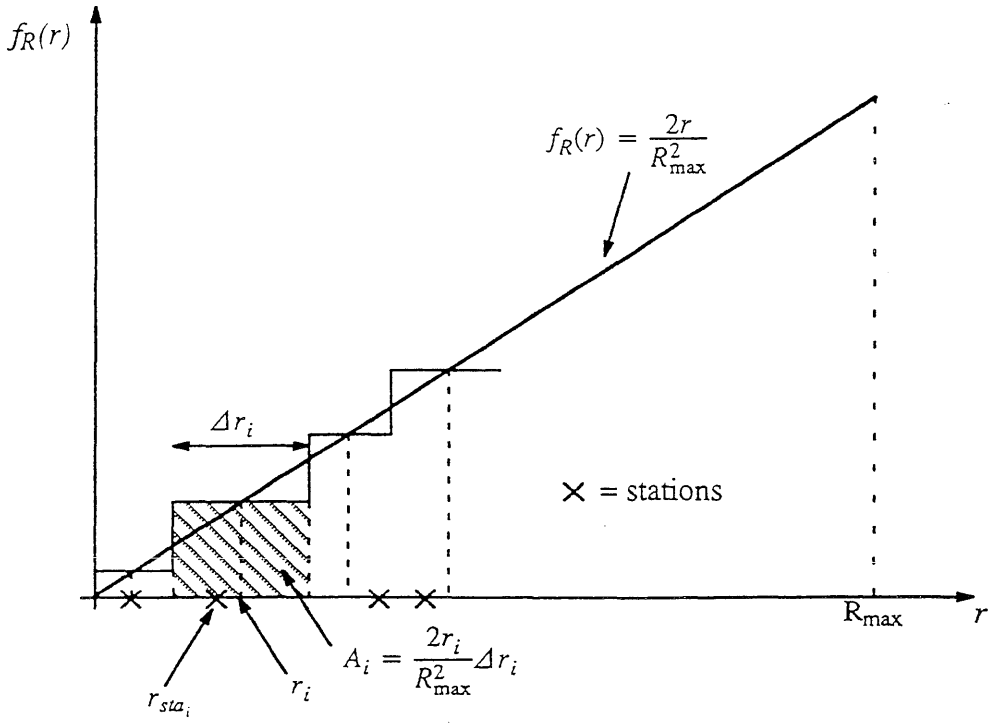

Figure 5.9: Numerical Integration of Equation 5.3

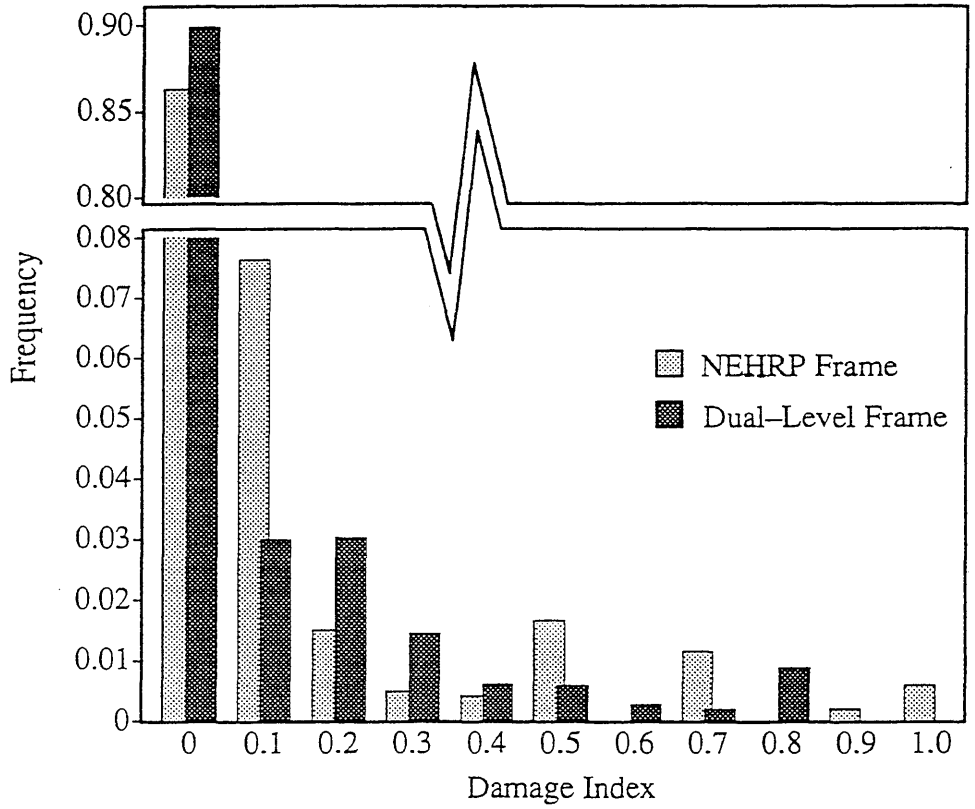

Figure 5.10: Histogram of Damage Indices Considering Effect of Epicentral Distance

(note: DI = 0 indicates elastic response)

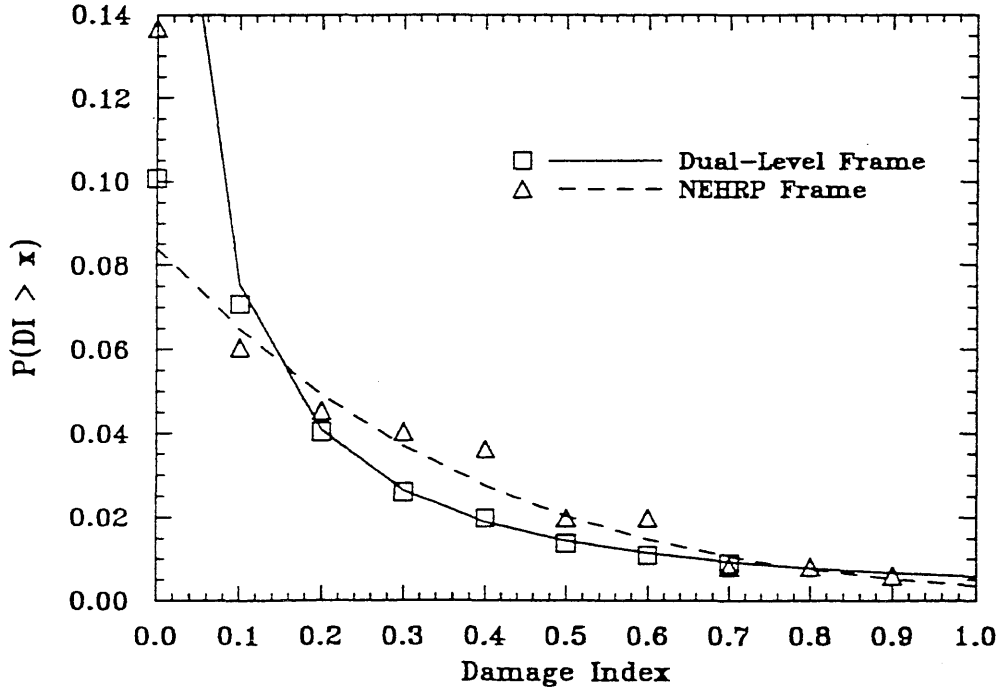

Figure 5.11: Probability of Exceedance for Damage Indices Considering Effect of Epicentral Distance and Fitted with Tail Biased Generalized Extreme Value Distributions

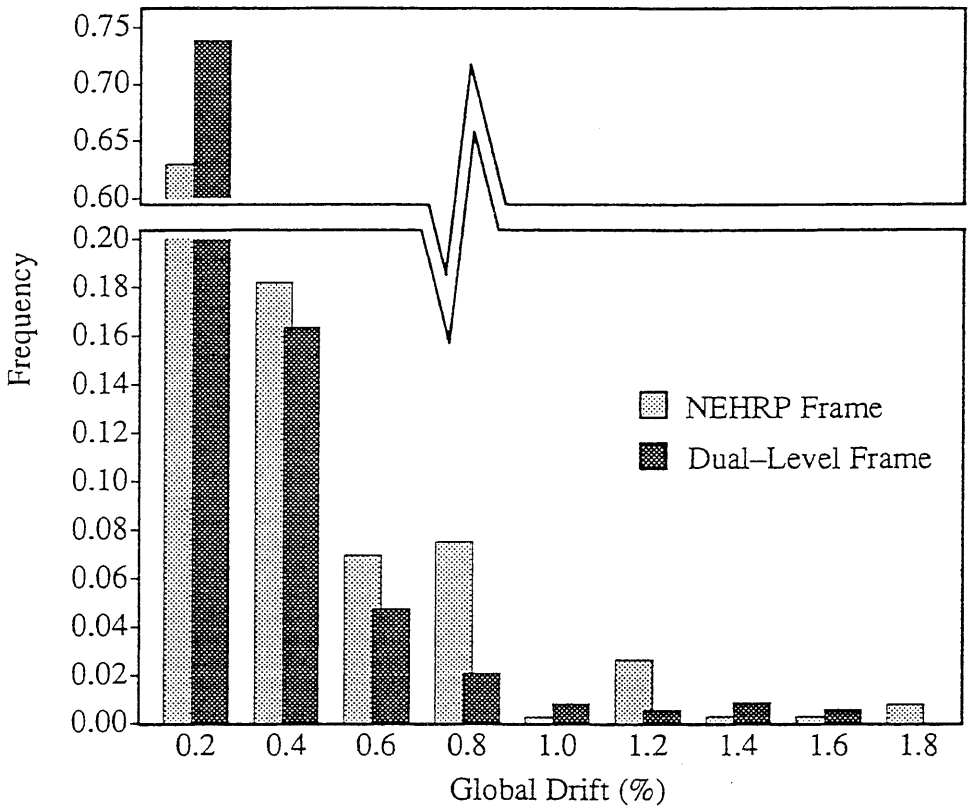

Figure 5.12: Histogram of Global Drifts Considering Effect of Epicentral Distance

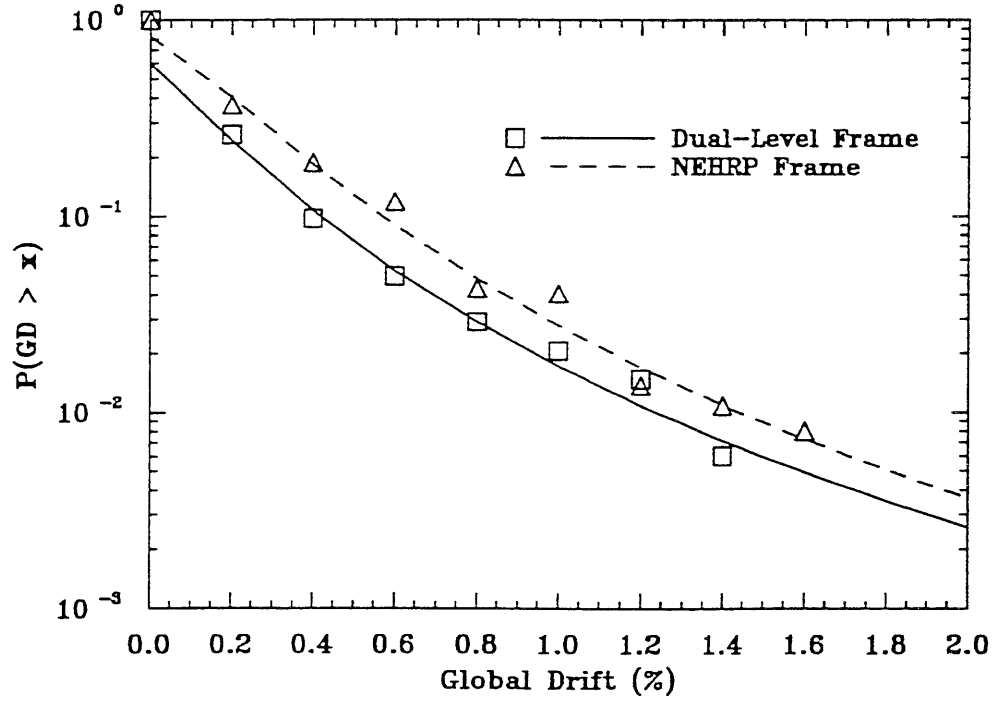

Figure 5.13: Probability of Exceedance for Global Drift Considering Effect of Epicentral Distance and Fitted with Tail Biased Generalized Extreme Value Distributions

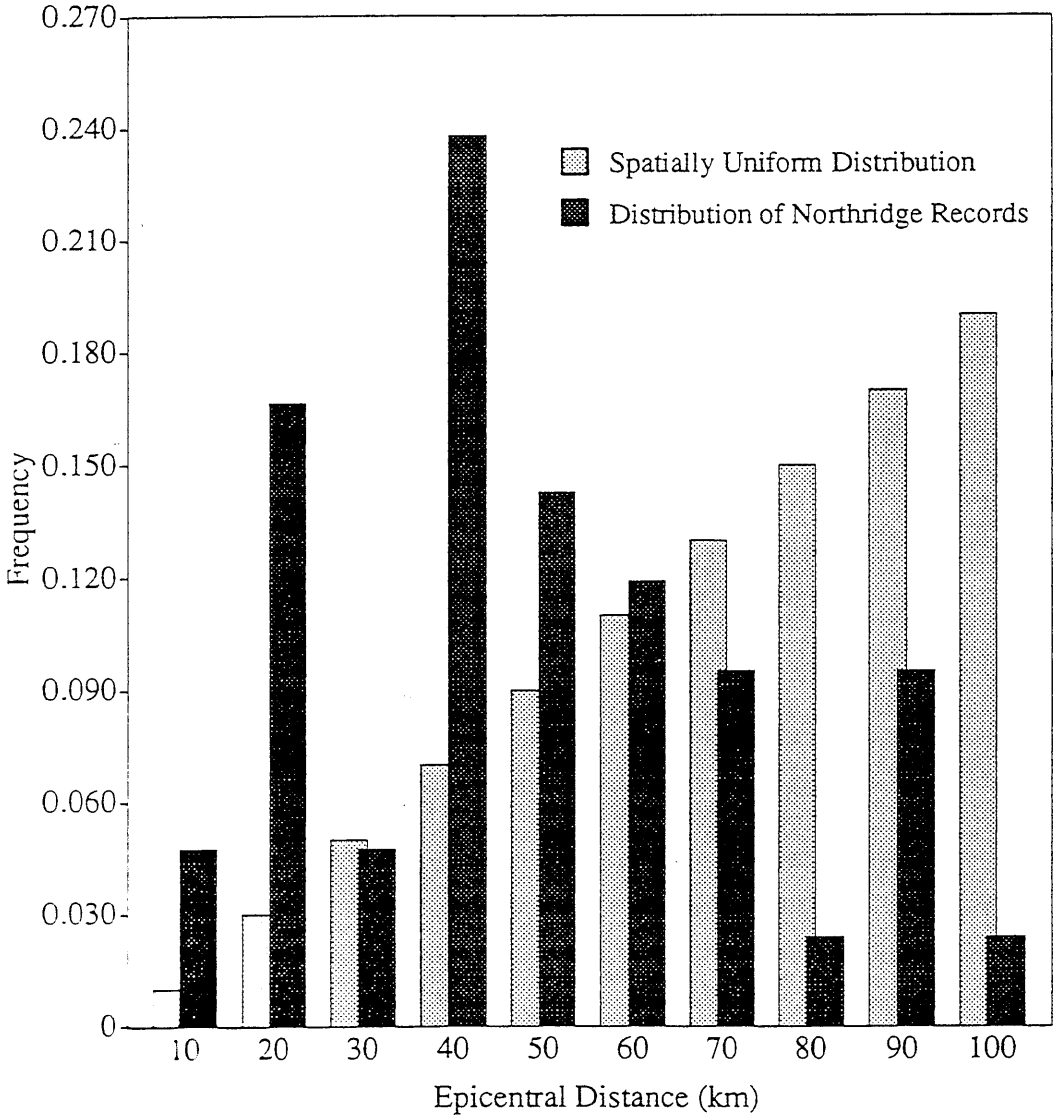

Figure 5.14: Histograms of Epicentral Distances

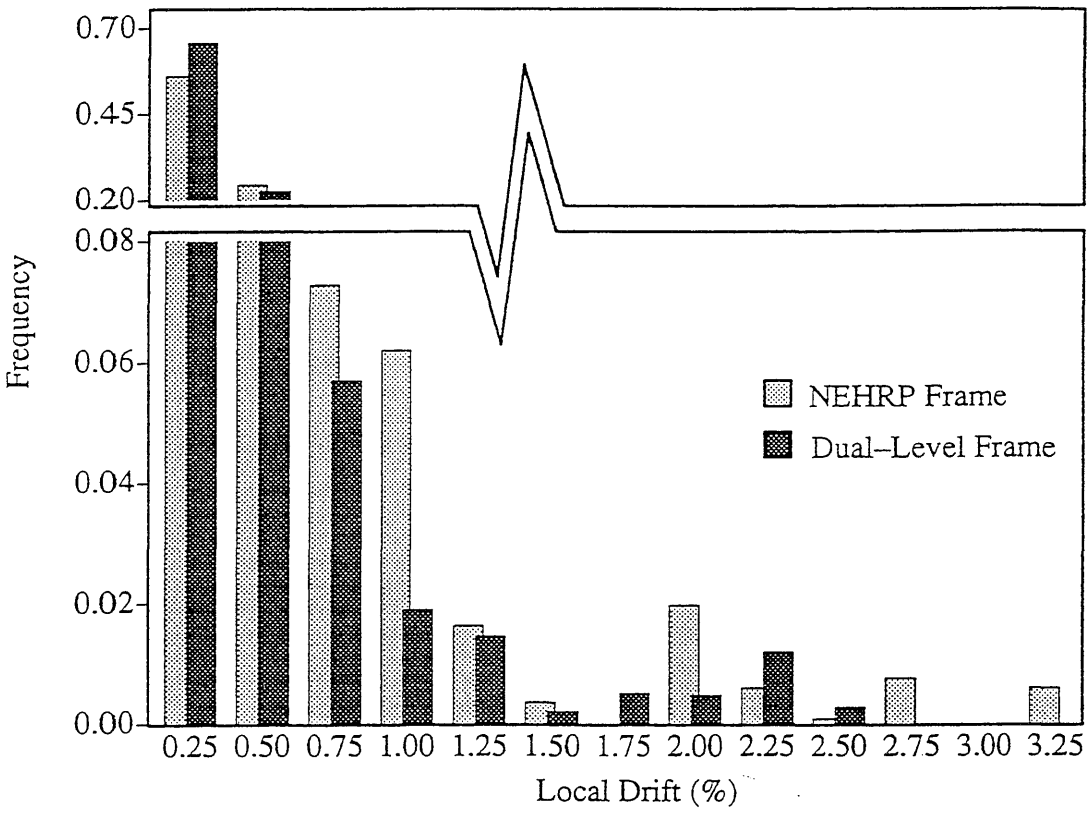

Figure 5.15: Histogram of Local Drifts
Considering Effect of Epicentral Distance

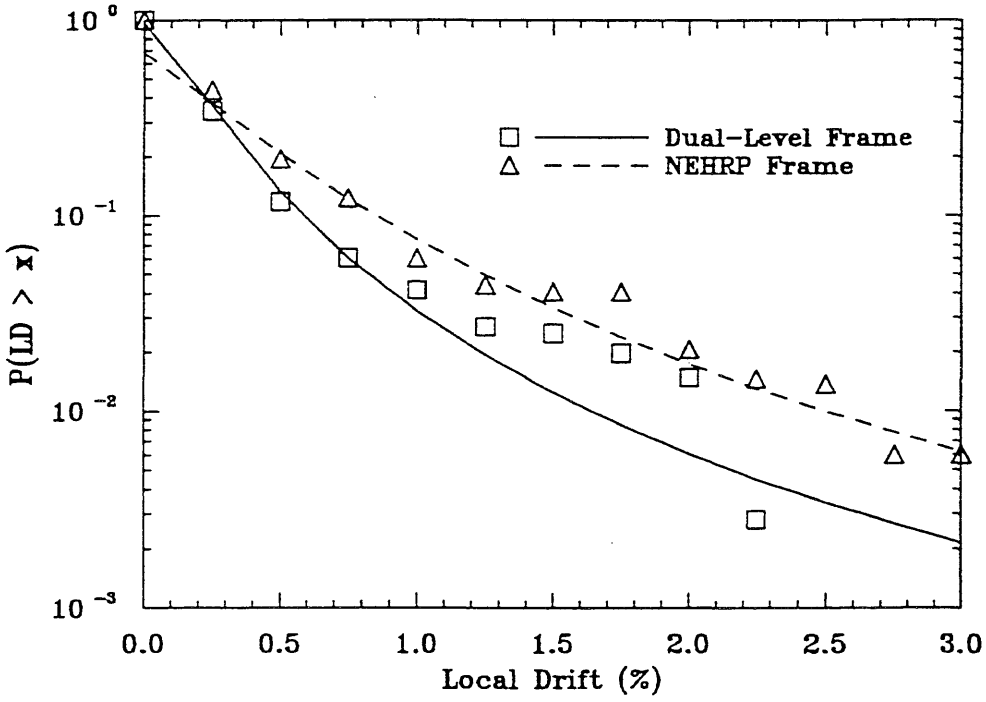

Figure 5.16: Probability of Exceedance for Local Drift
Considering Effect of Epicentral Distance and
Fitted with Tail Biased Generalized Extreme Value Distributions

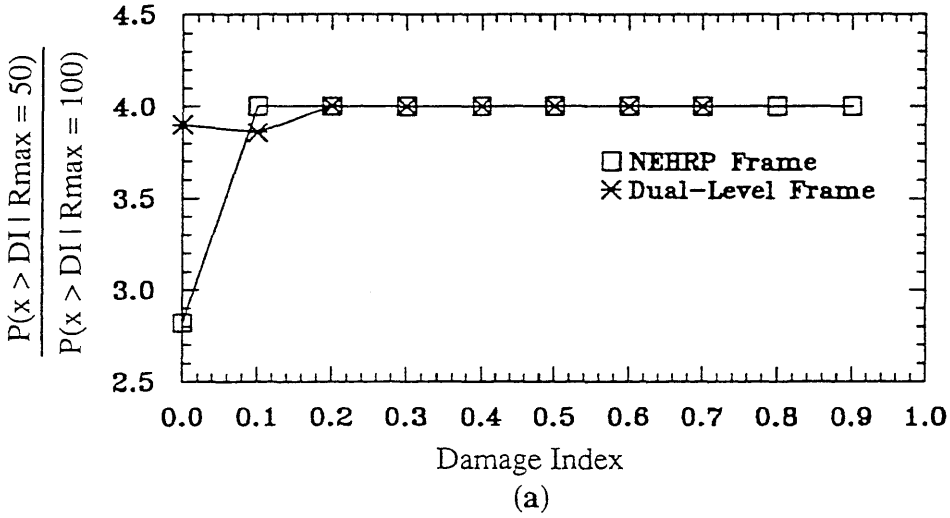

(a)

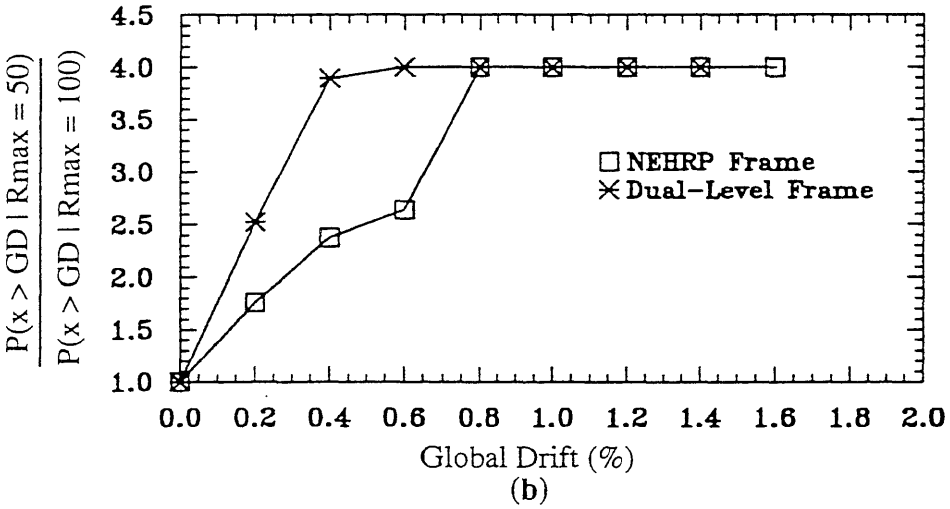

(b)

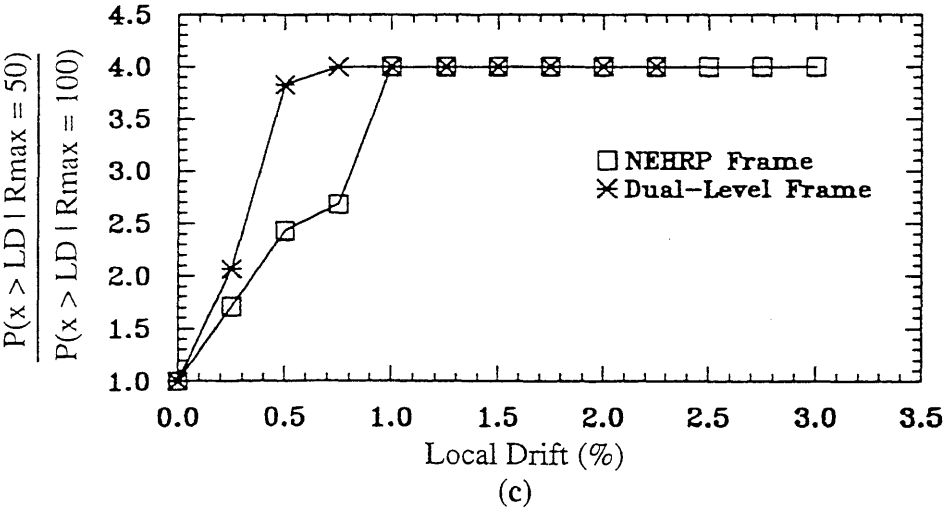

(c)

Figure 5.17: Ratios of Probabilities of Exceedance for R_{max} = 50 km and R_{max} = 100 km

CHAPTER 6

SUMMARY AND CONCLUSIONS

6.1 Summary

The performance of a RC building designed in accordance with a Dual–level seismic design procedure is evaluated using 1994 Northridge earthquake records. This design procedure requires the building to be designed for both an ultimate and a serviceability force level. Furthermore, the performance under both force levels must be evaluated using a nonlinear pushover analysis. The return periods for the ultimate and serviceability design earthquakes were chosen as 475 and 10 years, respectively. Under the serviceability force level the building should remain elastic, while under the ultimate force level limited inelastic response is allowed. For the purpose of comparison, the performance of a similar building designed according to the 1991 NEHRP provisions is also evaluated.

The proposed Dual–level design procedure resulted in a frame with a fundamental period of only 1.47 seconds, while the NEHRP design exhibited a fundamental period of 2.12 seconds. Thus, the relative response of the two designs varied depending on the characteristics of the ground motion. For example, for the most severe records (i.e. Sylmar County Hospital and Newhall Fire Station), the global drift of the NEHRP design was approximately 1.5 times the global drift of the Dual–level design. On the other hand, for less severe records where both frames remained nearly elastic, the maximum roof displacements of the Dual–level design were nearly the same or greater than the those of the NEHRP design.

It should also noted that although both frames were designed according to the strong–column– weak–beam requirement of the ACI building code, the Dual–level design exhibited the desired collapse mechanism during severe excitation, while the NEHRP design often formed a weak story collapse mechanism. This difference can be attributed to the performance check required by the Dual–level design procedure at the ultimate force level.

Using the extensive number of strong ground motion records available from the 1994 Northridge earthquake, the reliabilities of the NEHRP and Dual–level designs given the occurrence of an event similar to the Northridge earthquake (i.e. M ≈ 6.7 on a blind thrust fault) were evaluated. The overall frame damage indices, global drifts, and local drifts were chosen as the response quantities to measure the performance of the structures. A method was developed to account for the effect of random epicentral distances in the reliability calculations.

6.2 Conclusions

The Dual–level design procedure results in better drift control for severe ground motions that force the building into the inelastic range. Thus, excessive structural and non–structural damage may be avoided, and with little or no interruption to the building occupation after the earthquake. Furthermore, under small and moderate ground motions the Dual–level design remains nearly elastic, while under severe ground motions a soft story collapse is avoided; thus, the design comes closer to attaining the desired design philosophy stated in most current building codes.

The reliability (i.e. the probability of not exceeding given response thresholds) of the Dual–level design is consistently higher than the reliability of the NEHRP design for each of the response quantities considered. In other words, for the same probability level, the response or damage index of the Dual–level frame is much smaller than that of the NEHRP frame. The difference between the reliabilities of the two frames is much larger when the effect of distribution of epicentral distance is not considered, reflecting the over–representation of near–source stations in the ground motion records.

The reliabilities of the two designs given the occurrence of a future event similar to the Northridge earthquake (i.e., M≈6.7 on a blind thrust fault) within a circular area with a radius of 100 km, are (Fig. 5.13 and Fig. 5.16):

For the Dual–level design:

- the probability of exceeding a global drift of 1.5% is approximately 0.003
- the probability of exceeding a global drift of 0.5% is approximately 0.075
- the probability of exceeding a local drift of 2.0% is approximately 0.006

- the probability of exceeding a local drift of 0.5% is approximately 0.150

For the NEHRP design:

- the probability of exceeding a global drift of 1.5% is approximately 0.006
- the probability of exceeding a global drift of 0.5% is approximately 0.125
- the probability of exceeding a local drift of 2.0% is approximately 0.018
- the probability of exceeding a local drift of 0.5% is approximately 0.200

6.3 Recommendations for Future Research

Several aspects of the current study deserve further investigation.

- Appropriate values for the base shear reduction factor, K, must be investigated. This research could draw on recent studies by Uang (1992) and others to determine R_w and R factors for the UBC and NEHRP provisions.

- More realistic material models should be used to develop the moment–curvature and interaction diagrams. This could include considering strain hardening in the steel, and using a confinement model, such as the modified Kent and Park model (Park et al., 1982), for the concrete core.

- More advanced DRAIN–2DX elements currently under investigation should be used in the nonlinear dynamic model. Such elements could include a fiber model where the properties of the concrete and steel are considered separately and a stiffness degrading hysteresis can be included.

- The closest distance to the rupture surface should be used in the reliability calculations, in place of the epicentral distance. This may account for the high response values at stations in the north–west San Fernando valley.

- Directivity effects should be considered in the reliability calculations. This may be accomplished by including the distribution of the orientation of the path from the Northridge epicenter to the station under consideration. However, records must be generated for the regions where no real records are available.

LIST OF REFERENCES

ACI Committee 318 (1992). *Building Code Requirements for Reinforced Concrete (ACI 318–89) (Revised 1992)*, American Concrete Institute, Detroit, MI.

Allahabadi, R. and Powell, G.H. (1988). "DRAIN–2DX User Guide," *Report No. UCB/EERC–88/06*, University of California at Berkeley, Berkeley, CA.

Ang, A. H–S., and Tang, W. H. (1975). *Probability Concepts in Engineering Planning and Design: Volume I – Basic Principles*, John Wiley & Sons, New York, NY.

Ang, A. H–S., and Tang, W. H. (1984). *Probability Concepts in Engineering Planning and Design: Volume II – Decision, Risk, and Reliability*, John Wiley & Sons, New York, NY.

ATC (Applied Technology Council) (1986). "Comparison of Code Provisions," *Proceedings of Second U.S. – Japan Workshop on Improvement of Seismic Design and Construction Practices, ATC 15–1*.

Bertero, V. V., Anderson, J. C., Krawinkler H., and Miranda, E. (1991). "Design Guidelines for Ductility and Drift Limits," *Report No. UCB/EERC–91/15*, University of California at Berkeley, Berkeley, CA.

Bertero, R. D., and Bertero, V. V. (1992). "Tall Reinforced Concrete Buildings: Conceptual Earthquake–Resistant Design Methodology," *Report No. UCB/EERC–92/16*, University of California at Berkeley, Berkeley, CA.

BSSC (Building Seismic Safety Council) (1992). *NEHRP Recommended Provisions for the Development of Seismic Regulations for New Buildings (1991 Ed.)*, FEMA.

Clough, R. W. and Penzien, J. (1993). *Dynamics of Structures*, Second Ed., McGraw–Hill, New York, NY.

Collins, K. R., Wen, Y. K., and Foutch, D. A., (1995). "Investigation of Alternative Seismic Design Procedures for Standard Buildings," *Structural Research Series Report No. 600*, Department of Civil Engineering, University of Illinois at Urbana–Champaign, Urbana, IL.

Corley, W.G. (1966). "Rotational Capacity of Reinforced Concrete Beams," *Journal of the Structural Division*, ASCE, Vol. 92, No. ST5.

Cosenza, E., Manfredi, G., and Ramasco, R. (1993) "The Use of Damage Functionals in Earthquake Engineering: A Comparison Between Different Methods," *Earthquake Engineering and Structural Dynamics*, John Wiley & Sons, Vol. 22, pp. 855–868.

CSA (Canadian Standards Association) (1984). *Design of Concrete Structures for Buildings (CAN3–A23.3–M84)*, CSA, Toronto, ON.

EERI (Earthquake Engineering Research Institute) (1994). *Northridge Earthquake, January 17, 1994: Preliminary Reconnaissance Report*, EERI, Oakland, CA.

EQE International, Ltd. (1994) *The January 17, 1994 Northridge, California Earthquake*, EQE International, Ltd., San Francisco, CA.

Foutch, D.A., Yu, C. Y., and Wen, Y. K. (1992) "Reliability of Steel Frame Buildings Under Seismic Load," *Proceedings of Tenth World Conference on Earthquake Engineering*, Madrid, pp. 4423–4427.

French, C.W. and Moehle, J.P. (1991). "Effect of Floor Slab on Behavior of Slab–Beam–Column Connections," *ACI Special Publication SP 123*, ACI, Detroit, MI.

Goel, R.K., and Chopra, A.K. (1994). "Dual–Level Earthquake Resistant Design Approach for Asymmetric–Plan Buildings," *Proceedings of the Fifth U.S. National Conference on Earthquake Engineering*, EERI, V. 2, Chicago, IL, 253–262.

IGRESS–2 (1989). Interactive Graphic Environment for Steel Structures Analysis and Computer –Aided Design, *User's Manual*, Prairie Technologies Inc.

Kunnath, S.K., Reinhorn, A.M., and Park, Y.J. (1990). "Analytical Modeling of Inelastic Seismic Response of R/C Structures," *Journal of Structural Engineering*, ASCE, Vol. 116, No. 4.

Kunnath, S.K., Reinhorn, A.M., and Lobo, R.F. (1992). "IDARC Version 3.0: A Program for the Inelastic Damage Analysis of Reinforced Concrete Structures," *Technical Report NCEER–92–0022*, Buffalo, NY.

MacGregor, J. G. (1992). *Reinforced Concrete: Mechanics and Design*, Prentice Hall, Englewood Cliffs, NJ.

Maes, M.A. and Breitung, K. (1993). "Reliability–Based Tail Estimation," *Proceedings, IUTAM Symposium on Probabilistic Structural Mechanics (Advances in Structural Reliability Methods)*, San Antonio, TX, pp. 335–346.

Miranda, E. and Bertero, V.V. (1989). "Performance of Low Rise Buildings in Mexico City," *Earthquake Spectra*, EERI, Vol. 5, No. 1.

Mirza, S.A. and MacGregor, J.G. (1979). "Variability of Mechanical Properties of Reinforcing Bars," *Journal of the Structural Division*, ASCE, Vol. 105, No. ST5.

Naeim, F. (1995). "On Seismic Design Implications of the 1994 Northridge Earthquake Records," *Earthquake Spectra*, EERI, Vol. 11, No. 1.

Naeim, F., and Anderson, J.C. (1993). *Classification and Evaluation of Earthquake Records for Design*, The 1993 NEHRP Professional Fellowship Report, EERI, Oakland, CA.

Nassar, A.A., and Krawinkler, H. (1991). "Seismic Demands for SDOF and MDOF Systems," *Report No. 95*, John A. Blume Earthquake Engineering Center, Department of Civil Engineering, Stanford University, Stanford, CA.

Otani, S. (1992). "Concept Behind Ultimate Strength Design Guidelines for Reinforced Concrete Buildings in Japan," *The Third Meeting of the U.S.–Japan Joint Technical Committee on Precast Seismic Structural Systems*, San Diego, CA.

Park, R. and Paulay, T. (1975) *Reinforced Concrete Structures*, John Wiley & Sons, New York, NY.

Park, R., Priestley, M.J.N., and Gill, W.D. (1982). "Ductility of Square–Confined Concrete Columns," *Journal of the Structural Division*, ASCE, Vol. 108, No. ST4.

Park, R. and Sampson, R. A. (1972). "Ductility of RC Column Sections in Seismic Design," *Journal of American Concrete Institute*, Vol. 69, No. 9.

Park, Y.J., Ang, A.H.–S., and Wen, Y.K. (1984). "Seismic Damage Analysis and Damage–Limiting Design of R.C. Buildings," *Structural Research Series Report No. 516*, Department of Civil Engineering, University of Illinois at Urbana–Champaign, Urbana, IL.

Paulay, T. and Priestley, M. J. N. (1992). *Seismic Design of Reinforced Concrete and Masonry Buildings*, John Wiley and Sons, Inc., New York, NY.

Prakash, V., Powell, G. H., and Campbell, S. (1993). "DRAIN–2DX Base Program Description and User Guide, Version 1.10," *Report No. UCB/SEMM–93/17*, University of California at Berkeley, Berkeley, CA.

Pillai, S. U., and Kirk, D. W. (1988). *Reinforced Concrete Design*, Second Ed., McGraw–Hill, Toronto, ON.

Powell, G. H. (1993). "DRAIN–2DX Element Description Description and User Guide for Element TYPE01, TYPE02, TYPE04, TYPE06, TYPE09, and TYPE15, Version 1.10," *Report No. UCB/SEMM–93/18*, University of California at Berkeley, Berkeley, CA.

PRESSS Guidelines Drafting Working Group (1992). *Design Guidelines (Draft) for Reinforced Concrete Buildings*, The Third Meeting of the U.S.–Japan Joint Technical Committee on Precast Seismic Structural Systems, San Diego, CA.

Saito, T., and Wen, Y. K. (1994). "Seismic Risk Evaluation of R.C. Buildings in Japan Designed in Accordance with 1990 AIJ Guidelines," *Structural Research Series Report No.587*, Department of Civil Engineering, University of Illinois at Urbana–Champaign, Urbana, IL.

Saito, T. – personal correspondence (1994).

Shakal, A., Huang, M., Darragh, R., Cao, T., Sherburne, R., Malhotra, P., Cramer, C., Sydnor, R., Graizer, V., Maldonado, G., Petersen, C., and Warmpole, J. (1994). "CSMIP Strong–Motion Records from the Northridge, California Earthquake of January 17, 1994", *Report OSMS 94–07*, CSMIP (California Strong Motion Intrumentation Program), Sacramento, CA.

Shibata, A. – personal correspondence (1994).

Sozen, M.A. (1981). "Review of Earthquake Response of R.C. Buildings with a View to Drift Control," *State of the Art in Earthquake Engineering*, Kelaynak Press, Ankara, Turkey.

STAAD–III (Structural Analysis and Design) (1993). *User's Manual*, Research Engineers, Inc., Orange, CA.

Teran–Gilmore, A. and Bertero, V.V. (1993). "Seismic Performance of a 30–Story Building Located on Soft Soil and Designed According to UBC 1991," *Report No. UCB/EERC–93/04*, University of California at Berkeley, Berkeley, CA.

Trifunac, M.D., Todorovska, M.I., and Ivanovic, S.S. (1994). "A note on distribution of uncorrected peak ground accelerations during the Northridge, California, earthquake of 17 January 1994," *Soil Dynamics and Earthquake Engineering*, Vol. 13, pp. 187–196.

Uang, C.M. (1992). "Seismic Force Reduction and Displacement Amplification Factors," *Proceedings of the Tenth World Conference on Earthquake Engineering*, Madrid, Spain, pp. 5875–5880.

Wang, C.–H. (1995) research in progress, Department of Civil Engineering, University of Illinois at Urbana–Champaign, Urbana, IL.

Wen, Y. K. (1995). "Building Reliability and Code Calibration," accepted for publication in *Earthquake Spectra*, EERI, Vol. 11, No. 2.

APPENDIX A

PROCEDURE FOR TENSION DESIGN OF COLUMNS

- First design the column for load cases where column is in compression.
- Let M_1 be the unfactored pure moment capacity of the column designed for compression load cases. Let P_1 be the unfactored pure axial tensile capacity of the column designed for compression load cases.
- Using the factored moment and axial load resulting from the "tensile" load case, calculate M_u/ϕ and P_u/ϕ, where $\phi = 0.9$.
- Plot M_1, P_1, M_u/ϕ, and P_u/ϕ as shown below.

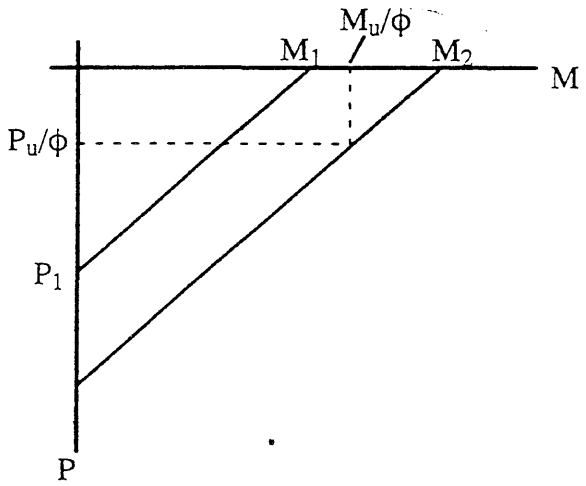

- Calculate M_2 as follows:

$$M_2 = \frac{M_u}{\phi} + \frac{P_u}{\phi}\left[\frac{M_1}{P_1}\right]$$

- If $M_2 > M_1$, re–design column to achieve unfactored pure moment capacity of M_2.
- Check all load cases again.

APPENDIX B

FORTRAN PROGRAMS

B.1 Program to calculate required steel areas for beams

```
*******************************
* This program will calculate the   *
* steel area needed to resist given  *
* forces on a beam.                  *
*******************************
      PROGRAM MAIN
C**
      IMPLICIT REAL*8 (A–H,O–Z)
      COMMON FY,FC,BN,BP,D
      CHARACTER*1 DM
      DATA FY,FC,BN,BP,D/60.,4.,20.,50.,32.5/
C**
      open (unit=1, file='beam.inp')
      open (unit=3, file='beam.out')
      write (3,1000) 'node','Negative','Required'
      write (3, 1005) '/Positive','Steel Area'
      read (1,*) N
      do 50 I=1,N
        READ(1,*) node, AM, DM
        CALL BEAM(AM,DM,AS)
        write (3,1010) node, DM, AS
 50   continue
 1000 format (A5,3X,A9,3X,A9)
 1005 format (8X,A9,3X,A10)
 1010 format (I5,A9,3X,F10.2)
      STOP
      END

      SUBROUTINE BEAM(AM,DM,AS)
C**
      IMPLICIT REAL*8 (A–H,O–Z)
      COMMON FY,FC,BN,BP,D
      CHARACTER*1 DM
C**
      C1=0.9*FY*D
      IF (DM .EQ. 'N' .OR. DM .EQ. 'n') THEN
        C2=0.9*FY**2/(1.7*FC*BN)
      ELSEIF (DM .EQ. 'P' .OR. DM .EQ. 'p') THEN
        C2=0.9*FY**2/(1.7*FC*BP)
      ENDIF
      AS=(C1–DSQRT(C1**2–4.*C2*AM))/2./C2
```

```
      RETURN
      END
```

B.2 Program to calculate design forces due to SCWB requirement

```
**********************************
* This program will calculate the forces  *
* to be resisted to meet the SCWB         *
* requirement of ACI, given the steel     *
* areas of the beams                      *
**********************************
      PROGRAM MAIN
C**
      IMPLICIT REAL*8 (A-H,O-Z)
      COMMON FY,FC,BN,BP,D
      CHARACTER*1 DM
      DATA FY,FC,BN,BP,D/60.,4.,20.,50.,32.5/
C**
      open (unit=1, file='scwb.inp')
      open (unit=3, file='scwb.out')
      write (3,1000) 'node','Design Mom.','Beam 1','Beam 2'
      write (3,1005) 'for SCWB','Capacity','Capacity'
 10   read (1,*) node, DM, As
      call CAPACITY(As, DM, cap)
      if (((node .eq. 5) .or. (node .eq. 13) .or. (node .eq. 21))
     & .and. (DM .EQ. 'N' .OR. DM .EQ. 'n')) then
        scwb=6./5.*cap/2.
        write (3,1008) node, scwb, cap
      elseif ((node .eq. 6) .or. (node .eq. 14) .or. (node .eq. 22))
     & then
        node1=node
        read (1,*) node, DM, As
        if (node1 .ne. node) then
          print *, 'invalid input order'
          stop
        endif
        call CAPACITY(As, DM, cap2)
        scwb=6./5.*(cap+cap2)/2.
        write (3,1010) node, scwb, cap, cap2
      elseif (node .eq. 999) then
        stop
      endif
      go to 10
1000 format (A5,3X,A11,3X,A7,4X,A7)
1005 format (8X,A9,5X,A8,3X,A8)
1008 format (I5,3X,F9.2,5X,F8.2)
1010 format (I5,3X,F9.2,5X,F8.2,3X,F8.2)
      end
```

```
      subroutine CAPACITY(As, DM, cap)
C**
      IMPLICIT REAL*8 (A–H,O–Z)
      COMMON FY,FC,BN,BP,D
      CHARACTER*1 DM
C**
      IF (DM .EQ. 'N' .OR. DM .EQ. 'n') THEN
        cap=0.9*As*FY*(D–(As*FY)/(1.7*FC*BN))
      ELSEIF (DM .EQ. 'P' .OR. DM .EQ. 'p') THEN
        cap=0.9*As*FY*(D–(As*FY)/(1.7*FC*BP))
      ENDIF
      return
```

B.3 Program to calculate the Moment–Curvature relationships

```
************************************************************
*      Moment – Curvature Generation Program               *
*              by  Ken Elwood                              *
*    Dept. of Civil Eng., University of Illinois           *
*            September 19, 1994                            *
*                                                          *
* Given details of column cross section and axial          *
* load, the program will calculate the Moment              *
* curvature relationship. Note ecmax is needed to          *
* to be large enough to attain the axial load alone.       *
*                                                          *
* Input file: input.col                                    *
* Output file: M_phi.col#                                  *
************************************************************
*
* Variable definition
*
      real b, h, d, dh, fcmax, enot, fy, Es, ecmax
      real sumf, conc, steel, x, sumfp, cprev, c, As, ds
      real csoln, M, phi, P, decmax
      integer nstrip, a, count, nsteel
      character*1000 junk, ending*5, outfile*14
      dimension conc(1000), x(1000), M(1000), phi(1000),
     & As(20), ds(20)
*
* Find input values
*
      open (unit=1, file='input.col')
      read (1, '(A)') junk
      read (1, '(A)') junk
      read (1, *) b
      read (1, *) h
      read (1, *) dh
```

```
      read (1, *) fcmax
      read (1, *) enot
      read (1, *) fy
      read (1, *) Es
      read (1, *) a
      read (1, *) nsteel
      do 5 I=1, nsteel
        read (1, *) As(I), ds(I)
5     continue
      read (1, *) P
      read (1, *) ecmax
      read (1, '(A)') ending
      outfile='M_phi.col'//ending
      open (unit=3, file=outfile)
*
* Find # of strips
*
      nstrip=nint(h/dh)
*
* intialize variables
*
*       ecmax=0.0
      count=0
*
* choose ecmax
*
      decmax=(0.004-ecmax)/real(a)
      do 50 count=1, a
       n=0
       sumfp=0.0
       ecmax=ecmax+decmax
*
* choose c
*
20      c=(dh/2.0)+(real(n)*dh)
*
* calc forces in strips and steel
*
        call FORCES (b, d, dh, fcmax, enot, fy, Es, conc, x,
     &  sumf, steel, c, ecmax, nstrip, Ac, ds, As, nsteel)
*
* determine if sum of forces is greater than P, less than P, or P (not very likely!)
*
        if (sumf .lt. P) then
*
* recalc with lower NA (ie larger c)
```

```
*
        sumfp=sumf
        n=n+1
        go to 20
      else if (sumf .gt. P) then
*
* interpolate to find c with sum of forces equal to zero,
* then recalc forces and then find corresponding moment and phi
*
        cprev=c–dh
        call INTER (c, cprev, sumf, sumfp, csoln, P, count)
        c=csoln
        call FORCES (b, d, dh, fcmax, enot, fy, Es, conc, x,
     &    sumf, steel, c, ecmax, nstrip, Ac, ds, As, nsteel)
        call SOLN (M, phi, d, steel, x, conc, ecmax, c,
     &    nstrip, count, nsteel, ds, P, h)
      else
*
* just in case sum of forces happens to hit P
*
        call SOLN (M, phi, d, steel, x, conc, ecmax, c,
     &    nstrip, count, nsteel, ds, P, h)
      end if
50    continue
      end


      subroutine FORCES (b, d, dh, fcmax, enot, fy, Es, conc, x,
     & sumf, steel, c, ecmax, nstrip, Ac, ds, As, nsteel)
**********************************************************************
* This routine will calculate the forces in each strip an the steel *
* then sum the forces.  Uses Hognstad's parabola for concrete.      *
**********************************************************************
      real b, d, dh, fcmax, enot, fy, Es, conc, x, sumf
      real steel, c, ecmax, e, fc, Ac
      real ds, As, h
      integer nstrip, nsteel
      dimension e(1000), fc(1000), conc(1000), x(1000), ds(5),
     & As(5), steel(5)
*
      sumf=0.0
      do 300 I=1, nstrip
        x(I)=(dh/2.0)+((real(I)–1)*dh)
        e(I)=(ecmax/c)*(c–x(I))
        if (e(I) .lt. (–0.05*enot))then
          fc(I)=0.0
        else if (e(I) .gt. enot) then
```

```
        fc(I)=fcmax*(1.0-0.15*((e(I)-enot)/enot))
      else
        fc(I)=fcmax*(2.0*(e(I)/enot)-(e(I)/enot)**2)
      end if
      Ac=b*dh
      do 200 J=1, nsteel
        if ((x(I-1) .lt. ds(J)) .and. (x(I) .ge. ds(J))) then
          Ac=b*dh-As(J)
        end if
200     continue
      conc(I)=fc(I)*Ac
      sumf=sumf+conc(I)
300   continue
    do 400 K=1, nsteel
      esteel=(ecmax/c)*(c-ds(K))
      if ((abs(esteel)) .le. (fy/Es)) then
        fs=Es*esteel
      else if (esteel .lt. (-(fy/Es))) then
        fs=-fy
      else
        fs=fy
      end if
      steel(K)=fs*As(K)
      sumf=sumf+steel(K)
400   continue
    end


    subroutine INTER (c, cprev, sumf, sumfp, csoln, P, count)
*************************************************************************
* This routine interpolates between the sum of forces greater than P and the *
* sum of forces less than P to find csoln where sum should be P          *
*************************************************************************
    real c, cprev, sumf, sumfp, csoln, slope, P
    integer count
*
    slope=(sumf-sumfp)/(c-cprev)
    csoln=cprev+(P-sumfp)/slope
    end



    subroutine SOLN (M, phi, d, steel, x, conc, ecmax, c,
   & nstrip, count, nsteel, ds, P, h)
*************************************************************************
* This routine calculates the moment and phi for the given ecmax  *
* and write the results to data.out.  Moment taken about one side *
* of the cross section                                    *
```

```
*********************************************************************
      real M, phi, d, steel, x, conc, ecmax, c, Mconc, Msteel
      real P, ds, h
      integer nstrip, count, nsteel
      dimension conc(1000), x(1000), M(100), phi(100), ds(*),
     &          steel(*)
*
      Mconc=0.0
      Msteel=0.0
      do 400 I=1, nstrip
        Mconc=Mconc+x(I)*conc(I)
400   continue
      do 500 J=1, nsteel
        Msteel=Msteel+ds(J)*steel(J)
500   continue
      M(count)=-1*(Mconc+Msteel-P*h/2)
      phi(count)=ecmax/c
      write (3, *) phi(count), M(count)
      end
```

B.4 Program to calculate the axial force–moment interaction diagrams

```
*********************************************************
*     Moment–Curvature–Axial Load Interaction           *
*              Diagram Program                          *
*                                                       *
*                KEN ELWOOD                             *
*                                                       *
*  Dept. of Civil Eng., University of Illinois          *
*                                                       *
*            September 28, 1994                         *
*                                                       *
* Given details of column cross section the program     *
* will produce the P–M and P–phi interaction diagrams   *
* and at the bottom of the output is a summary of the   *
* curve including My, Mbal/My, Pc, Pbal/Pc and Pt.      *
*                                                       *
* Input file: input.inter                               *
* Output file: inter.col#_#                             *
*********************************************************
*
*
      Program interaction
*
*        Variable definition
*
      real b, h, d, dh, fcmax, enot, fy, Es, ecmax
```

```
      real sumf, conc, steel, x, sumfp, cprev, c, As, ds
      real csoln, M, phi, Mbal,  Pbal
      integer nstrip, div, count, nsteel
      character*1000 junk, ending*5, outfile*14
      dimension conc(999),x(999),M(999),phi(999),As(20),ds(20),P(999)
*
*       Find input values
*
      open (unit=1, file='input.inter')
      read (1, '(A)') junk
      read (1, '(A)') junk
      read (1, *) b
      read (1, *) h
      read (1, *) dh
      read (1, *) fcmax
      read (1, *) enot
      read (1, *) fy
      read (1, *) Es
      read (1, *) div
      read (1, *) nsteel
      do I=1, nsteel
        read (1, *) As(I), ds(I)
      end do
      read (1, '(A)') ending
      outfile='inter.col'//ending
      open (unit=3, file=outfile)
*
*       Find number of strips
*
      nstrip=nint(h/dh)
*
*       Intialize variables
*
      ecmax=0.004
* Note: the next three lines are needed to initialize M to zero even though
* M is not used before it is defined.  A print statement prior to the FORCES
* routine will also correct this misterious problem!  M is not sent to the
* FORCES routine and therefore should not be influenced by it.
      do I=1, div
        M(I)=0.0
      end do
*
*       Find maximum axial load and increment of axial load
*
      call AXIAL (fcmax, b, h, As, fy, Es, enot, Pmax, Pmin,
     &     div, Pincr, nsteel)
```

```
      write(3,*) ' PHI    M     P'
      write(3,*) 0.0, 0.0, Pmin
*
*       start loop for each P
*
      do count=1, div
        n=0
        sumfp=0.0
        P(count)=real(count-1)*Pincr
*
*       choose c
*
 20     c=(dh/2.0)+(real(n)*dh)
*
*       calc forces in strips and steel
*
        call FORCES (b, d, dh, fcmax, enot, fy, Es, conc, x,
     &       sumf, steel, c, ecmax, nstrip, Ac, ds, As, nsteel)
*
*       determine if sum of forces is greater than P, less than P, or P
*
        if (sumf .lt. P(count)) then
*
*       recalc with lower NA (ie larger c)
*
          sumfp=sumf
          n=n+1
          go to 20
        else if (sumf .gt. P(count)) then
*
*       interpolate to find c with sum of forces equal to zero,
*       then recalc forces and then find corresponding moment and phi
*
          cprev=c-dh
          call INTER (c, cprev, sumf, sumfp, csoln, P, count)
          c=csoln
          call FORCES (b, d, dh, fcmax, enot, fy, Es, conc, x,
     &       sumf, steel, c, ecmax, nstrip, Ac, ds, As, nsteel)
          call SOLN (M, phi, d, steel, x, conc, ecmax, c,
     &       nstrip, count, nsteel, ds, P, h, Mbal,  Pbal)
        else
*
*       just in case sum of forces happens to hit P
*
          call SOLN (M, phi, d, steel, x, conc, ecmax, c,
     &       nstrip, count, nsteel, ds, P, h, Mbal,  Pbal)
```

```
      end if
*
*       find when c >= h to leave loop
*
      if (c .ge. h) go to 100
    end do
 100  write (3,*) 0.0, 0.0, Pmax
    write (3,*)
    write (3,*)
    write (3,*) 'Pt = ',Pmin
    write (3,*) 'Pc = ',Pmax
    write (3,*) 'My = ',M(1)
    write (3,*) 'Mbal/M = ',Mbal/M(1)
    write (3,*) 'Pbal/Pc = ',Pbal/Pmax
    end

    subroutine FORCES (b, d, dh, fcmax, enot, fy, Es, conc, x,
   &     sumf, steel, c, ecmax, nstrip, Ac, ds, As, nsteel )
*************************************************************************
*    This routine will calculate the forces in each strip an the steel   *
*    then sum the forces.  Uses Hognstad's parabola for concrete.        *
*************************************************************************
    real b, d, dh, fcmax, enot, fy, Es, conc, x, sumf
    real steel, c, ecmax, e, fc, Ac
    real ds, As
    integer nstrip, nsteel
    dimension e(999), fc(999), conc(999), x(999), ds(20), As(20),
   & steel(20)
*
    sumf=0.0
    do I=1, nstrip
      x(I)=(dh/2.0)+((real(I)-1)*dh)
      e(I)=(ecmax/c)*(c-x(I))
      if (e(I) .lt. (-0.05*enot)) then
        fc(I)=0.0
      else if (e(I) .gt. enot) then
        fc(I)=fcmax*(1.0-0.15*((e(I)-enot)/enot))
      else
        fc(I)=fcmax*(2.0*(e(I)/enot)-(e(I)/enot)**2)
      end if
      Ac=b*dh
      do J=1, nsteel
        if ((x(I-1) .lt. ds(J)) .and. (x(I) .ge. ds(J))) then
          Ac=b*dh-As(J)
        end if
      end do
      conc(I)=fc(I)*Ac
```

```
      sumf=sumf+conc(I)
    end do
    do K=1, nsteel
      esteel=(ecmax/c)*(c–ds(K))
      if ((abs(esteel)) .le. (fy/Es)) then
        fs=Es*esteel
      else if (esteel .lt. (–(fy/Es))) then
        fs=–fy
      else
        fs=fy
      end if
      steel(K)=fs*As(K)
      sumf=sumf+steel(K)
    end do
    end

    subroutine INTER (c, cprev, sumf, sumfp, csoln, P, count)
*************************************************************************
*    This routine interpolates between the sum of forces greater    *
*    than P and the sum of forces less than P to find csoln where   *
*    sum should be P                                                *
*************************************************************************
    real c, cprev, sumf, sumfp, csoln, slope, P
    integer count
    dimension P(999)
*
    slope=(sumf–sumfp)/(c–cprev)
    csoln=cprev+(P(count)–sumfp)/slope
    end

    subroutine SOLN (M, phi, d, steel, x, conc, ecmax, c,
   &    nstrip, count, nsteel, ds, P, h, Mbal,  Pbal)
*************************************************************************
*    This routine calculates the moment and phi for the given ecmax    *
*    and write the results to data.out.  Moment taken about one side   *
*    of the cross section                                               *
*************************************************************************
    real M, phi, d, steel, x, conc, ecmax, c, Mconc, Msteel
    real P, ds, h, Mbal,  Pbal
    integer nstrip, count, nsteel
    dimension conc(999), x(999), M(999), phi(999), ds(20),
   & P(999), steel(20)
*
    Mconc=0.0
    Msteel=0.0
    do I=1, nstrip
      Mconc=Mconc+x(I)*conc(I)
    end do
```

```
      do J=1, nsteel
        Msteel=Msteel+ds(J)*steel(J)
      end do
      M(count)=-1*(Mconc+Msteel-P(count)*h/2)
      phi(count)=ecmax/c
      write (3, *) phi(count), M(count), P(count)
      if (M(count) .gt. M(count-1)) then
        Mbal=M(count)
        Pbal=P(count)
      end if
      end

      subroutine AXIAL (fcmax, b, h, As, fy, Es, enot, Pmax, Pmin,
     &     div, Pincr, nsteel)
*******************************************************************************
*    This routine finds the maximum and minimum (i.e. tension) axial loads *
*******************************************************************************
      real fcmax, b, h, As, fy, Es, enot, Pmax, Pmin, Pincr, Asteel
      real fs, Ac, Fconc, Fsteel
      integer div, nsteel
      dimension As(20)
*
      Asteel=0.0
      do I=1, nsteel
        Asteel=Asteel+As(I)
      end do
      Ac=b*h-Asteel
      Fconc=fcmax*Ac
      if (enot .gt. (fy/Es)) then
        fs=fy
      else
        fs=enot*Es
      end if
      Fsteel=fs*Asteel
      Pmax=Fconc+Fsteel
      Pmin=-Asteel*fy
      Pincr=Pmax/div
      end
```

B.5 Program to calculate the damage indices given the DRAIN–2DX output

```
*********************************************
* This program will calculate the damage     *
* indices (Park and Ang model) given a       *
* DRAIN output file and yeild and ultimate   *
* capacities of the members.  A weighted     *
* Index for the frame will also be calc.     *
*                                            *
*       Ken Elwood, March 1995               *
*                                            *
*********************************************
      program Damage
*
      implicit double precision (a–h,o–z)
*     double precision
      character junk*100, drain*10
      dimension bmyp(21),bmyn(21),bphiyp(21),bphiyn(21),bphiup(21),
     & bphiun(21),cmy(28),cphiy(28),cphiu(28),colmaxp(28,2),
     & colmaxn(28,2),colaccp(28,2),colaccn(28,2),bmaxp(21,2),
     & bmaxn(21,2), baccp(21,2),baccn(21,2),Ehbem(21,2),Ehcol(28,2),
     & DIbem(21,2),DIcol(21,2)
      data beta/0.15/
*
* open input and output files
*
      open (4,file='infile')
      read (4,'(A)') drain
      if (drain .eq. '7S_10Y.out') then
        iflag=0
        open (5,file='7S_10Y.out')
        open (6,file='dual.col')
        open (7,file='dual.bem')
        open (8,file='7s10y.di')
        open (9,file='dual.sum',access='append')
      else
        iflag=1
        open (5,file='NEHRP.out')
        open (6,file='nehrp.col')
        open (7,file='nehrp.bem')
        open (8,file='nehrp.di')
        open (9,file='nehrp.sum',access='append')
      end if
*
* Read in capacities
*
      read (7,'(A)') junk
```

```
      read (7,*) nbeam,dat1,dat2,dat3,dat4,dat5,dat6
      do I=1,6
        bmyp(I)=dat1
        bmyn(I)=dat2
        bphiyp(I)=dat3
        bphiyn(I)=dat4
        bphiup(I)=dat5
        bphiun(I)=dat6
      end do
      read (7,*) nbeam,dat1,dat2,dat3,dat4,dat5,dat6
      do I=7,12
        bmyp(I)=dat1
        bmyn(I)=dat2
        bphiyp(I)=dat3
        bphiyn(I)=dat4
        bphiup(I)=dat5
        bphiun(I)=dat6
      end do
      read (7,*) nbeam,dat1,dat2,dat3,dat4,dat5,dat6
      do I=13,21
        bmyp(I)=dat1
        bmyn(I)=dat2
        bphiyp(I)=dat3
        bphiyn(I)=dat4
        bphiup(I)=dat5
        bphiun(I)=dat6
      end do
*
      read (6,'(A)') junk
      read (6,'(A)') junk
      read (6,*) ncol,dat1,dat2,dat3
      do I=1,4,3
        cmy(I)=dat1
        cphiy(I)=dat2
        cphiu(I)=dat3
      end do
      read (6,*) ncol,dat1,dat2,dat3
      do I=2,3
        cmy(I)=dat1
        cphiy(I)=dat2
        cphiu(I)=dat3
      end do
      read (6,*) ncol,dat1,dat2,dat3
      do I=5,8,3
        cmy(I)=dat1
        cphiy(I)=dat2
```

```
  cphiu(I)=dat3
end do
read (6,*) ncol,dat1,dat2,dat3
do I=6,7
  cmy(I)=dat1
  cphiy(I)=dat2
  cphiu(I)=dat3
end do
read (6,*) ncol,dat1,dat2,dat3
do I=9,12,3
  cmy(I)=dat1
  cphiy(I)=dat2
  cphiu(I)=dat3
end do
read (6,*) ncol,dat1,dat2,dat3
do I=10,11
  cmy(I)=dat1
  cphiy(I)=dat2
  cphiu(I)=dat3
end do
read (6,*) ncol,dat1,dat2,dat3
do I=13,16,3
  cmy(I)=dat1
  cphiy(I)=dat2
  cphiu(I)=dat3
end do
read (6,*) ncol,dat1,dat2,dat3
do I=14,15
  cmy(I)=dat1
  cphiy(I)=dat2
  cphiu(I)=dat3
end do
read (6,*) ncol,dat1,dat2,dat3
do I=17,20,3
  cmy(I)=dat1
  cphiy(I)=dat2
  cphiu(I)=dat3
end do
read (6,*) ncol,dat1,dat2,dat3
do I=18,19
  cmy(I)=dat1
  cphiy(I)=dat2
  cphiu(I)=dat3
end do
read (6,*) ncol,dat1,dat2,dat3
do I=21,24,3
```

```
        cmy(I)=dat1
        cphiy(I)=dat2
        cphiu(I)=dat3
      end do
      read (6,*) ncol,dat1,dat2,dat3
      do I=22,23
        cmy(I)=dat1
        cphiy(I)=dat2
        cphiu(I)=dat3
      end do
      read (6,*) ncol,dat1,dat2,dat3
      do I=25,28,3
        cmy(I)=dat1
        cphiy(I)=dat2
        cphiu(I)=dat3
      end do
      read (6,*) ncol,dat1,dat2,dat3
      do I=26,27
        cmy(I)=dat1
        cphiy(I)=dat2
        cphiu(I)=dat3
      end do
*
*  set depth of members
*
      if (iflag .eq. 1) then
        colh=30.0
        bemh=35.0
      else
        colh=28.0
        bemh=34.0
      end if
*
*  get data from DRAIN output
*
      do I=1,64
        read (5,'(A)') junk
      end do
*
* Read in max top displ.
*
      read (5,50) top1,top2
      topmax=dmax1(top1,dabs(top2))
      topdr=topmax/1128.0*100.0
      do I=1,8
        read (5,'(A)') junk
```

```
      end do
*
* Read in column rotations (two maximum rotation arrays and two accumulated
* rotation array – 1st col –> bottom
*              2nd col –> top
* Note: first node sign convention is opposite to sign convention used for
*       above calculations (i.e. positive is tension on bottom or right side)
*
      do I=1, 28
        read (5,100) colmaxn(I,1),colaccn(I,1)
        read (5,100) colmaxp(I,1),colaccp(I,1)
        read (5,100) colmaxp(I,2),colaccp(I,2)
        read (5,100) colmaxn(I,2),colaccn(I,2)
      end do
*
* Read in beam rotations (two maximum rotation arrays and two accumulated
* rotation array – 1st col –> left
*              2nd col –> right
* Note: first node sign convention is opposite to sign convention used for
*       above calculations (i.e. positive is tension on bottom or right side)
*
      do I=1,8
        read (5,'(A)') junk
      end do
*
      do I=1, 21
        read (5,100) bmaxn(I,1),baccn(I,1)
        read (5,100) bmaxp(I,1),baccp(I,1)
        read (5,100) bmaxp(I,2),baccp(I,2)
        read (5,100) bmaxn(I,2),baccn(I,2)
      end do
*
* Read in max interstory drift
*
      do I=1,39
         read (5,'(A)') junk
      end do
*
      drmax=0.0
      do I=1,7
        read (5,500) nstory,drift1,drift2
        if ((drmax .lt. drift1) .or. (drmax .lt. dabs(drift2))) then
          drmax=dmax1(drift1,dabs(drift2))
          mstory=nstory
        end if
      end do
```

```
*
*  calculate damage index for each beam hinge
*
     write (8,1100) 'Beam','End','Damage Index'
     write (8,1100) '——','——','————————'
     Ehtot=0.0
     do I=1,21
       rotup=bemh/2.0*(bphiup(I)–bphiyp(I))
       rotun=bemh/2.0*(bphiun(I)–bphiyn(I))
       Ehnorm=(bmyp(I)*rotup+bmyn(I)*rotun)/2.0
       do J=1,2
         Ehbem(I,J)=bmyp(I)*dabs(baccp(I,J))+bmyn(I)*
    &               dabs(baccn(I,J))
         Ehtot=Ehtot+Ehbem(I,J)
         if (dabs(bmaxp(I,J)) .ge. dabs(bmaxn(I,J))) then
           rotmax=dabs(bmaxp(I,J))
           rotnorm=rotup
         else
           rotmax=dabs(bmaxn(I,J))
           rotnorm=rotun
         end if
         DIbem(I,J)=rotmax/rotnorm+beta*Ehbem(I,J)/Ehnorm
*          write (8,*) rotmax,rotnorm,beta,Ehbem(I,J),Ehnorm
         write (8,1000) I, J, DIbem(I,J)
       end do
     end do
*
*  calculate the damage for each column hinge
*
     write (8,*)
     write (8,1100) 'Col.','End','Damage Index'
     write (8,1100) '——','——','————————'
     do I=1,28
       rotu=colh/2.0*(cphiu(I)–cphiy(I))
       Ehnorm=cmy(I)*rotu
       do J=1,2
         Ehcol(I,J)=cmy(I)*dabs(colaccp(I,J))+cmy(I)*
    &               dabs(colaccn(I,J))
         Ehtot=Ehtot+Ehcol(I,J)
         if (dabs(colmaxp(I,J)) .ge. dabs(colmaxn(I,J))) then
           rotmax=dabs(colmaxp(I,J))
           rotnorm=rotu
         else
           rotmax=dabs(colmaxn(I,J))
           rotnorm=rotu
         end if
```

```
        DIcol(I,J)=rotmax/rotnorm+beta*Ehcol(I,J)/Ehnorm
        write (8,1000) I, J, DIcol(I,J),rotmax/rotnorm
      end do
    end do
*
* calculate overall damage index
*
    write (8,*)
    DItot=0.0
    if (Ehtot .le. 0.000001) go to 10
    do I=1,21
      do J=1,2
        DItot=DIbem(I,J)*Ehbem(I,J)/Ehtot+DItot
      end do
    end do
    do I=1,28
      do J=1,2
        DItot=DIcol(I,J)*Ehcol(I,J)/Ehtot+DItot
      end do
    end do
*
* output final results
*
10  write (8,1200) 'The overall damage index is ',DItot
    write (8, 1300) 'The maximum top drift is ',topdr,'%'
    write (8, 1400) 'The maximum interstory drift is ',drmax*100,
   & '% (at story ',mstory,')'
*
    write (9,1500) DItot, topdr, drmax*100
*
50  format (14X,E12.4,5X,E12.4)
100 format (75X,E11.3,5X,E12.4)
500 format (I5,E12.4,5X,E12.4)
1000 format (1X,I6,I6,2F15.2)
1100 format (1X,2A6,A15)
1200 format (1X,A28,F4.2)
1300 format (1X,A26,F7.4,A1)
1400 format (1X,A28,F7.4,A12,I1,A1)
1500 format (1X,F4.2,2X,F7.4,2X,F7.4)
    end
```

B.6 Program to calculate the probabilities of exceeding given threshold values (considering epicentral distance)

```
************************************
* This program will calculate the  *
* probability of exceeding given   *
* threshold responce values by     *
* considering the epicentral dist. *
*                                  *
*   by Ken Elwood, April 1995      *
************************************
      program probability
*
      implicit double precision (a-h,o-z)
      double precision LD,LDo
      character junk*70
      dimension dist(100),DI(100),GD(100),LD(100),DIo(15),
     & GDo(15),LDo(15),nrec(50),r(50),A(50),probtot(15)
*
      open (5,file='epicen.dat')
      open (8,file='prob_50.out')
*
      do I=1,3
        read (5,'(A)') junk
      end do
*
      nrad=0
      do I=1,84
        read (5, 1000) dist(I),DI(I),GD(I),LD(I)
        if (dist(I) .gt. 50.0) go to 10
        if ((I .ne. 1) .and. (dist(I) .eq. dist(I-1))) then
          nrec(nrad)=nrec(nrad)+1
        else
          nrad=nrad+1
          nrec(nrad)=1
          r(nrad)=dist(I)
        end if
      end do
*
 10   dDIo=0.1
      dGDo=0.2
      dLDo=0.25
      do I=1,14
        DIo(I)=dble(I-1)*dDIo
        GDo(I)=dble(I-1)*dGDo
        LDo(I)=dble(I-1)*dLDo
      end do
```

```
*
* Calculate areas under prob. density function
*
      Rmax=50.0
      rlast=0.0
      area=0.0
      do I=1,nrad
        if (I .eq. 1) then
          dr=(r(I)+r(I+1))/2
        else if (I .eq. nrad) then
          dr=Rmax-(r(I)+r(I-1))/2
        else
          dr=((r(I)+r(I+1))/2)-((r(I)+r(I-1))/2)
        end if
        rcenter=rlast+dr/2
        h=2*rcenter/(Rmax**2)
        A(I)=h*dr
        rlast=rlast+dr
        area=area+A(I)
      end do
*
* Calc prob of exceeding given thresholds
*
* Damage Index
*
      write (8,1500) 'Damage Index','Threshold','Prob. of Exceedence'
      do I=1,11
        thresh=DIo(I)
        ncount=1
        probtot(I)=0.0
        do J=1,nrad
          nexceed=0
          do K=1,nrec(J)
            if (DI(ncount) .gt. thresh) then
              nexceed=nexceed+1
            end if
            ncount=ncount+1
          end do
          prob=dble(nexceed)/dble(nrec(J))
          probtot(I)=prob*A(J)+probtot(I)
        end do
        write (8,2000) thresh,probtot(I)
      end do
      write (8,*)
*
* Global Drift
```

```
*
      write (8,1500) 'Global Drift','Threshold','Prob. of Exceedence'
      do I=1,11
        thresh=GDo(I)
        ncount=1
        probtot(I)=0.0
        do J=1,nrad
          nexceed=0
          do K=1,nrec(J)
            if (GD(ncount) .gt. thresh) then
              nexceed=nexceed+1
            end if
            ncount=ncount+1
          end do
          prob=dble(nexceed)/dble(nrec(J))
          probtot(I)=prob*A(J)+probtot(I)
        end do
        write (8,2000) thresh,probtot(I)
      end do
      write (8,*)
*
* Local Drift
*
      write (8,1500) 'Local Drift','Threshold','Prob. of Exceedence'
      do I=1,14
        thresh=LDo(I)
        ncount=1
        probtot(I)=0.0
        do J=1,nrad
          nexceed=0
          do K=1,nrec(J)
            if (LD(ncount) .gt. thresh) then
              nexceed=nexceed+1
            end if
            ncount=ncount+1
          end do
          prob=dble(nexceed)/dble(nrec(J))
          probtot(I)=prob*A(J)+probtot(I)
        end do
        write (8,2000) thresh,probtot(I)
      end do
 1500 format (1X,A12,//,1X,A9,A25)
 2000 format (1X,F9.2,F25.6)
 1000 format (20X,F3.0,3F12.4)
      end
```

APPENDIX C

RESPONSES TO NORTHRIDGE STRONG GROUND MOTION RECORDS

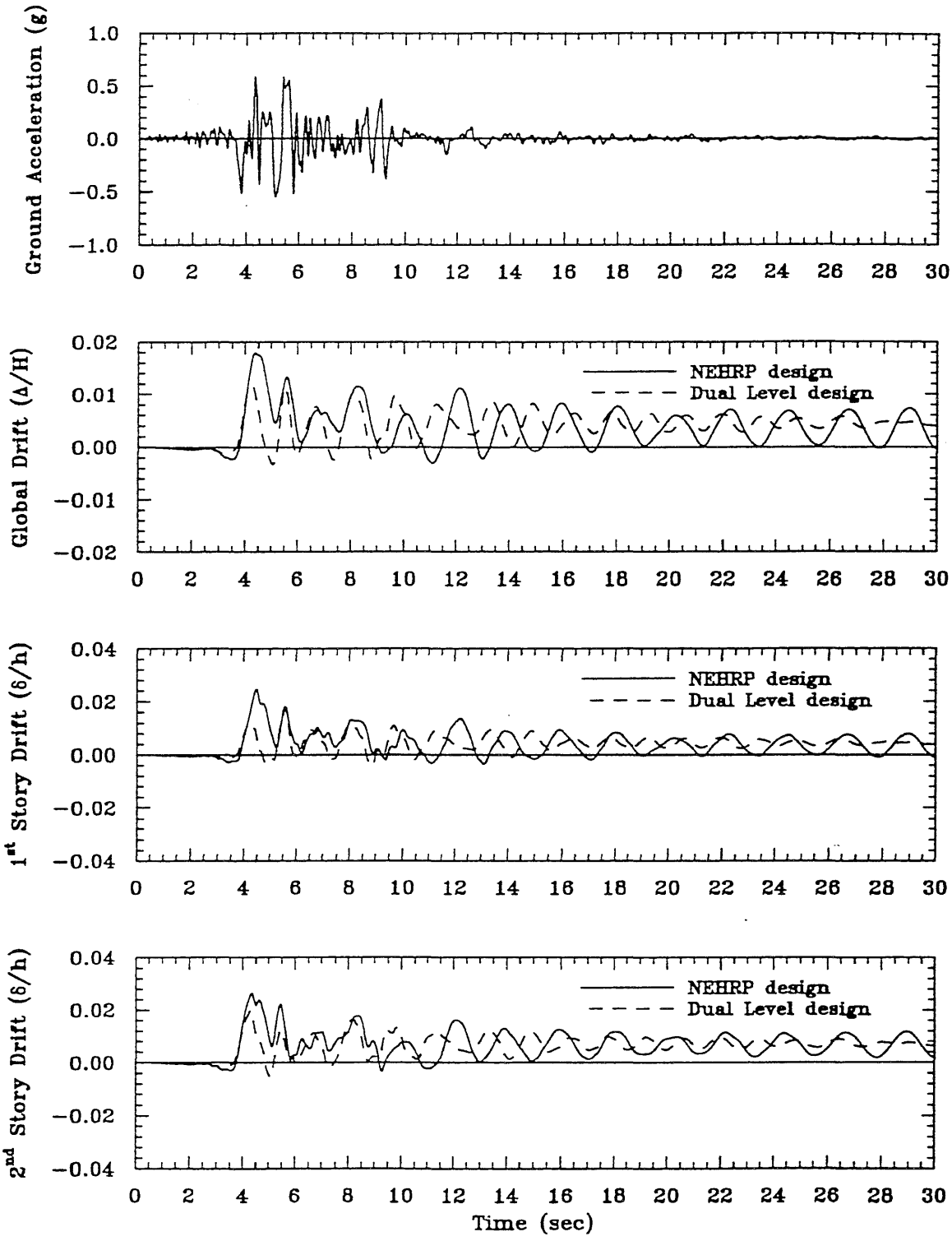

Figure C.1: Ground Motion and Structural Responses for Newhall Record
(a) ground acceleration, (b) global drift, (c) first story drift, (d) second story drift

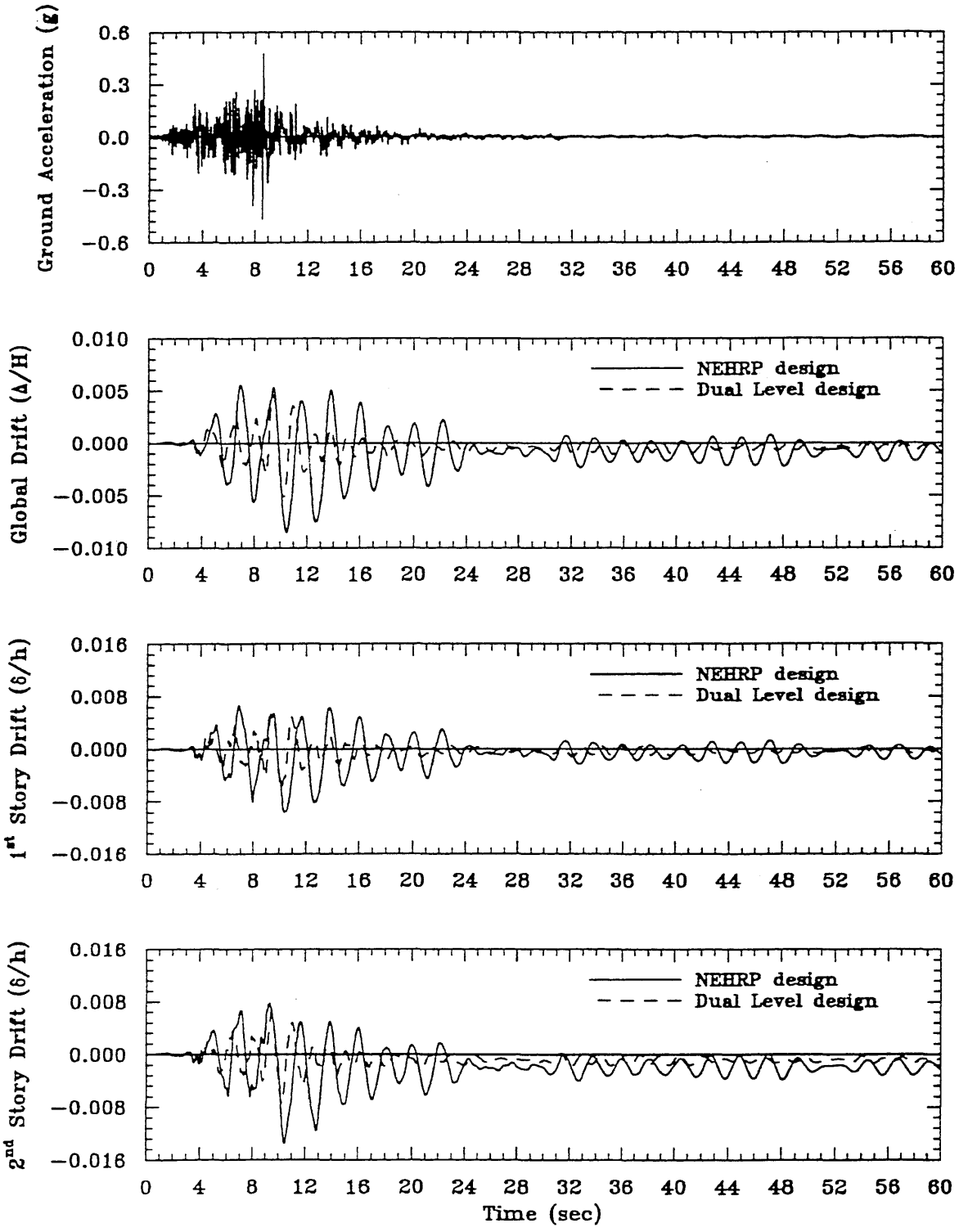

Figure C.2: Ground Motion and Structural Responses for UCLA Grounds Record
(a) ground acceleration, (b) global drift, (c) first story drift, (d) second story drift

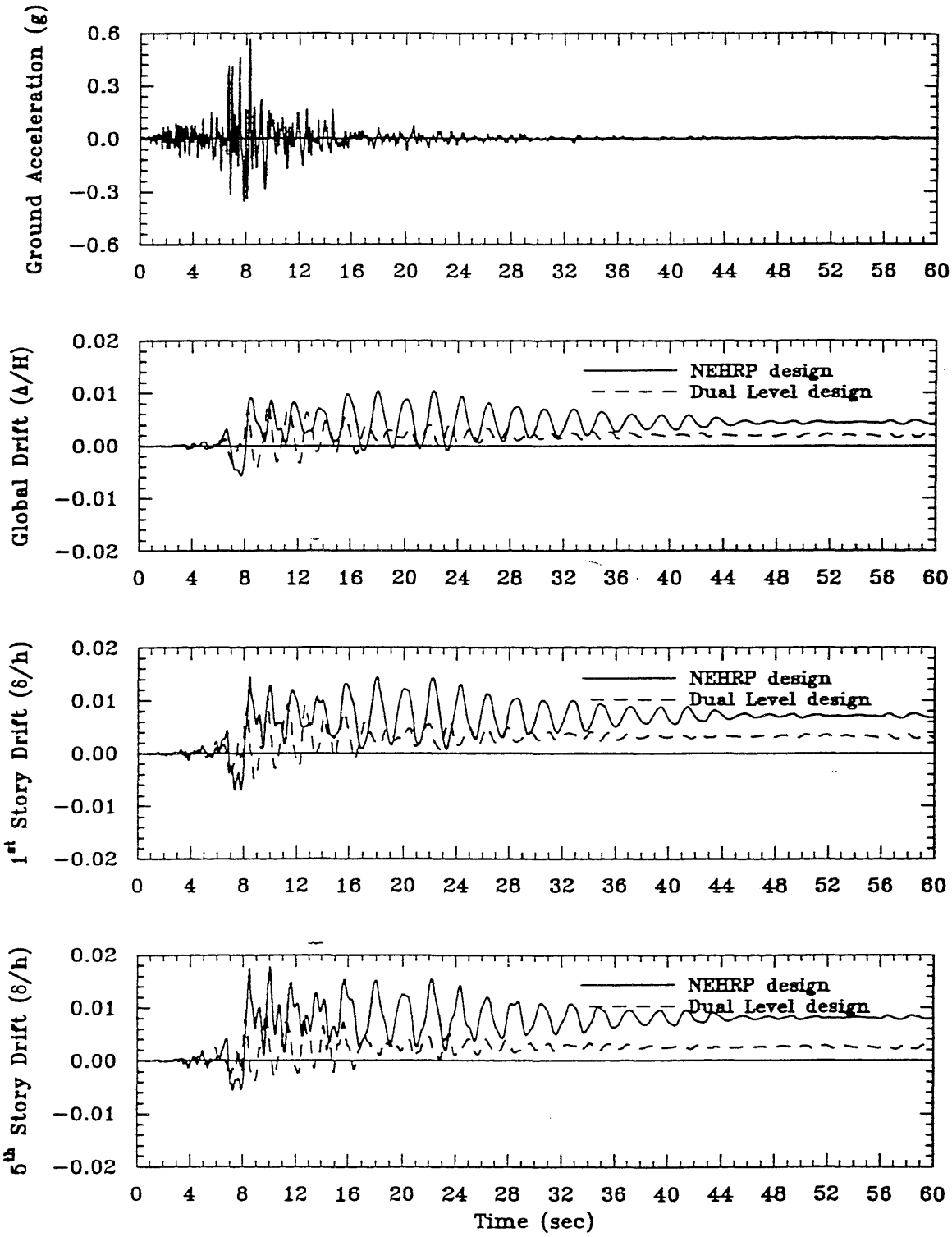

Figure C.3: Ground Motion and Structural Responses for Castaic Record (Northridge Earthquake)
(a) ground acceleration, (b) global drift, (c) first story drift, (d) second story drift

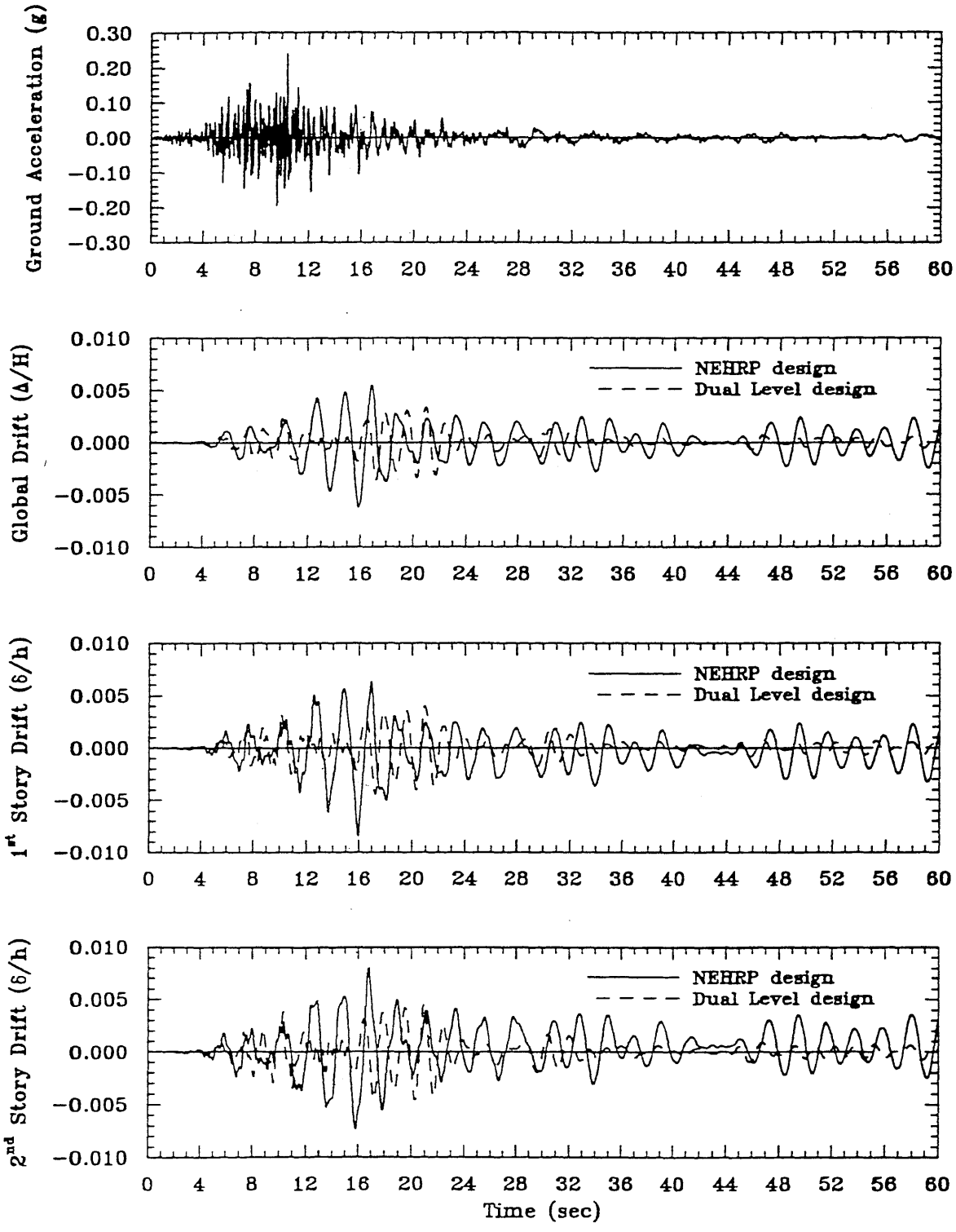

Figure C.4: Ground Motion and Structural Responses for Baldwin Hills Record
(a) ground acceleration, (b) global drift, (c) first story drift, (d) second story drift

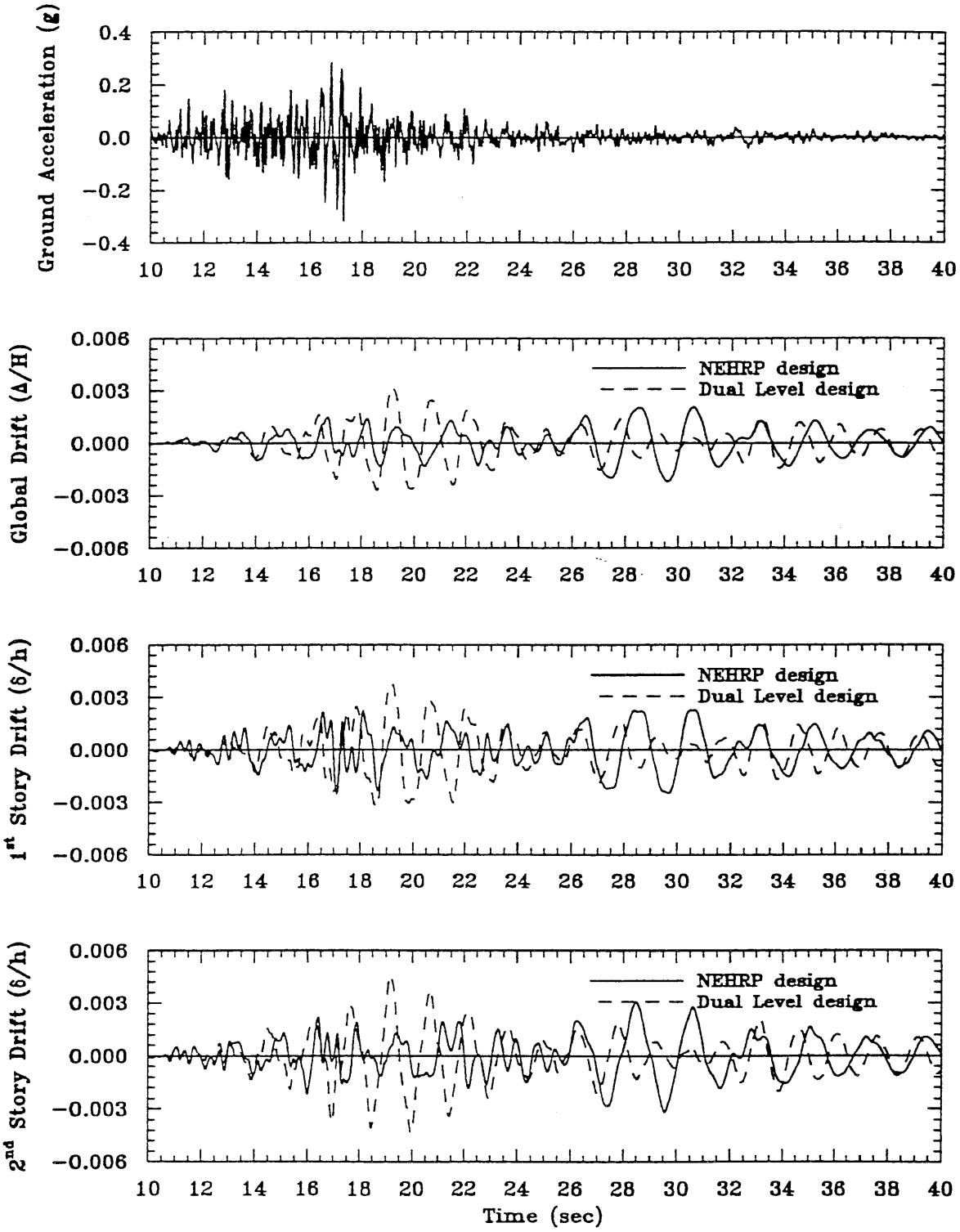

Figure C.5: Ground Motion and Structural Responses for City Terrace Record
(a) ground acceleration, (b) global drift, (c) first story drift, (d) second story drift

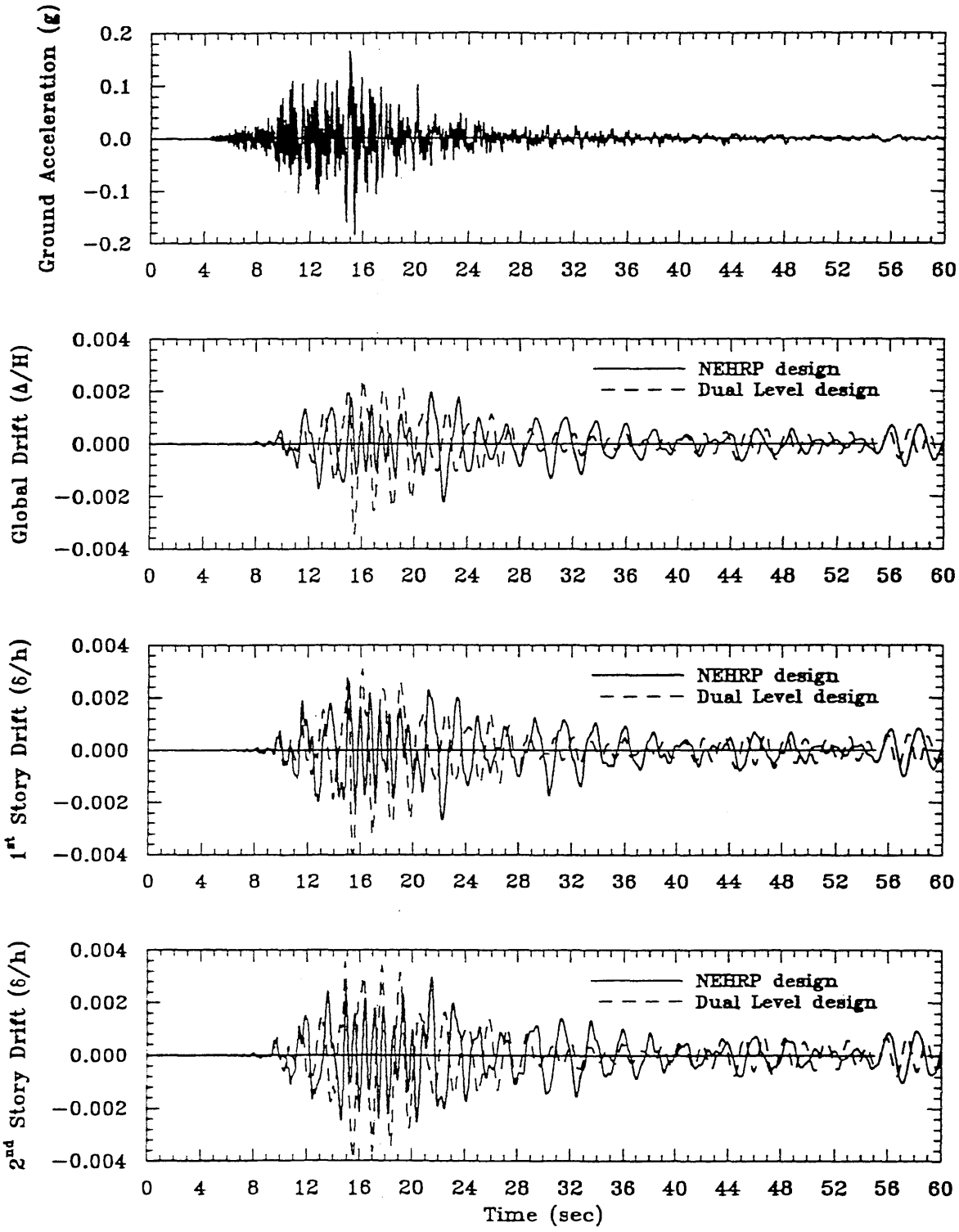

Figure C.6: Ground Motion and Structural Responses for Temple & Hope Record
(a) ground acceleration, (b) global drift, (c) first story drift, (d) second story drift